

7-1-2024

# Modulating Covalency in a Ni-H-Al Subunit: Synthesis and Characterization of a Series of Electronically Differentiating Ni-Al Heterometallics

Aleida Guadalupe Gonzalez  
*The University of Texas Rio Grande Valley*

Follow this and additional works at: <https://scholarworks.utrgv.edu/etd>

 Part of the [Inorganic Chemistry Commons](#)

---

## Recommended Citation

Gonzalez, Aleida Guadalupe, "Modulating Covalency in a Ni-H-Al Subunit: Synthesis and Characterization of a Series of Electronically Differentiating Ni-Al Heterometallics" (2024). *Theses and Dissertations*. 1544.  
<https://scholarworks.utrgv.edu/etd/1544>

This Thesis is brought to you for free and open access by ScholarWorks @ UTRGV. It has been accepted for inclusion in Theses and Dissertations by an authorized administrator of ScholarWorks @ UTRGV. For more information, please contact [justin.white@utrgv.edu](mailto:justin.white@utrgv.edu), [william.flores01@utrgv.edu](mailto:william.flores01@utrgv.edu).

MODULATING COVALENCY IN A Ni-H-AI SUBUNIT: SYNTHESIS  
AND CHARACTERIZATION OF A SERIES OF ELECTRONICALLY  
DIFFERENTIATING Ni-AI HETEROMETALLICS

A Thesis

by

ALEIDA GUADALUPE GONZALEZ

Submitted in Partial Fulfillment of the  
Requirements for the Degree of  
MASTER OF SCIENCE

Major Subject: Catalysis and Sustainability

The University of Texas Rio Grande Valley

July 2024



MODULATING COVALENCY IN A Ni-H-Al SUBUNIT: SYNTHESIS  
AND CHARACTERIZATION OF A SERIES OF ELECTRONICALLY  
DIFFERENTIATING Ni-Al HETEROMETALLICS

A Thesis  
by  
ALEIDA GUADALUPE GONZALEZ

COMMITTEE MEMBERS

Dr. Manar M. Shoshani  
Chair of Committee

Dr. Haoyuan Chen  
Committee Member

Dr. Arnulfo O. Mar  
Committee Member

Dr. Jason Parsons  
Committee Member

July 2024



Copyright 2024 Aleida Guadalupe Gonzalez

All Rights Reserved



## ABSTRACT

Gonzalez, Aleida G. Modulating Covalency in a Ni-H-Al Subunit: Synthesis and Characterization of a Series of Electronically Differentiating Ni-Al Heterometallics. Master of Science in Biochemistry and Molecular Biology (M.S.), July 2024, 88 pp., 12 tables, 67 figures, 63 references.

Metal hydrides are moieties that are present in a variety of applications as intermediates in catalysis. Despite the vast utilization of metal hydrides, monometallic metal hydride complexes bear limitations in inert-bond activation and functionalization. A strategy to overcome these limitations and access more challenging reactivity is utilizing metal-metal cooperativity on a single platform to further activate hydride moieties. Although incorporating multiple metal centers on a single ligand scaffold has been realized, access to heterometallic hydride-bearing complexes is a greater synthetic challenge. Given the limitations in accessing such systems, the reactivity and electronic structure of heterometallic hydrides are seldom studied. Recently, our group reported a novel nickel-aluminum heterotrimetallic hydride complex demonstrating enhanced reactivity in comparison to monometallic precursors in the hydroboration of *N*-heterocycles.

Our work features a rare report of three-center bonding within an Al-H-Ni subunit with sterically accessible Lewis-acidic Al centers. To aid in our understanding of the electronic structure and enhanced catalytic reactivity of this system, the synthesis of related heterometallic complexes, bearing a Ni-H-Al subunit, with electronically differentiating ancillary ligands was undertaken. Synthesis, characterization, and electronic structure studies will be discussed.



## DEDICATION

To my family.



## ACKNOWLEDGMENTS

I would like to express my deepest appreciation to my two advisors, Professor Manar M. Shoshani and Professor Haoyuan Chen, who have motivated and guided me throughout my studies. For their availability and persistent help this thesis would not have been possible.

I would like to thank my committee members and staff, Professor Arnulfo O. Mar and Professor Jason Parsons, Ms. Helia Morales, Mr. Joe Lara, and Dr. Erik Plata, who always supported and motivated me to keep me engaged with the continuation of my studies. Thank you for your time and encouraging words whenever I needed to.

I would like to thank the COS Dean's Graduate Assistantship that provided me with the funds to accomplish my Master of Science in Biochemistry and Molecular Biology.

I would like to thank my friends, Frank Garcia and Rafael Gonzalez for always being available whenever I had an issue with my codes, programs, and CPU issues. For being patient teaching me whenever I had an error and encouraging me to keep learning whenever I felt stuck. Thank you for all your time and knowledge, I hope one day to be as good as you are.

I would like to thank my lab members for their constant support whenever I needed help and for making these past two years full of memories and great moments together.

I would like to thank my family, friends, and God for always being by my side whenever I needed someone. For constantly checking on my well-being and listening to all my struggles. I wouldn't have done it without you.



## TABLE OF CONTENTS

	Page
ABSTRACT.....	iii
DEDICATION.....	iv
ACKNOWLEDGMENTS.....	v
LIST OF TABLES.....	viii
LIST OF FIGURES.....	ix
CHAPTER I: INTRODUCTION.....	1
1.1 Homogenous Ni Catalysis.....	1
1.2 Cooperative Catalysis.....	2
1.3 Heterometallic Complexes.....	4
1.4 Metal Hydrides in Catalysis.....	6
1.5 Examples of Multimetallic Hydrides in Catalysis.....	7
1.6 Heterometallic Hydrides in Catalysis.....	9
1.7 Electronic Structure of the Ni-H-Al Motif.....	12
1.8 Addition of Ancillary Ligands to Parent complex.....	13

CHAPTER II: SYNTHESIS AND CHARACTERIZATION OF HETEROMETALLIC HYDRIDES.....	16
2.1 Synthesis and Characterization of Heterometallic Hydrides.....	16
2.2 Synthesis and Characterization of New Heterometallic NiAl-Hydride Complexes....	20
2.3 Ancillary Ligands Employed Leading to Auxiliary/Negligible Reactivity.....	51
2.4 Catalytic Trials with Heterometallics.....	53
CHAPTER III: ELECTRONIC STRUCTURE STUDIES OF HETEROMETALLIC HYDRIDES.....	60
3.1 Wiberg Bond Index and QTAIM Analyses of Heterometallic Molecules, Heterotrimetallic molecule, and Alane.....	60
3.2 T1 Time Analysis of Heterometallic Molecules, Heterotrimetallic molecule, and Alane.....	69
CHAPTER IV: CONCLUSION.....	78
4.1 Future work.....	80
REFERENCES.....	82
VITA.....	88

## LIST OF TABLES

Table 1: Properties of Bond Distances of NiAl-(PPh <sub>3</sub> ) <sub>2</sub> .....	27
Table 2: Properties of Bond Distances of NiAl-(dppm) <sub>2</sub> .....	34
Table 3: Properties of Bond Distances of NiAl-(PMe <sub>3</sub> ) <sub>2</sub> .....	41
Table 4: Properties of Bond Distances of NiAl-(PMe <sub>3</sub> ) <sub>2</sub> -NHC-IPr(3).....	48
Table 5: Overall comparison table of properties between all complexes.....	50
Table 6: List of ligands used, # of equivalence, temperature, and attempts.....	52
Table 7: WBIs, Rho values, and Bond distances of NiAl-(PPh <sub>3</sub> ) <sub>2</sub> .....	62
Table 8: WBIs, Rho values, and Bond distances of NiAl-(dppm) <sub>2</sub> .....	64
Table 9: WBIs, Rho values, and Bond distances of NiAl-(PMe <sub>3</sub> ) <sub>2</sub> .....	65
Table 10: WBIs, Rho values, and Bond distances of NiAl-P(Me <sub>3</sub> ) <sub>2</sub> + NHC-IPr.....	67
Table 11: Overall comparison table of WBIs and Rho values between all complexes.....	69
Table 12: Overall comparison table of T1 times between all complexes.....	77



## LIST OF FIGURES

Figure 1: Ni-SHOP catalysts for ethylene oligomerization.....	2
Figure 2: Modes of Cooperativity.....	3
Figure 3: Monometallic complexes.....	5
Figure 4: Heterobimetallic complexes.....	5
Figure 5: Multimetallic complexes .....	6
Figure 6: Sterically Accessible using a secondary metal for Multimetallic complex.....	7
Figure 7: Fe-Al system of Cooperative Heterometallic.....	8
Figure 8: Sterics in multimetallic complexes.....	9
Figure 9: Reaction of Heterotrimetallic NiAl <sub>2</sub> .....	10
Figure 10: Hydroboration of quinoline using NiAl <sub>2</sub> .....	11
Figure 11: Kinetics studies between LAIH vs. NiAl <sub>2</sub> .....	11
Figure 12: General Electronic structure of NiAl <sub>2</sub> complex .....	12
Figure 13: Ni-H-Al subunits between Al-based or Ni-based .....	13
Figure 14: Al-based vs. Ni-based scale.....	14
Figure 15: Alane-Ni(0) vs. Aluminly-Ni(II).....	14
Figure 16: Nature of bonding motif of Ni-H-Al.....	15
Figure 17: Overall Synthesis of Precursors for LAIH and NiAl <sub>2</sub> .....	17
Figure 18: Synthesis of 1,3-bis(2,6-diisopropylphenyl)imidazole-2-ylidene.....	19
Figure 19: Synthesis of NHC-Me and NHC-IPr.....	19
Figure 20: Reaction of LAIH + TPP.....	21
Figure 21: Reaction of NiAl <sub>2</sub> + TPP.....	22
Figure 22: <sup>1</sup> H NMR spectrum of <b>NiAl-(PPh<sub>3</sub>)<sub>2</sub></b> in C <sub>6</sub> D <sub>6</sub> .....	24
Figure 23: <sup>13</sup> C{ <sup>1</sup> H} NMR spectrum of <b>NiAl-(PPh<sub>3</sub>)<sub>2</sub></b> in C <sub>6</sub> D <sub>6</sub> .....	25

Figure 24: $^{31}\text{P}\{^1\text{H}\}$ NMR spectrum of <b>NiAl-(PPh<sub>3</sub>)<sub>2</sub></b> in C <sub>6</sub> D <sub>6</sub> .....	26
Figure 25: XRD crystal structure of <b>NiAl-(PPh<sub>3</sub>)<sub>2</sub></b> .....	27
Figure 26: Reaction of LAIH + dppm.....	29
Figure 27: $^1\text{H}$ NMR spectrum of <b>NiAl-(dppm)<sub>2</sub></b> in C <sub>6</sub> D <sub>6</sub> .....	31
Figure 28: $^{13}\text{C}\{^1\text{H}\}$ NMR spectrum of <b>NiAl-(dppm)<sub>2</sub></b> in C <sub>6</sub> D <sub>6</sub> .....	32
Figure 29: $^{31}\text{P}\{^1\text{H}\}$ NMR spectrum of <b>NiAl-(dppm)<sub>2</sub></b> in C <sub>6</sub> D <sub>6</sub> .....	33
Figure 30: XRD crystal structure of <b>NiAl-(dppm)<sub>2</sub></b> .....	33
Figure 31: Reaction of LAIH + TMP.....	36
Figure 32: Reaction of NiAl <sub>2</sub> + TMP.....	36
Figure 33: $^1\text{H}$ NMR spectrum of <b>NiAl-(PMe<sub>3</sub>)<sub>2</sub></b> in C <sub>6</sub> D <sub>6</sub> .....	38
Figure 34: $^{13}\text{C}\{^1\text{H}\}$ NMR spectrum of <b>NiAl-(PMe<sub>3</sub>)<sub>2</sub></b> in C <sub>6</sub> D <sub>6</sub> .....	39
Figure 35: $^{31}\text{P}\{^1\text{H}\}$ NMR spectrum of <b>NiAl-(PMe<sub>3</sub>)<sub>2</sub></b> in C <sub>6</sub> D <sub>6</sub> .....	40
Figure 36: XRD crystal structure of <b>NiAl-(PMe<sub>3</sub>)<sub>2</sub></b> .....	41
Figure 37: Reaction of NiAl-(PMe <sub>3</sub> ) <sub>2</sub> and NHC-IPr.....	43
Figure 38: $^1\text{H}$ NMR spectrum of <b>NiAl-(PMe<sub>3</sub>)<sub>2</sub>-NHC-IPr</b> in C <sub>6</sub> D <sub>6</sub> .....	45
Figure 39: $^{13}\text{C}\{^1\text{H}\}$ NMR spectrum of <b>NiAl-(PMe<sub>3</sub>)<sub>2</sub>-NHC-IPr</b> in C <sub>6</sub> D <sub>6</sub> .....	46
Figure 40: $^{31}\text{P}\{^1\text{H}\}$ NMR spectrum of <b>NiAl-(PMe<sub>3</sub>)<sub>2</sub>-NHC-IPr</b> in C <sub>6</sub> D <sub>6</sub> .....	47
Figure 41: XRD crystal structure of <b>NiAl-(PMe<sub>3</sub>)<sub>2</sub>-NHC-IPr</b> .....	48
Figure 42: General methodology behind the small-scale reaction with unsuccessful ligands.....	51
Figure 43: Reaction of Quinoline and H-BPin with 5% NiAl <sub>2</sub> catalyst.....	54
Figure 44: $^1\text{H}$ NMR spectrum of catalytic reaction using 5 % <b>NiAl<sub>2</sub></b> in C <sub>6</sub> D <sub>6</sub> .....	55
Figure 45: $^{31}\text{P}\{^1\text{H}\}$ NMR spectrum of catalytic reaction using 5 % <b>NiAl<sub>2</sub></b> in C <sub>6</sub> D <sub>6</sub> .....	56
Figure 46: Reaction of Quinoline and H-BPin with 5% NiAl-(PPh <sub>3</sub> ) <sub>2</sub> catalyst.....	56
Figure 47: $^1\text{H}$ NMR spectrum of catalytic reaction using 5 % <b>NiAl-(PPh<sub>3</sub>)<sub>2</sub></b> in C <sub>6</sub> D <sub>6</sub> .....	58
Figure 48: $^{31}\text{P}\{^1\text{H}\}$ NMR spectrum of catalytic reaction using 5 % <b>NiAl-(PPh<sub>3</sub>)<sub>2</sub></b> in C <sub>6</sub> D <sub>6</sub> .....	59
Figure 49: Optimized structure of NiAl-(PPh <sub>3</sub> ) <sub>2</sub> .....	62
Figure 50: Optimized structure of NiAl-(dppm) <sub>2</sub> .....	63
Figure 51: Optimized structure of NiAl-(PMe <sub>3</sub> ) <sub>2</sub> .....	65

Figure 52: Optimized structure of NiAl-(PMe <sub>3</sub> ) <sub>2</sub> -NHC-IPr.....	66
Figure 53: Experimental molecular structure of all complexes.....	68
Figure 54: Structure of NiAl-(PPh <sub>3</sub> ) <sub>2</sub> .....	71
Figure 55: T1 Time Plot NiAl-(PPh <sub>3</sub> ) <sub>2</sub> in C <sub>6</sub> D <sub>6</sub> .....	71
Figure 56: T1 Time Plot NiAl-(PPh <sub>3</sub> ) <sub>2</sub> in THF.....	72
Figure 57: Structure of NiAl-(PMe <sub>3</sub> ) <sub>2</sub> .....	72
Figure 58: T1 Time Plot NiAl-(PMe <sub>3</sub> ) <sub>2</sub> in C <sub>6</sub> D <sub>6</sub> .....	73
Figure 59: T1 Time Plot NiAl-(PMe <sub>3</sub> ) <sub>2</sub> in THF.....	73
Figure 60: Structure of NiAl-(PMe <sub>3</sub> ) <sub>2</sub> -NHC-IPr.....	74
Figure 61: T1 Time Plot NiAl-(PMe <sub>3</sub> ) <sub>2</sub> -NHC-IPr in THF.....	74
Figure 62: Structure of LAIH.....	75
Figure 63: T1 Time Plot LAIH in C <sub>6</sub> D <sub>6</sub> .....	75
Figure 64: Structure of NiAl <sub>2</sub> .....	76
Figure 65: T1 Time Plot NiAl <sub>2</sub> in C <sub>6</sub> D <sub>6</sub> .....	76
Figure 66: T1 Time Plot NiAl <sub>2</sub> in THF.....	77
Figure 67: Future work.....	81



## CHAPTER I

### INTRODUCTION

#### 1.1. Homogenous Ni Catalysis

Leveraging the natural abundance of certain metals found on the Earth's crust is potentially a cost-effective method to access sustainable catalysis. Currently, several industrial processes rely on catalysts that incorporate precious metals such as Pd, Pt, Ir, and Rh.<sup>53,54</sup> The late-metal nature of those metals provides functional group tolerance, which is needed to avoid catalyst poisoning in the presence of polar functionalities. A metal that has been growingly utilized in the past few decades is nickel.<sup>30</sup> The low cost of Ni, the functional group tolerance, and the large abundance on the Earth's crust are some of the main reasons that its utilization has garnered high interest.<sup>49</sup> Though heterogeneous Ni catalysts are well known in their usage, Homogenous Ni-based catalysts have been growing in their utility both for academic purposes as well as industry.<sup>41,42</sup> Homogeneous systems also bear the advantage of providing a greater level of mechanistic detail in comparison to ill-defined heterogeneous variants. Lastly, a homogeneous Ni system can be relatively straightforward to synthesize.<sup>28</sup> For these and among other reasons, chemists are interested in building new homogenous Ni complexes that range in complexity to leverage in catalysis.

Homogenous Ni complexes have shown substantial value in industry. For example, the Ni phosphino-enolate complex shown in Figure 1 is just one example of the Shell Higher-Olefin Process (SHOP) catalysts which are competent in the oligomerization of ethene to higher alpha olefins (Figure 1) and can then be used as a precursor or hydroformylation. The Keim group

published a paper on how using nickel industrial chemicals may improve by about 60-70% when modifying C-C coupling reactions using nickel catalysis.<sup>30</sup>

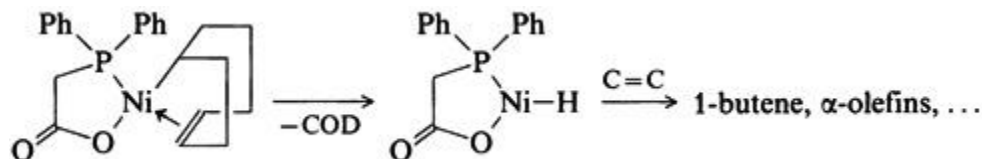


Figure 1: Ni-SHOP catalysts for ethylene oligomerization.<sup>30</sup>

Though over the past few decades, the number of reports of Ni-mediated catalytic transformations has only grown, and the scope of transformations has widened substantially, several drawbacks are still present. High catalyst loadings, low yields, and selectivity are often observed for a slew of Ni-catalyzed transformations.<sup>41</sup> Small molecule and inert-bond activation is also very limited without the aid of a directing group, whereas complexes of Ir and Rh are able to facilitate C-C and C-H bond activations under relatively mild conditions, mononuclear Ni complexes that can serve the same purpose are lacking.<sup>42</sup> To this end, new strategies to leverage Ni are needed.

## 1.2. Cooperative Catalysis

There are several strategies to enhance the ability of molecular complexes to serve as better catalysts. One recent strategy is through the design and synthesis of homogenous complexes that

invoke “cooperative reactivity”. Cooperativity is a common concept across many fields including biological chemistry, surface chemistry, as well as organometallic chemistry. With respect to organometallic chemistry, complexes can invoke cooperativity by having metals and ligands working together, as well as multiple metal centers working together. Focusing on metal-metal cooperativity, common ways to distinguish the types are shown in Figure 2 limiting examples to an encapsulated bimetallic site. In the top example,  $M_A$  is a transition metal that is redox-active, and  $M_B$  is the encapsulated metal that bears a primary goal of changing the electron density of  $M_A$ .  $M_B$  helps  $M_A$  by functioning as a sigma acceptor which renders  $M_A$  more electrophilic and primed for bond activation. On the other hand, a cooperative coordination site involves utilizing two redox-active metals that can undergo cooperative cleavage of bonds in the second example of cooperativity shown below. The vacant coordination sites are necessary to carry this out.

(Figure 2).

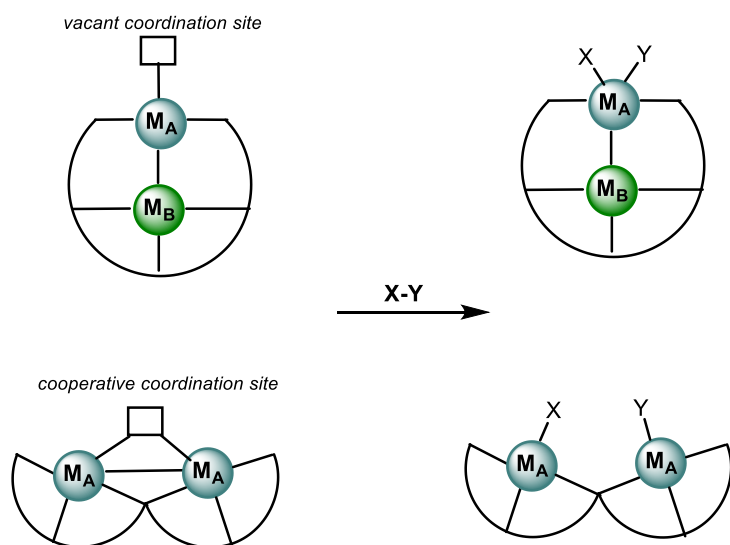


Figure 2: Modes of Cooperativity.

While the bottom example from Figure 2 is thoroughly investigated, representative examples of the top image of Figure 2 are an emerging field. This is partially related to the challenges associated with the synthesis of well-defined heterometallic complexes. Furthermore, select examples have shown  $M_B$  can directly participate in substrate binding and bond activation which serves as a highly promising advancement in the field.

As is important to differentiate which method is going to be performed while synthesizing. During this methodology, it was utilized a vacant coordination site with the expectation to have heterobimetallic complexes and obtained a better understanding of utilizing two different metals in a single catalyst in order to improve modulation of electron donation around them. For this reason, it is essential to differentiate between homometallic and heterometallic complexes. Having a different metal in your complex may improve reactivity and steric hindrance.

### **1.3. Heterometallic Complexes**

Homometallic and heterometallic complexes can exist as bimetallic, and multimetallic complexes. Determining the nuclearity of the complexes synthesized can be challenging as many of these complexes use terminal ancillary ligands and rely on self-assembly; this is further complicated when different metal and their respective preferences in molecular geometry are incorporated.<sup>7</sup> It is crucial to predict the number of metals in complexes since it can directly influence the behavior of the complex. While monometallic complexes are easier to synthesize, monometallic complexes featuring Earth-abundant metals have limitations in their capabilities in molecular reactivity, as discussed above (Figure 3).<sup>6</sup> Monometallic complexes have been found easy to produce. However, monometallic complexes have limitations in regard to steric hindrance and reactivity (Figure 3).

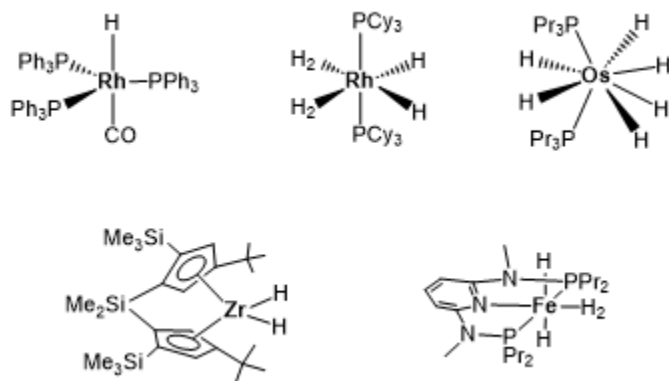


Figure 3: Monometallic complexes.<sup>6</sup>

The main challenge that plagues multimetallic complexes is that they are much complex to synthesize which results on having multistep mechanisms in comparison to monometallic complexes (Figure 4).<sup>24</sup> Ways to help alleviate this issue are to include ligand design elements that incorporate site-specific binding sites. Having a specific arrangement of electronic influence and bulky substituents surrounding the complex has been a successful strategy in ligand design.<sup>45</sup> As a consequence, heterobimetallic complexes incorporating these ligand design features have been of recent interest for exploration.

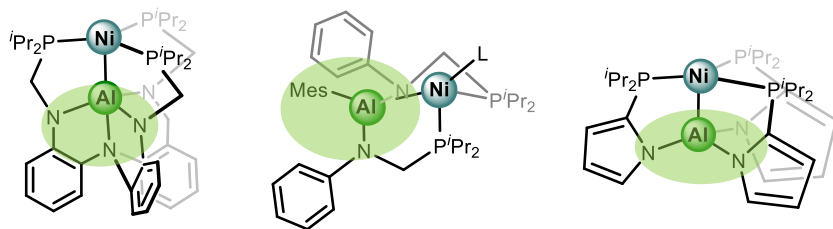


Figure 4: Heterobimetallic complexes.<sup>8, 53, 34</sup>

## 1.4. Metal Hydrides in Catalysis

Heterometallic complexes are an important part of catalysis and one of the main ones are hydrides. The term “hydride” is defined as the ionic bonding between a hydrogen atom with another element, in the field of inorganic chemistry mainly with a metal.<sup>34</sup> Metal hydride complexes are known catalysts of choice in many catalytic reactions including ethylene polymerization, oligomerization, hydroformylation, and many others.<sup>50</sup> Though monometallic complexes have had extensive studies on metal hydrides in their electronic structure and catalytic capabilities, the metal-hydrogen subunit in multimetallic complexes often shows the most impressive reactivity (Figure 5).<sup>6</sup> While there is a clear motivation to study multimetallic hydride complexes, harnessing the reactivity has not been fully realized, and in many cases, the increase in reactivity has not been fully understood (Figure 5). Electronic structure studies have the capability of offering a better understanding of the M-H-M subunits. Currently, there are limited studies on metal hydride-containing heterometallic complexes.<sup>24</sup> However, leveraging these potential complexes in catalysis is exciting to explore given the potential to alter electron density within the metal hydride subunit.

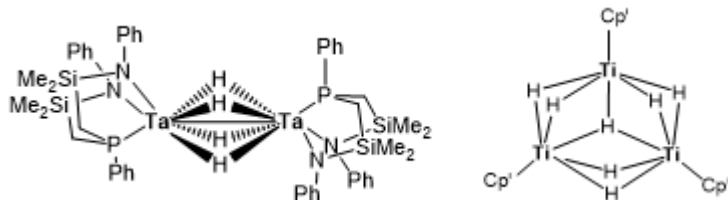


Figure 5: Multimetallic complexes.<sup>6</sup>

In order to have a deeper understanding of electron density modulation, it is important to understand the sterics surrounding the secondary metal while having a multimetallic complex. Figure 6 shows how having an encapsulated secondary metal leads to having a hydride subunit in between both metals (When R=H). The interaction between metals in a heterobimetallic complex is difficult to understand due to both having a strong influence on one another, however, it is essential to have a deep understanding of the subunit to improve the reaction dynamics of the complex. For this reason, having examples to implement and produce multimetallic hydrides is important to improve mechanistic studies.

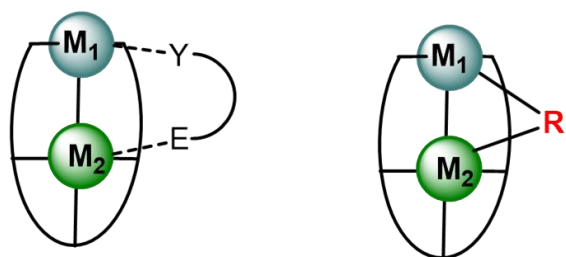


Figure 6: Sterically Accessible using a secondary metal for Multimetallic complex.

### 1.5. Examples of Multimetallic Hydrides in Catalysis

Multimetallic hydrides form often via multi-step synthesis which make them difficult to synthesize and may result in low yields. However, the benefits of multimetallic hydrides in their unique reactivity outweigh their disadvantages in their synthesis. Some of the benefits of multimetallic hydrides, such as having more than one hydride in between the bimetallic subunit, can lead to higher reactivity and better accessibility and selectivity in reactivity. Figure 7 shows a novel Fe-Al system reported by the Crimmin group. This complex employs primarily

monodentate donors on the redox-active metal which is only bridged to the Al center via hydride ligands.

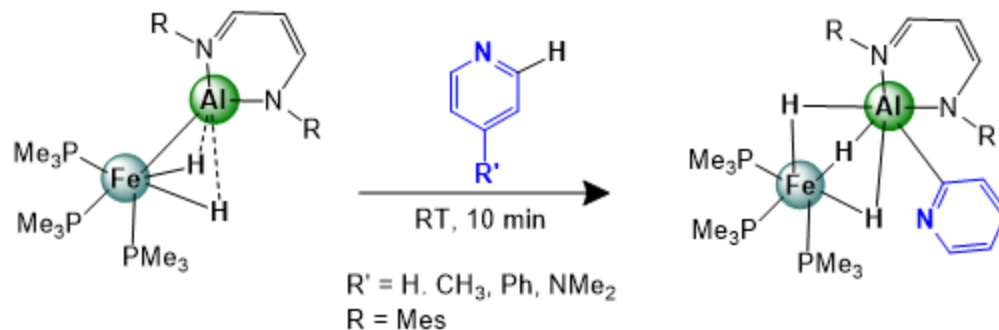


Figure 7: Fe-Al system of Cooperative Heterometallic.<sup>52</sup>

In this reaction, we can observe the multiple hydrides in between the Fe-Al subunit which result in selective C-H activation of pyridine.<sup>52</sup> The secondary metal, in this case, Al, is proposed to hinder poisoning from incoming substrates and direct reactivity, as well as potentially enhance the reactivity of bridged atoms. Some other synthetic methods for heterometallic complexes tend to rely on the self-assembly of metal cations that have multidentate ligand scaffolds. Dealing with multimetallic complexes gives us access to multiple bridged atoms which will give us a higher opportunity of reactivity and lead to better catalysts.<sup>52</sup> As observed in Figure 8, the complex on top offers two hydrides per bridged atoms, and the complex on the bottom offers only one, however multiple modulations of electron density around the Ni atom which is the primary metal.<sup>7,26</sup>

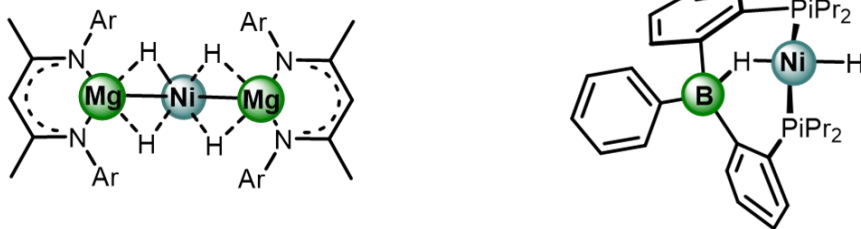


Figure 8: Sterics in multimetallic complexes.<sup>7,26</sup>

### 1.6. Heterometallic Hydrides in Catalysis

Catalysis consists of different types of complexes, but one of the least understood is heterometallic hydrides. As discussed above, having two different kinds of metals in a complex may have multiple access to more than one hydride.<sup>48</sup> Heterometallic hydrides have become essential in a variety of catalytic processes.<sup>6</sup> Since heterometallic hydride complexes have the properties of two different metals, this brings favorable novel properties in a single complex that may improve reactivity compared to homometallic complexes.<sup>34,36</sup> For these and more reasons, heterometallic hydrides are under interest among plenty of scientists due to their promising features.

Heterometallic hydride complexes consist of at least two different types of metals, along with a hydrogen atom bridging both metals. Having these types of hydrides helps improve reactivity and sterics among the heterometallic subunit.<sup>40</sup> Heterometallic hydride subunits are not fully understood. For this reason, we focused on mechanistic and computational studies to further understand the unknown interactions among the subunits. Our parent structure is a heterotrimetallic hydride which implies two Ni-H-Al subunit. In order to understand further the

electronic structure of this Ni-H-Al motif, we decided to add electron-rich ligands to our complex to donate the electron density to the Ni center to improve reactivity and versatility.

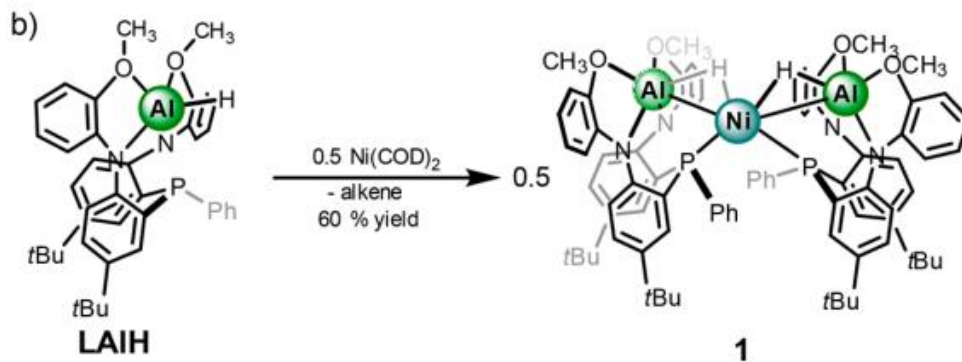


Figure 9: Reaction of Heterotrimetallic NiAl<sub>2</sub>.<sup>16</sup>

Recently, our group reported the use of the heterotrimetallic Ni-H-Al complex in the hydrofunctionalization of *N*-heterocycles. The reactivity is proposed to proceed in a cooperative manner, in which LAlH (Ligand Aluminum Hydride) metalloligand works with a Ni center. As is shown in Figure 9, the precursor that we synthesized for the parent structure consists of a LAlH complex and adding Ni(COD)<sub>2</sub> inside a glovebox in a standard temperature and pressure setting, a 60% yield of the parent structure NiAl<sub>2</sub> was achieved.<sup>16</sup>

In order to determine the catalytic capabilities of NiAl<sub>2</sub> and LAlH, comparative kinetics studies were performed by hydroboration of *N*-heterocycles. The kinetic studies were performed using 5 mol % of NiAl<sub>2</sub> and 10 mol % LAlH with 1 equivalence of quinoline and 3 equivalence of H-Bpin.<sup>16</sup> The number of reactions was four using a variety of quinoline substrates but matching parameters. When the NiAl<sub>2</sub> complex is used as a catalyst, the activity is substantially higher likely owing to the cooperative nature between Ni and Al (Figure 10).

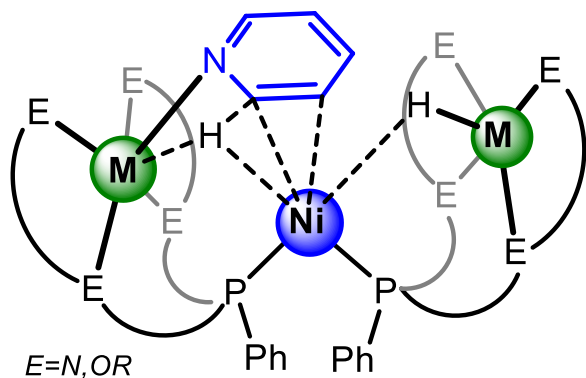


Figure 10: Hydroboration of quinoline using  $NiAl_2$ .

Using the information obtained from the kinetics studies, a plot of the natural logarithm of the concentration of quinoline versus time clearly shows a linear behavior (Figure 11). The  $k_{obs}$  values are  $4.66 \times 10^{-2} \text{ min}^{-1}$  for  $NiAl_2$  and  $1.06 \times 10^{-4} \text{ min}^{-1}$  for LAIH, which indicates a 400X enhancement in activity.<sup>16</sup> Due to these results, it is fundamental to understand the electronic structure of the Ni-H-Al motif in the  $NiAl_2$  complex to further extend our understanding of amplifying reactivity among our complexes.

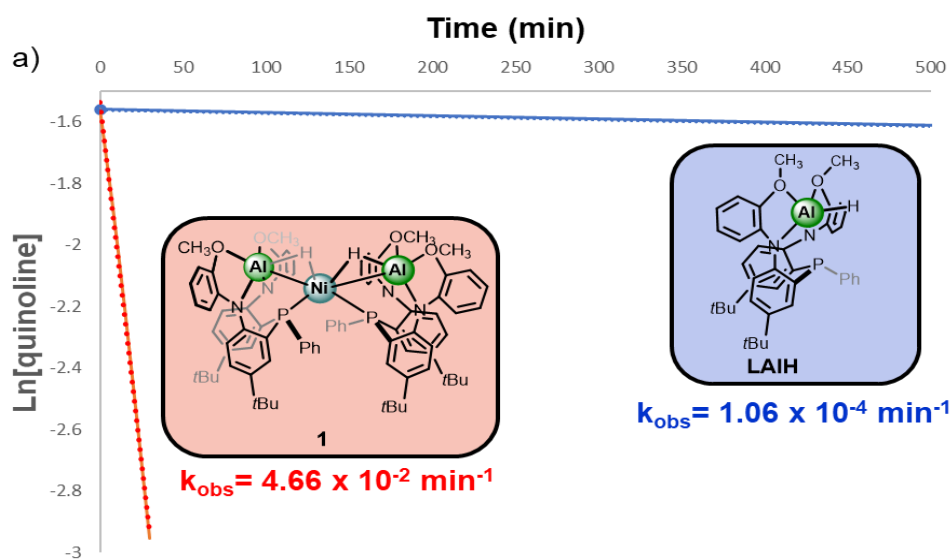


Figure 11: Kinetics studies between LAIH vs  $NiAl_2$ .<sup>16</sup>

## 1.7. Electronic Structure of the Ni-H-Al Motif

A method to gain insight into the electronic structure of heterometallic complexes is by performing computational analyses. These computational analyses may be where the majority of electron density arises through varying metrics of analysis. The computational analyses used Natural Bond Orbital (NBO) and Quantum Theory of Atoms in Molecules (QT-AIM).<sup>2, 3,47</sup> These computational analyses were performed in several of our complexes to better understand the Ni-H-Al subunit.

Figure 12 shows the general  $\text{NiAl}_2$  complex which contains two hydrides in particular that are the main Ni-H-Al subunit in the complex. These Ni-H-Al subunits are uncommon since there are only a few complexes that exist with these characteristics. As a result, computational studies were performed on the  $\text{NiAl}_2$  complex to better understand the electronic interactions around the complex.

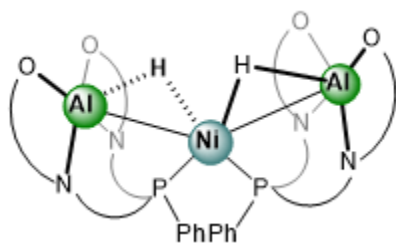
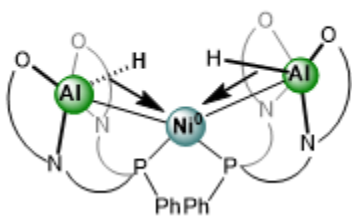


Figure 12: General Electronic structure of  $\text{NiAl}_2$  complex.

Aside from determining the electron density around the complex, computational studies also aid in determining if the complex is an Al-based hydride  $\text{Ni}(0)$  or a Ni-based hydride  $\text{Ni}(II)$ . It is important to clarify that either of the following will help establish a fundamental pathway to improve the catalytic activity to obtain adjusted complexes. As shown in Figure 13, an Al-based

hydride Ni(0) donates its electron density to the nickel center, otherwise, a nickel-based hydride Ni(II) donates its electron density to the Aluminum secondary metal.<sup>48</sup> Aside from computational studies, the addition of a competitive ancillary ligand to the NiAl<sub>2</sub> complex will allow us to observe to which metal the ligand will donate its electron density. These studies will provide valuable insight in understanding if NiAl<sub>2</sub> bears an Al-based hydride or a Ni-based hydride.

### Al-based Hydride Ni(0)



or

### Ni-based Hydride Ni(II)

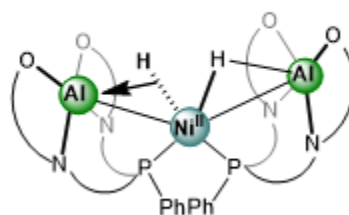


Figure 13: Ni-H-Al subunits between Al-based or Ni-based.

## 1.8. Addition of Ancillary Ligands to Parent complex

Ancillary ligands are generally described as having a primary role of donating electron density to a metal center and not playing an auxiliary role in redox-based chemistry. The degree of donation with the ancillary ligands varies depending on their electronic and steric properties.<sup>14</sup> Common ancillary ligands include CO, phosphines, nitriles, and N-heterocyclic carbenes. Additionally, a comparison with electron-donating groups is important to have a contrast using electron-withdrawing (EW) groups. The spectrochemical series is a common way to qualitatively assign these properties.<sup>14</sup>

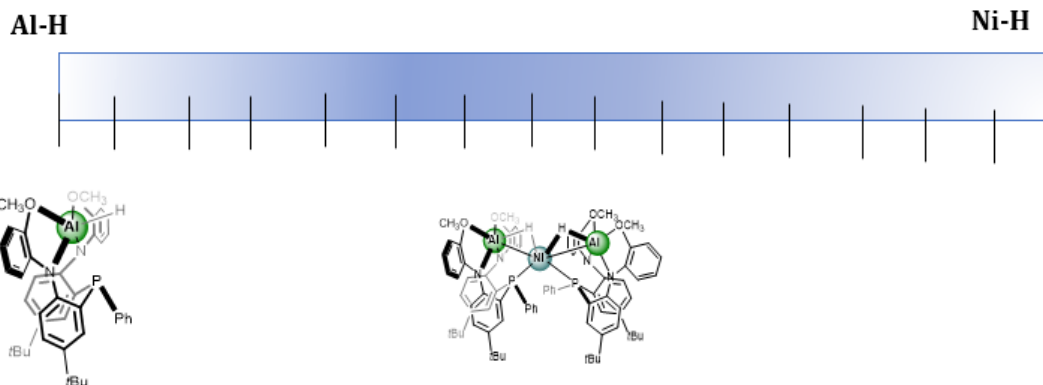


Figure 14: Al-based vs. Ni-based scale.

A scale shown in Figure 14 describes that the  $\text{LAiH}$  was under the most Al-character and  $\text{NiAl}_2$  was somewhere between both characters. This approach was studied and discussed below using ED and EW ligands to generate heterobimetallic complexes with varying hydride character. As is observed in Figure 15 and mentioned before, adding ancillary ligands to both complexes will offer insight towards the degree of donation to Ni from an Al-H bond as well as backdonation from Ni to the Al-H antibonding orbital. The degree of each of these interactions directly relates to the level of Al-H vs Ni-H.



Figure 15: Alane-Ni(0) vs. Aluminyl-Ni(II).

### Nature of bonding motif

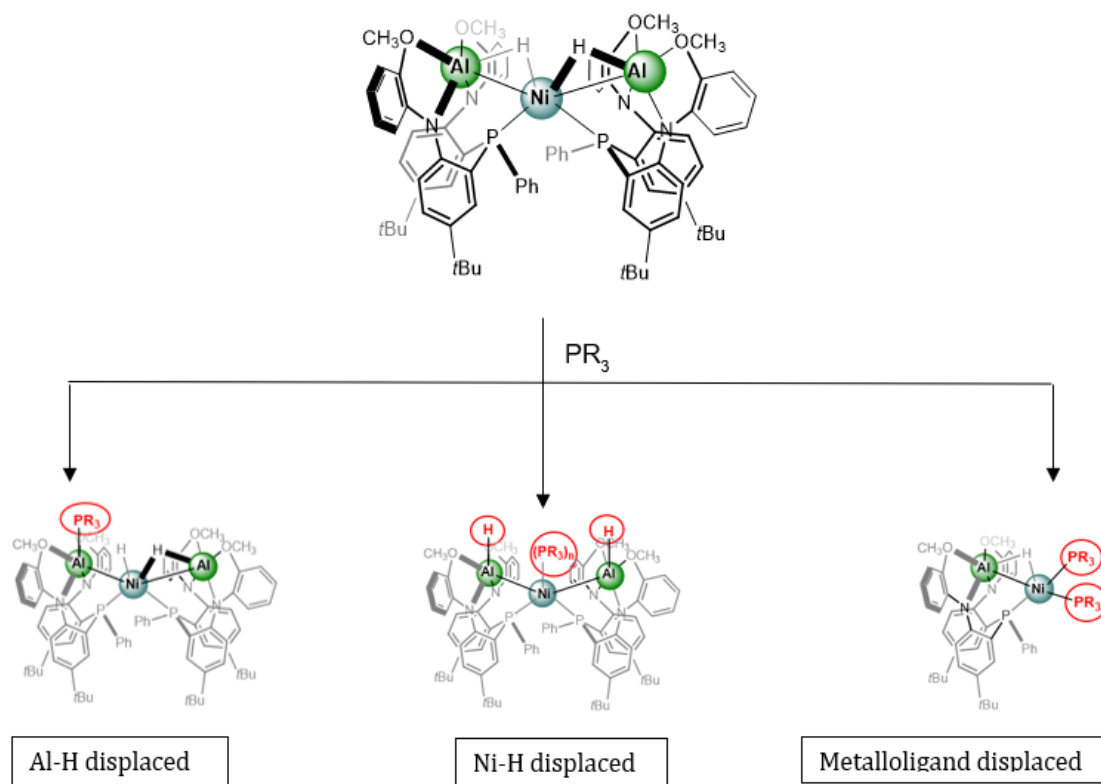


Figure 16: Nature of bonding motif of Ni-H-Al.

One can envision that the addition of ED or EW ligands to the parent NiAl<sub>2</sub> complex can result in different outcomes. Figure 16 shows the parent structure and for this example phosphines (PR<sub>3</sub>) was used. The first possibility is having an Al-H displaced in which PR<sub>3</sub> is bonded to one of the aluminums. The second possibility is having a Ni-H displaced in which PR<sub>3</sub> is bonded to the nickel and then the aluminums will be bonded to the hydrogens making it a bona fide aluminum-hydride. Finally, the third possibility is having a metalloligand displaced in which more than one phosphine is bonded to the nickel and it creates a Ni-H-Al subunit.

## CHAPTER II

### SYNTHESIS AND CHARACTERIZATION OF HETEROMETALLIC HYDRIDES

#### 2.1 Synthesis and Characterization of Heterometallic Hydrides

The main components of this chapter stem from the reactivity of the parent  $\text{NiAl}_2$  complex from the previous chapter which has been previously reported. This parent complex coined  $\text{NiAl}_2$ , is under investigation in its electronic structure to better understand its bonding as well as improve its reactivity towards catalytic insertion chemistry.<sup>18</sup> For that reason, the addition of ancillary ligands was sought. In this section, we explore the impact of the addition of varying ancillary ligands to the  $\text{NiAl}_2$  complex. Namely, we sought to investigate whether the ligand will coordinate with the Al, Ni, neither, nor both. Select complexes were isolated and fully characterized and will be discussed in the subsequent sections.

##### 2.1.1 Overall synthesis of LAIH and $\text{NiAl}_2$

As was previously studied, the  $\text{NiAl}_2$  is synthesized in a multistep synthesis which begins with a C-N cross-coupling of 2-bromo-4-tert-butyl-aniline and 2-iodoanisole to produce **A**. When **A** is clean, then it proceeds to the addition of 2 eq. of n-butyllithium for the deprotonation halogen exchange to generate **B**. Once **B** is cleaned up and isolated, then 0.5 eq. of phenyldichlorophosphine is used to produce the phosphine ( $\text{LH}_2$ ). When ligand  $\text{LH}_2$  is isolated, addition of a 1 eq. of alane-dimethylethylamine complex is then carried out to synthesize metalloligand (LAIH). The hydride of the LAIH species resonates at 5.1 ppm. The last step to

accomplish the NiAl<sub>2</sub> synthesis is via addition of 0.5 eq. of Ni(COD)<sub>2</sub>. The full synthetic scheme is outlined in Figure 17.<sup>16</sup>

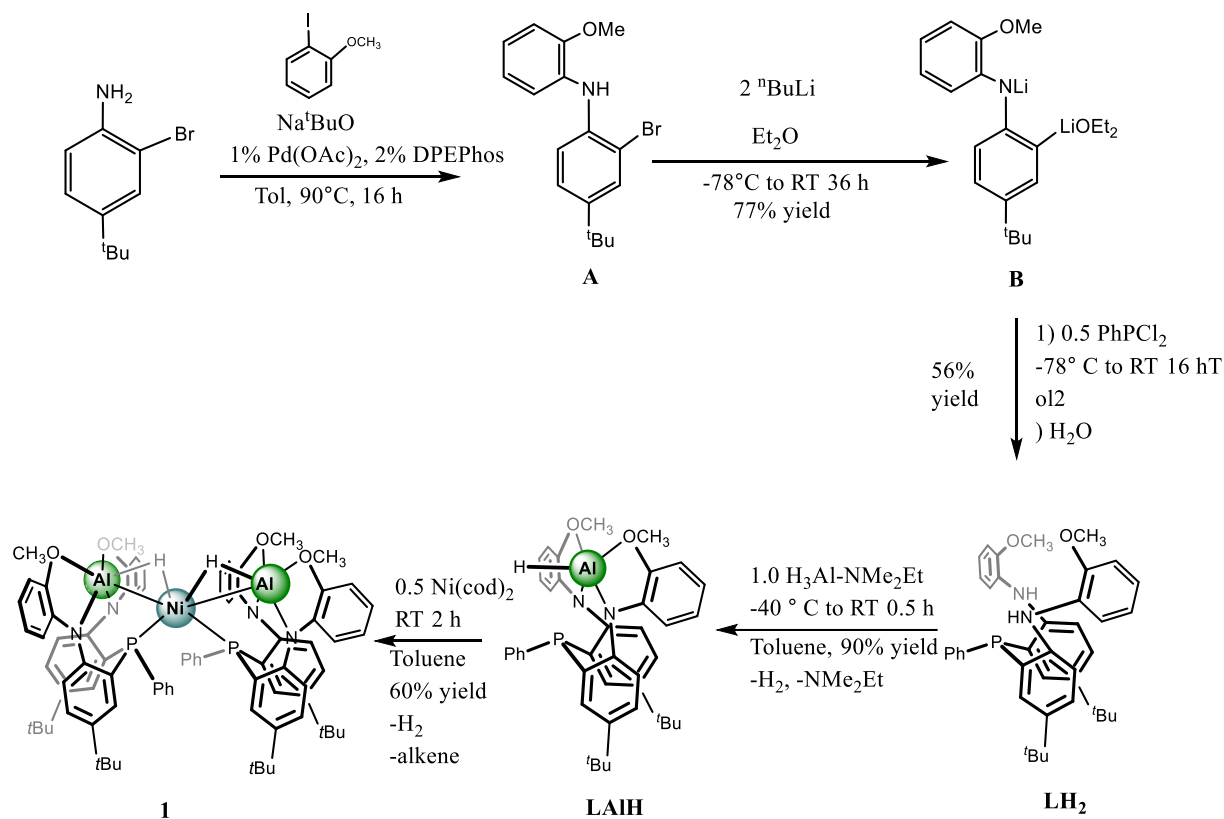


Figure 17: Overall Synthesis of Precursors for LAIH and NiAl<sub>2</sub>.<sup>16</sup>

Though the NiAl<sub>2</sub> complex is generally the subject of interest given the heterometallic hydride nature, using LAIH has a distinct advantage in that it decreases an isolation step and the kinetics for dissociation need not be considered. Therefore, for this study, the majority of the small-scale syntheses targeting additional ancillary ligands NiAl<sub>2</sub> and LAIH were used.

### 2.1.2 Ancillary Ligand Hypothesis

When considering the coordination environment about Ni, two phosphine donors are employed and what can be considered a sigma interaction with an Al-H bond. The main two interactions with the Al-H bond are a sigma interaction to the Ni center and a back bonding interaction to an antibonding orbital. The two interactions there provide a glimpse into whether there is more Al-hydride or Ni-hydride character within the complex. The benefit of adding ancillary ligands is that those interactions can be tuned and potentially modulate the degree of hydride character. The results in both characterization of resultant species and relative catalytic performance would be highly instructive.

Given the fact that the current NiAl<sub>2</sub> is supported by sigma donors such as phosphine ligands, sigma donors were primarily targeted for this study. This includes phosphine donors of varying sigma-donating capabilities as well as other donors such as N-heterocyclic carbenes (NHC) ligands. Strong sigma donors such as NHCs have opened the door to scientists to explore and guide themselves to use them on important metal complexes.<sup>1,15</sup> Having such electron-rich groups derived from heteroaromatic compounds. Among the different alternative atoms, NHCs can have, it can be sulfur, and oxygen that are accessible, but stable carbenes usually contain only nitrogen substituents.<sup>14</sup> For this set of carbenes, it was essential to use carbenes with a different electronic or steric parameter.

The vast majority of ancillary ligands used within our study were purchased; however, the carbene ligands were synthesized in our lab. The first carbene utilized for this small-scale reaction was 1,3-Bis(2,6-diisopropylphenyl)imidazole-2-ylidene. The synthesis was performed followed by Jafarpour et al.<sup>29</sup> As shown in Figure 18, the synthesis was performed using 1,3-bis(2,6-diisopropyl phenyl) imidazolium chloride by the addition of Potassium Tert-butoxide in

THF, it was allowed to react for 15 minutes inside a glovebox. Once the reaction finished, it was then allowed to vacuum to remove any additional solvents. A white powder was obtained which was 1,3-Bis(2,6-diisopropylphenyl)imidazole-2-ylidene.

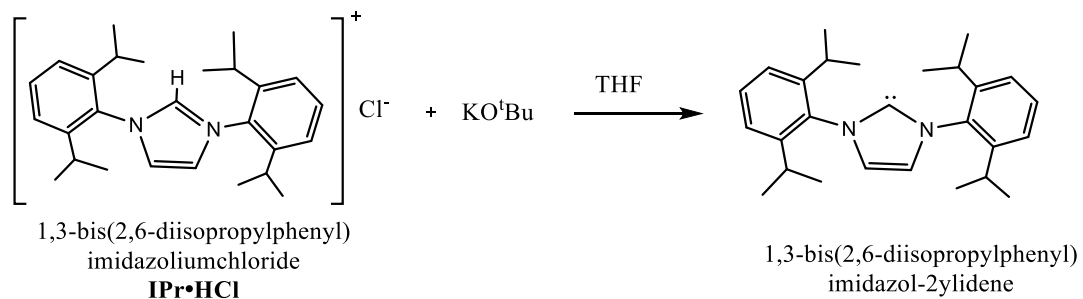


Figure 18: Synthesis of 1,3-bis(2,6-diisopropylphenyl) imidazole-2-ylidene.<sup>29</sup>

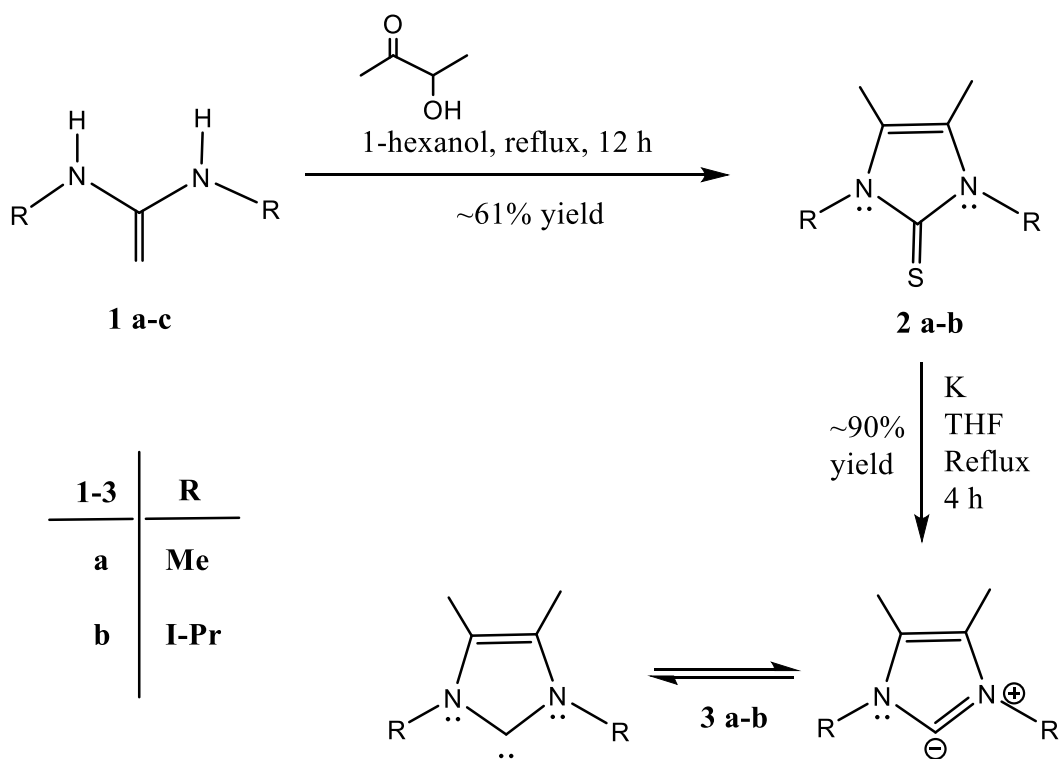


Figure 19: Synthesis of NHC-Me and NHC-IPr.<sup>32</sup>

Similarly, the second and third synthesized carbenes to explore a smaller substituent H-heterocycle carbene are 1,3,4,5-Tetramethyl Imidazole (NHC-Me) and 1,3-Diisopropyl-4,5-dimethyl imidazol-2-ylidene. These were synthesized following Kuhn & Kratz work.<sup>32</sup> As shown in Figure 19, the starting materials were for the second carbene N, N'-Dimethyl thiourea, and the third carbene 1,3-Diallyl-2-thiourea. In separate round bottom flasks, both compounds were allowed to reflux for 12 h along with 1-hexanol. For the second described carbene, 1,3,4,5-tetramethyl imidazole-2-(3H)-thione was obtained, and for the third described carbene, 1,3-Diisopropyl-4,5-dimethyl Imidazole-2-(3H)-Thione was isolated. Lastly, each thione was reduced with potassium metal under refluxing conditions in THF to produce the carbenes in moderate to good yields.

## 2.2 Synthesis and Characterization of New Heterometallic NiAl-Hydride Complexes

As discussed above, phosphines and carbene ligands were primarily employed given the strong sigma-donating nature of the ligands. In addition to exploring whether the coordination of the new donors would happen at Ni, Al, or both, we were intrigued to see if the hydride would continue to be in a shared designation. Below, are the results of the incorporation of four varying ligands: triphenylphosphine, bis-(diphenyl phosphino) methane, trimethyl phosphine, and diisopropyl-4,5-dimethyl-Imidazol-2-ylidene.

### 2.2.1 NiAl-(PPh<sub>3</sub>)<sub>2</sub> Complex

Triphenyl Phosphine (TPP) is a soft and bulky ligand that is a sigma donor that based on the Tolman map can bind 3-4 phosphines to a Ni.<sup>11, 12, 13</sup> In addition, TPP is one of the most common

ligands employed in catalysis given its air stability, price, and effectiveness in cross-coupling chemistry. TPP was sought due to the electronic similarities of the metalloligand phosphine which is also a triarylphosphine ligand.<sup>10</sup> Since this is possible, the stability of TPP may be effortlessly attached to a single metal.<sup>20, 37</sup> Triphenyl phosphine shows us that phosphine may increase the electron density of Ni since the bulkier the group the stronger or higher electron density it will add to the complex.

The addition of PPh<sub>3</sub> was carried out in two separate ways, from the addition of Ni(COD)<sub>2</sub> to LAIH and two equivalents of triphenylphosphine, as well as the addition of four equivalents of triphenylphosphine to NiAl<sub>2</sub> directly, balanced out with additional Ni(COD)<sub>2</sub> (Figures 20 and 21).

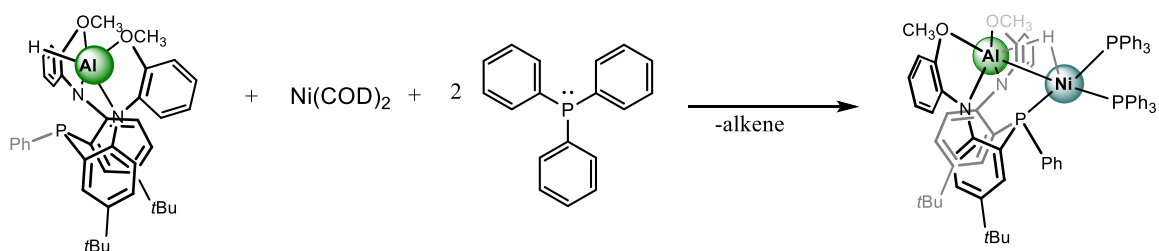


Figure 20: Reaction of LAIH + TPP.

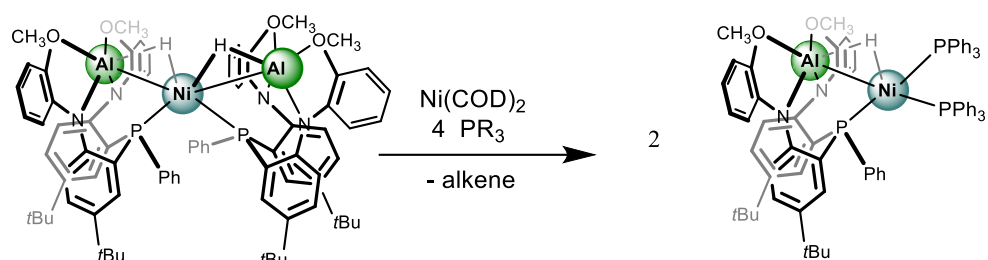


Figure 21: Reaction of  $\text{NiAl}_2 + \text{TPP}$ .

The requirement to titrate with an additional equivalent of Ni is due to synthesis of a heterobimetallic species from the heterotrimetallic  $\text{NiAl}_2$  compound. Intriguingly, the synthesis results in dissociation of a LAIH metalloligand indicating that the phosphine donors are likely better ligands than LAIH. Also, one of the metalloligands retains the bridged hydride between Al and Ni which is observed via NMR spectroscopy as well as single-crystal X-ray diffraction (SC-XRD) also reveals that there is a shortening of the Ni-Al bond length which may indicate that Al is accepting electron density more efficiently from Ni. This can be due to increased electron density from the  $\text{PPh}_3$  ligands in comparison to LAIH. The  $^{31}\text{P}\{^1\text{H}\}$  NMR spectrum presents as two different multiples with corresponding coupling constants as is expected for the bound  $\text{PPh}_3$  and LAIH moieties. This reactivity sparked substantial interest as a new methodology for accessing more of these rare motifs was determined. Examining the impact through the addition of varying ancillary ligands was then targeted. Below, the experimental for the synthesis and characterization of this compound is described. Including multinuclear NMR spectroscopy and single-crystal X-ray structure depictions.

Small scale synthesis: In a glovebox, using three different 20 mL scintillation vials were placed with LAIH (20 mg, 0.0311 mmol), Ni(COD)<sub>2</sub> (8.55 mg, 0.0311 mmol), and Triphenyl phosphine (16 mg, 0.0622 mmol). Using a whole pipette of C<sub>6</sub>D<sub>6</sub>, then it is added to the vial with LAIH. Once this is well dissolved, it is transferred to the vial with Triphenyl phosphine. Again, when this is well dissolved and integrated then it is transferred to the vial with the Ni(COD)<sub>2</sub>. The bright yellow solution displayed was then transformed into a burned orange solution. Once it is all incorporated, the small scale is transferred to a j-young tube with a Teflon-key cap. This j-young tube is taken out from the glovebox and placed in an oiled dish with a hot oil bath stirred for 45 min at 60 °C. After that, the J-young tube is allowed to cool down and then it is analyzed using an NMR. When the NMR is clean, then the j-young tube is taken inside the glovebox and all volatiles were then removed in vacuo and the crude material was triturated with n-pentane 3 x 1.5 mL. The crude solid was then extracted with diethyl ether and dried to afford 42.3 mg of Ni-Al-(PPh<sub>3</sub>)<sub>2</sub> in ~95% purity (87.62 % yield benzene, 6.82% ether, 5.54% pentane). <sup>1</sup>H NMR (400 MHz, C<sub>6</sub>D<sub>6</sub>, 298K): δ 7.56 (d, <sup>3</sup>J<sub>HH</sub> = 5.06 Hz, 2H, PhH) 7.36 (t, <sup>3</sup>J<sub>HH</sub> = 8.0 Hz, 12H, PhH), 7.25 (broad m, W<sub>1/2</sub> = 14.4 Hz, 2H, PhH), 6.94-6.88 (overlapping m, 21H, PhH), 6.69 (broad m, W<sub>1/2</sub> = 14.4 Hz, 4H, PhH), 6.46 (apparent t, <sup>3</sup>J<sub>HH</sub> = 8.1 Hz, 2H, PhH), 6.32 (broad m, W<sub>1/2</sub> = 12.3 Hz, 2H, PhH), 2.95 (broad s, 6H, OCH<sub>3</sub>), 1.14 (broad overlapping singlet, 18H, C(CH<sub>3</sub>)<sub>3</sub>), -1.78 (broad d, J<sub>HP</sub> W<sub>1/2</sub> = 53.3 Hz, 1H, Al-H-Ni). <sup>13</sup>C {<sup>1</sup>H} NMR (101 MHz, C<sub>6</sub>D<sub>6</sub>, 298 K) δ 140.34 (2<sup>nd</sup> order m, AXX'Y aryl-C), 137.53 (d, J<sub>CP</sub> = 5.4 Hz, aryl-C), 136.64 (overlapping s, aryl-C), 136.26 (dt, <sup>1</sup>J<sub>CP</sub> = 37.6 Hz, J<sub>CP</sub> = 3.5 Hz, aryl-C), 133.71 (2<sup>nd</sup> order multiplet AXXY'Y, aryl-C), 133.08 (d, J<sub>CP</sub> = 11.1 Hz, aryl-C), 129.54 (broad s, W<sub>1/2</sub> = 15.4 Hz, aryl-C), 128.24 (broad s, aryl-C), 127.95 (broad s, aryl-C), 127.71 (broad s, aryl-C), 127.47 (broad s, aryl-C), 127.26 (broad s, aryl-C), 126.94 (d, J<sub>CP</sub> = 9.29 Hz, aryl-C), 126.12 (s, aryl-C), 125.39 (s, aryl-C), 123.58 (broad

s,  $W_{1/2} = 24.8$  Hz, aryl-C), 122.38 (s, aryl-C), 120.69 (broad s,  $W_{1/2} = 181.5$  Hz, aryl-C), 120.25 (s, aryl-C), 115.20 (s,  $J_{CP} = 5.8$  Hz, aryl-C), 109.42 (broad s, aryl-C), 55.07 (s, OCH<sub>3</sub>), 33.83 (s, C(CH<sub>3</sub>)<sub>3</sub>), 31.30 (s, C(CH<sub>3</sub>)<sub>3</sub>), 28.03 (overlapping m, aryl-C). <sup>31</sup>P {<sup>1</sup>H} NMR (161.97 MHz, C<sub>6</sub>D<sub>6</sub>, 298 K)  $\delta$  29.23 (broad s,  $W_{1/2} = 57.59$  Hz, 2P, PPh<sub>3</sub>) -12.47 (t,  $^2J_{PP} = 11.2$  Hz, 1P, PPhAr). C<sub>76</sub>H<sub>74</sub>AlN<sub>2</sub>NiO<sub>2</sub>P<sub>3</sub> Theoretical: C % 74.45, H % 6.08, N % 2.28. Determined C % 74.47, H % 6.27, N % 2.04.

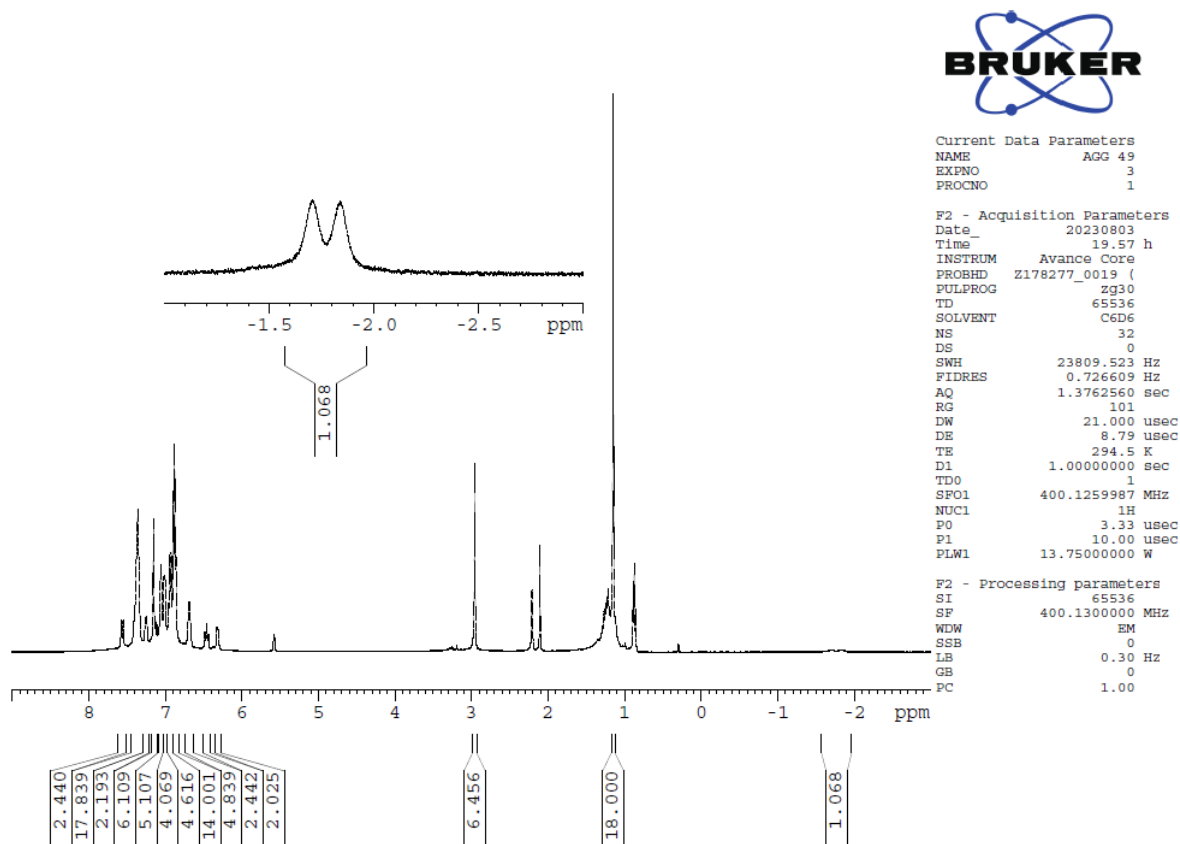


Figure 22: <sup>1</sup>H NMR spectrum of NiAl-(PPh<sub>3</sub>)<sub>2</sub> in C<sub>6</sub>D<sub>6</sub>.

The NMR data shows that the main groups in the complex which are the tert-butyls, methoxys, and phenyl groups, and lastly the Ni-H-Al showing at -1.78 ppm as a broad d. This peak is slightly more upfield than the reported NiAl<sub>2</sub> complex, compared to -1.50 ppm.<sup>16</sup> In addition, the triphenylphosphine is easier to identify by <sup>31</sup>P {<sup>1</sup>H} NMR, showing the peaks of a doublet around 29.23 ppm for PPh<sub>3</sub> and -12.47 ppm for PPhAr.

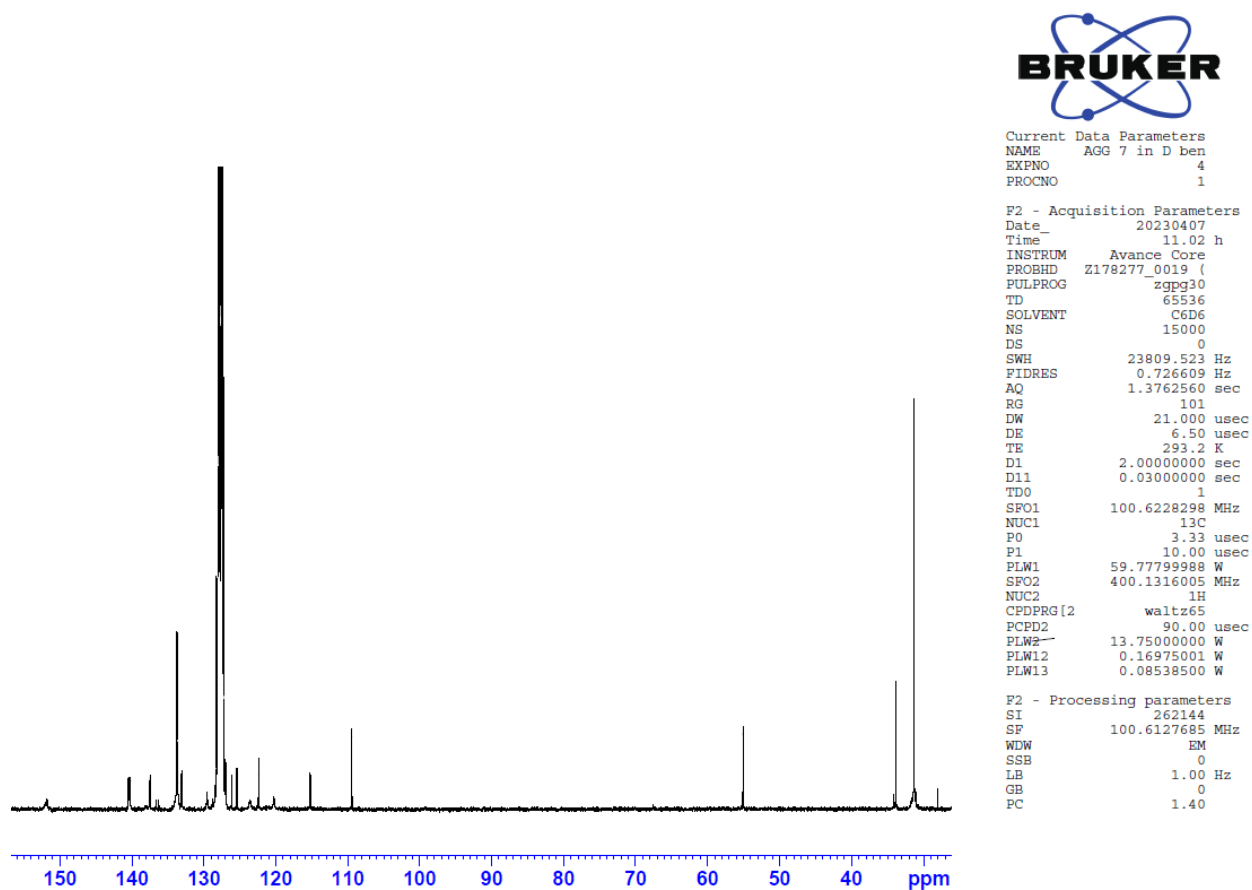


Figure 23: <sup>13</sup>C {<sup>1</sup>H} NMR spectrum of NiAl-(PPh<sub>3</sub>)<sub>2</sub> in C<sub>6</sub>D<sub>6</sub>.



Current Data Parameters  
NAME AGG 49  
EXPNO 4  
PROCNO 1

F2 - Acquisition Parameters  
Date\_ 20230803  
Time 20.05 h  
INSTRUM Avance Core  
PROBHD Z178277\_0019 (  
PULPROG zgpg30  
TD 65536  
SOLVENT C6D6  
NS 32  
DS 0  
SWH 65789.477 Hz  
FIDRES 2.007735 Hz  
AQ 0.4980736 sec  
RG 101  
DW 7.600 usec  
DE 6.50 usec  
TE 295.7 K  
D1 2.0000000 sec  
D11 0.0300000 sec  
TD0 1  
SFO1 161.9674942 MHz  
NUC1 31P  
P0 3.33 usec  
P1 10.00 usec  
PLW1 27.58300018 W  
SFO2 400.1316005 MHz  
NUC2 1H  
CPDPRG[2] waltz16  
PCPD2 90.00 usec  
PLW2 13.75000000 W  
PLW12 0.16975001 W  
PLW13 0.08538500 W

F2 - Processing parameters  
SI 32768  
SF 161.9755930 MHz  
WDW EM  
SSB 0  
LB 1.00 Hz  
GB 0  
PC 1.40

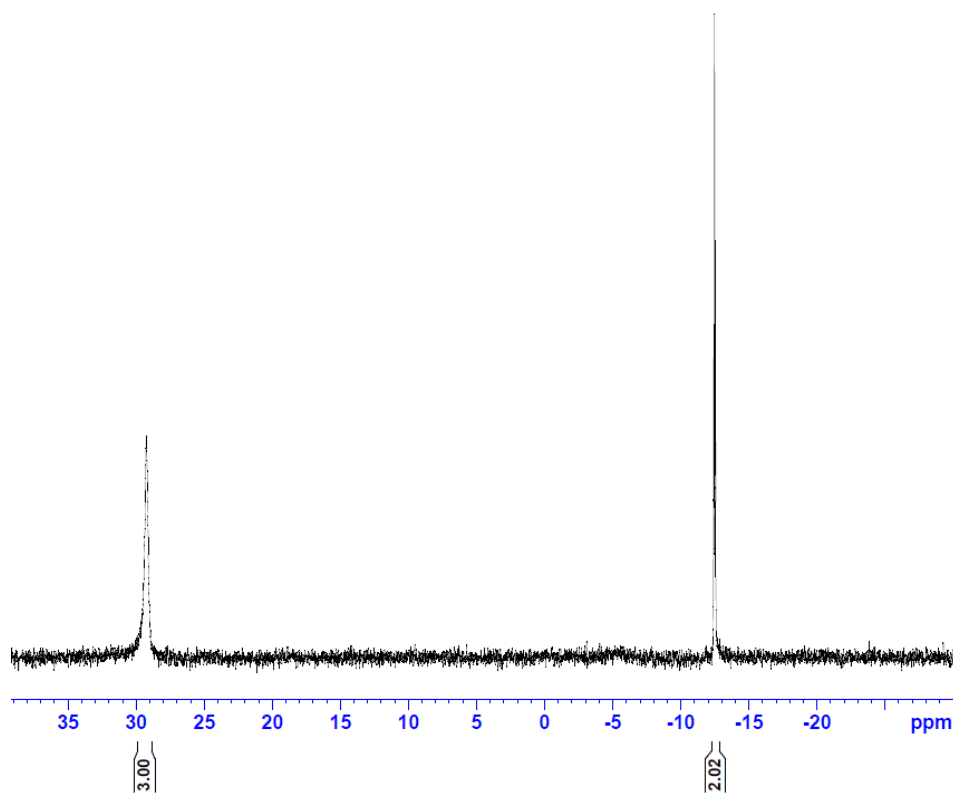


Figure 24:  $^{31}\text{P}\{^1\text{H}\}$  NMR spectrum of  $\text{NiAl}(\text{PPh}_3)_2$  in  $\text{C}_6\text{D}_6$ .

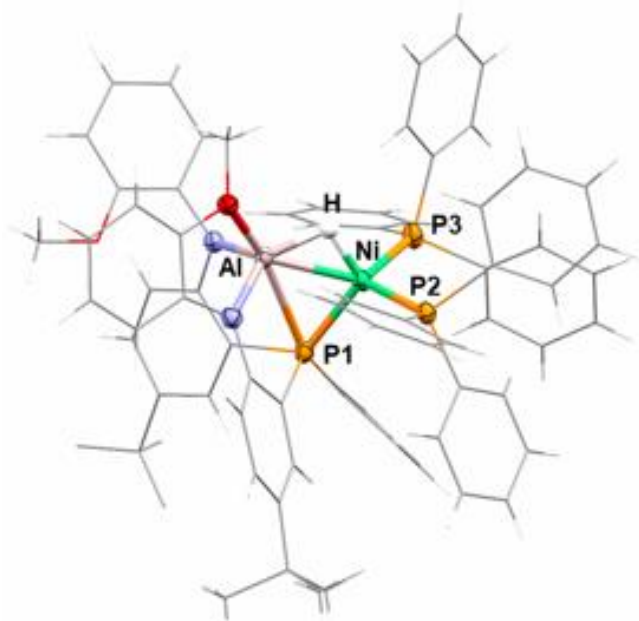


Figure 25: XRD crystal structure of **NiAl-(PPh<sub>3</sub>)<sub>2</sub>**.

Table 1: Properties of Bond Distances of NiAl-(PPh<sub>3</sub>)<sub>2</sub>.

NiAl-(PPh <sub>3</sub> ) <sub>2</sub>	Bond Distances Å
Ni-H	1.54(4)
Al-H	1.74(4)
Ni-Al	2.3222(16)
Ni-(P1)	2.1832(14)
Ni-(P2/P3)	2.2095(14)
	2.1915(16)

The crystal structure of NiAl-(PPh<sub>3</sub>)<sub>2</sub>, as shown in Figure 25 and Table 2, is composed of normal van der Waals' shortest bond distance is 1.54(4) Å which belongs to Ni-H. This is found to be far

smaller than the ranging of an optimized Ni-H bond distance which is 1.81-1.87 Å.<sup>60</sup> This was achievable since the triphenylphosphine donates its electron density to the Ni center. Then, Al-H is found to be 1.74(4) Å, which is longer than the expected Al-H bond distance previously reported to be 1.66-1.79 Å.<sup>9</sup> As one of the few complexes reported by Chen and colleagues the Ni-Al bond distance was found to be 2.35-2.41 Å, and the NiAl-(PPh<sub>3</sub>)<sub>2</sub> bond distance between Ni-Al was found to be 2.3222(16) Å.<sup>61</sup> For the Ni-P1 and Ni-(P2/P3) bond distances are between 2.18-2.20 Å which are also smaller than the expected of previously reported complexes which are around 2.28 Å.<sup>18</sup> The triphenylphosphine ligand brings together/assembles the overall complex variant to be closer, and the regioselectivity and electron density forces to be in close proximity.

### 2.2.2 NiAl-(dppm)<sub>2</sub> Complex

Inspired by the previous results and interested in utilizing a chelating ligand to see if coordination to both Ni and Al was achievable using Bis-(Diphenyl Phosphino) Methane (dppm). Dppm is a tertiary phosphine ligand that binds easily to a variety of transition metals in low oxidation state.<sup>43</sup> Since it plays a major role in stabilizing organometallic and hydride complexes, then it influences to isolate compounds for the major part in catalysis. Furthermore, given the vast literature shown to access dppm as a chelating ligand with both phosphines binding to one and two metals, exploring its coordination chemistry was of substantial interest. For dppm ability to either chelate or bridge coordination modes, this shows higher tendency to act as a monodentate or bridging bidentate ligand.<sup>17,25</sup> In addition, dppm has a similar, but more electron-rich profile when compared to PPh<sub>3</sub>, so exploring the impact of adjacent reaction to the

triphenylphosphine coordinated species was also of interest.<sup>46</sup> For all these reasons, dppm was chosen among phosphine ligands to be part of the list of ancillary ligands.

As shown in Figure 28, the reaction proceeded in the analogous manner as it did to the triphenylphosphine. No evidence of coordination between two metals or chelation is observed. However, interesting insights were still attained. For example, the hydride still shows a bridged nature between the Ni and Al center, however the chemical shift is now present at a resonance more consistent with Ni behavior. In addition, the Ni-Al bond distance is once again contracted which could again be due to the effect of a more donating ligand generating a more electron rich Ni center. The  $^3\text{P}\{^1\text{H}\}$  NMR spectrum of this species displays three peaks at room temperature which correspond to 1) the metalloligand phosphine 2) the bound dppm phosphorous centers, and 3) the unbound phosphorus centers. Similar to the triphenylphosphine coordination compounds, the geometry at Ni is tetrahedral with respect to the phosphine ligands and the Al-H donor. Given the pattern of reactivity, that there is a favorable generation of heterobimetallic complexes, more focus was emphasized on monitoring the impact of adding more electron-rich ligands than exploring coordination to Al. As such, sigma donors of increasing strength was targeted. Below, the experimental for the synthesis and characterization of this compound is described. Including multinuclear NMR spectroscopy and single-crystal X-ray structure depictions.

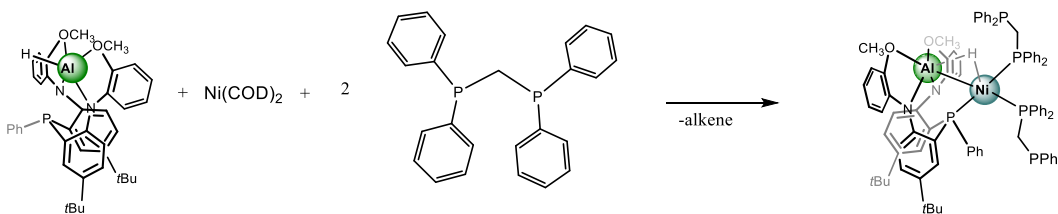


Figure 26: Reaction of LAlH + dppm.

Small scale synthesis: In a glovebox, using three different 20 mL scintillation vial were placed with LAIH (20 mg, 0.0311 mmol), Ni(COD)<sub>2</sub> (8.55 mg, 0.0311 mmol) and Bis-(diphenyl phosphino) methane (16 mg, 0.0622 mmol). Using a whole pipette of C<sub>6</sub>D<sub>6</sub>, then it is added to the vial with LAIH. Once this is well dissolved, it is transferred to the vial with Bis-(diphenyl phosphino) methane. Again, when this is well dissolved and integrated then it is transferred to the vial with the Ni(COD)<sub>2</sub>. The bright yellow solution displayed was then transformed into a burned orange solution. Once it is all incorporated, the small scale is transferred to a j-young tube with a Teflon-key cap. This J-young tube is taken out from the glovebox and placed in an oil dish with a hot oil bath stirred for 45 min at 60 °C. After that, the J-young tube is allowed to cool down and then it is analyzed using an NMR. When the NMR is clean, then the J-young tube is taken inside the glovebox and all volatiles were then removed in vacuo and the crude material was triturated with n-pentane 3 x 1.5 mL. The crude solid was then extracted with diethyl ether and dried to afford 40 mg of Ni-Al-(CH<sub>2</sub>(PPh<sub>2</sub>)<sub>2</sub>)<sub>2</sub> in ~90% purity (23.35 % yield benzene, 56.64% ether, and 20% pentane). <sup>1</sup>H NMR (400 MHz, C<sub>6</sub>D<sub>6</sub>, 298K): δ 7.62 (broad d, <sup>3</sup>J<sub>HH</sub> = 9.26 Hz, 2H, PhH), 7.53 (broad d, <sup>3</sup>J<sub>HH</sub> = 12.94 Hz, 2H, PhH), 7.29-6.65 (overlapping m, PPh), 6.44 (t, <sup>3</sup>J<sub>HH</sub> = 8.5 Hz, 2H, PhH), 6.35 (d, <sup>3</sup>J<sub>HH</sub> = 7.8 Hz, 2H, PhH), 3.17 (<sup>2</sup>J<sub>HP</sub> = 41.5 Hz, <sup>2</sup>J<sub>HP</sub> = 14.5 Hz, 4H, PCH<sub>2</sub>P), 3.08 (s, 6H, OCH<sub>3</sub>) 1.13 (s, 18H, (C(CH<sub>3</sub>)<sub>3</sub>) -2.14 (apparent d, J<sub>HP</sub> = 54.5 Hz W<sub>1/2</sub> = 62.09 Hz, Ni-H-Al). <sup>13</sup>C {<sup>1</sup>H} NMR (101 MHz, C<sub>6</sub>D<sub>6</sub>, 298 K) δ 152.17 (overlapping broad m, aryl-C), 141.24 (2<sup>nd</sup> order multiplet, aryl-C), 139.36 (2<sup>nd</sup> order multiplet, aryl-C), 138.54 (broad m, aryl-C), 137.53 (broad m, W<sub>1/2</sub> = 13.4 Hz, aryl-C), 137.02 (dt, J<sub>CP</sub> = 38.2 Hz, J<sub>CP</sub> = 4.7 Hz, aryl-C) 133.25, (broad d, J<sub>CP</sub> = 11.7 Hz, aryl-C), 132.81 (dd, J<sub>CP</sub> = 20.2 Hz, J<sub>CP</sub> = 9.50 Hz, aryl-C), 132.72 (doublet of m, J<sub>CP</sub> = 95.2 Hz, aryl-C), 132.50 (d, J<sub>CP</sub> = 12.7 Hz, aryl-C), 129.58 (broad m, W<sub>1/2</sub> = 19.6 Hz, aryl-C), 128.22 (s, aryl-C), 127.93-127.45 (overlapping m,

aryl-C), 126.95 (d,  $J_{CP} = 8.7$  Hz, aryl-C), 125.93 (s, aryl-C), 125.41 (s, aryl-C), 123.53 (broad s,  $W_{1/2} = 64.4$  Hz, aryl-C), 122.47 (s, aryl-C), 120.19 (broad s,  $W_{1/2} = 63.5$  Hz, aryl-C), 115.29 (d,  $J_{CP} = 5.6$  Hz, aryl-C), 109.38 (s, aryl-C), 55.20 (s, OCH<sub>3</sub>), 33.80 (s, C(CH<sub>3</sub>)<sub>3</sub>), 32.86 (2<sup>nd</sup> order multiplet AXX'YZ, Ni-Ph<sub>2</sub>P-CH<sub>2</sub>-PPh<sub>2</sub>), 31.28 (s, C(CH<sub>3</sub>)<sub>3</sub>), -0.34 (broad s, aryl-C). <sup>31</sup>P {<sup>1</sup>H} NMR (161.97 MHz, C<sub>6</sub>D<sub>6</sub>, 298 K)  $\delta$  20.77 (broad s,  $W_{1/2} = 188.50$  Hz, 2P, M-PPh<sub>2</sub>CH<sub>2</sub>PPh<sub>2</sub>), 5.07 (s, impurity), -12.29 (t,  $^2J_{PP} = 12.0$  Hz, 1P, PPhAr), -22.34 (s, impurity), -26.95 (apparent d,  $^2J_{PP} = 60.05$  Hz, 2P, M-PPh<sub>2</sub>CH<sub>2</sub>PPh<sub>2</sub>). C<sub>91</sub>H<sub>91</sub>AlN<sub>2</sub>NiO<sub>2</sub>P<sub>5</sub> Theoretical: C % 73.59, H % 6.18, N % 1.82. Determined C % 73.14, H % 6.21, N % 1.66.

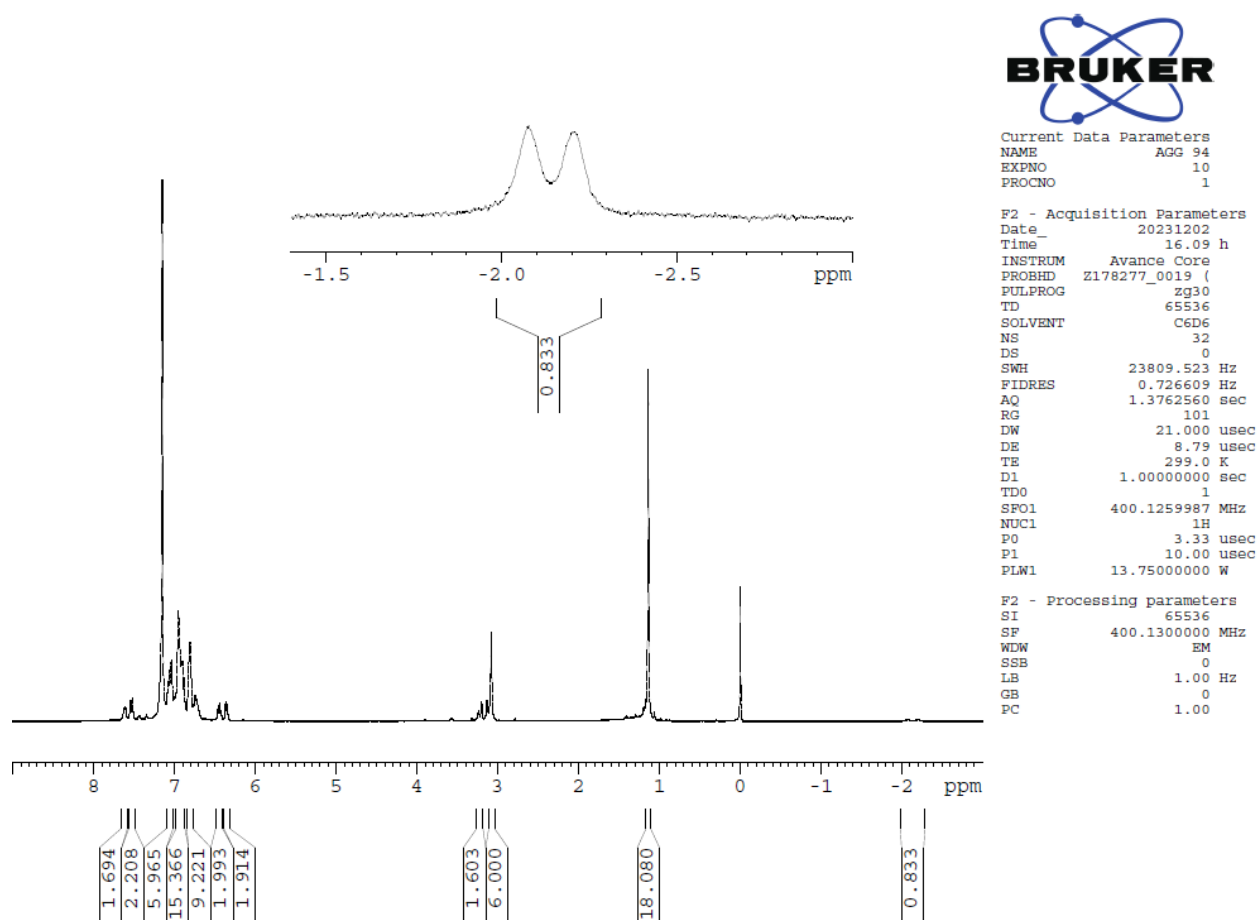


Figure 27: <sup>1</sup>H NMR spectrum of NiAl-(dppm)<sub>2</sub> in C<sub>6</sub>D<sub>6</sub>.

The NMR studies show that the main groups in the complex which are the tert-butyls, methoxys, and phenyl groups, and lastly the Ni-H-Al showing at -2.14 ppm as a broad d. This peak is slightly more upfield than the reported NiAl<sub>2</sub> and NiAl-(PPh<sub>3</sub>)<sub>2</sub> complexes, compared to -1.50 and -1.78 ppm.<sup>16</sup> In addition, the triphenylphosphine is easier to identify by <sup>31</sup>P {<sup>1</sup>H} NMR, showing the peaks of a broad s around 20.77 ppm for M-PPh<sub>2</sub>CH<sub>2</sub>PPh<sub>2</sub>, a t around -12.29 ppm for PPhAr, and a broad d around -26.95 ppm for M-PPh<sub>2</sub>CH<sub>2</sub>PPh<sub>2</sub>. The other two peaks on the <sup>31</sup>P {<sup>1</sup>H} NMR, at 5.07 ppm and -22.34 ppm are impurities.

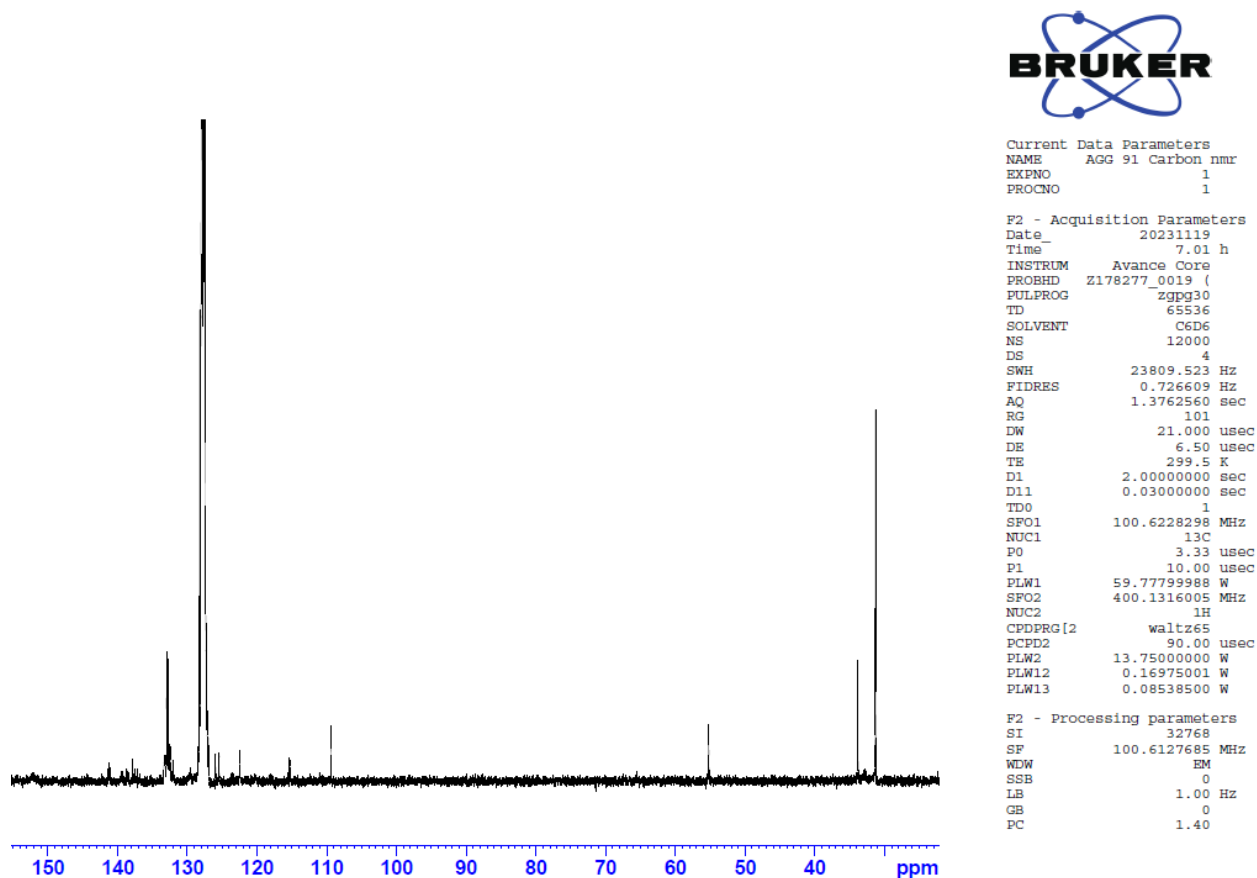
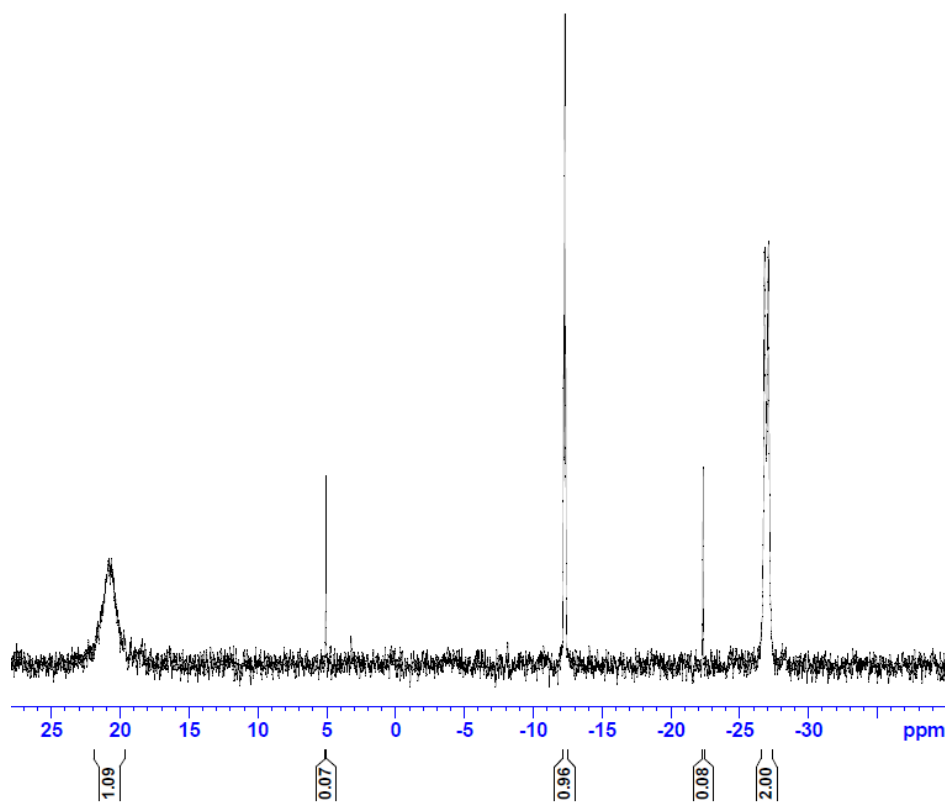


Figure 28: <sup>13</sup>C {<sup>1</sup>H} NMR spectrum of NiAl-(dppm)<sub>2</sub> in C<sub>6</sub>D<sub>6</sub>.



```
Current Data Parameters
NAME          AGG 94
EXPNO         11
PROCNO        1

F2 - Acquisition Parameters
Date_         20231202
Time          16.12 h
INSTRUM       Avance Core
PROBHD        Z178277_0019 (
PULPROG       zgpg30
TD            65536
SOLVENT       C6D6
NS            32
DS            0
SWH           65789.477 Hz
FIDRES        2.007735 Hz
AQ            0.4980736 sec
RG            101
DW            7.600 usec
DE            6.50 usec
TE            299.3 K
D1            2.0000000 sec
D11           0.03000000 sec
TD0           1
SFO1          161.9674942 MHz
NUC1          31P
P0            3.33 usec
P1            10.00 usec
PLW1          27.58300018 W
SFO2          400.1316005 MHz
NUC2          1H
CPDPRG[2]    waltz16
PCPD2         90.00 usec
PLW2          13.75000000 W
PLW12         0.16975001 W
PLW13         0.08538500 W

F2 - Processing parameters
SI            32768
SF            161.9755930 MHz
WDW           EM
SSB           0
LB            2.50 Hz
GB            0
PC            1.40
```

Figure 29:  $^{31}\text{P}\{^1\text{H}\}$  NMR spectrum of  $\text{Ni-Al}(\text{dppm})_2$  in  $\text{C}_6\text{D}_6$ .

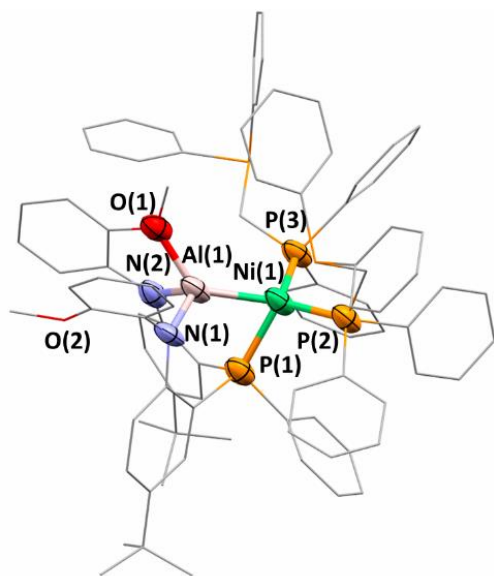


Figure 30: XRD crystal structure of  $\text{NiAl}(\text{dppm})_2$ .

Table 2: Properties of Bond Distances of NiAl-(dppm)<sub>2</sub>.

NiAl-(dppm) <sub>2</sub>	Bond distance Å
Ni-H	1.43(13)
	1.47(13)
Al-H	1.55(12)
	1.72(12)
Ni-Al	2.269 (4)
	2.276(4)
Ni-(P1)	2.169 (2)
	2.175(2)
Ni-(P2/P3)	2.171(2)
	2.186(2)

The crystal structure of NiAl-(dppm)<sub>2</sub>, as shown in Figure 30 and Table 3, is composed of normal van der Waals' shortest bond distance is 1.43-1.47(4) Å which belongs to Ni-H. This is found to be far smaller than the range from NiAl-(PPh<sub>3</sub>)<sub>2</sub> and NiAl<sub>2</sub> bond distance which is 1.54(4)-1.60(3)Å. This was achievable since the bis(diphenyl phosphino) methane donates its electron density to the Ni center. Then, Al-H is found to be 1.55(12)-1.72(12) Å, which is smaller than the expected Al-H bond distance previously reported of NiAl-(PPh<sub>3</sub>)<sub>2</sub>. Å, The NiAl-(dppm)<sub>2</sub> bond distance between Ni-Al was found to be 2.269(4)-2.276(4) Å, which is also smaller than the Ni-Al bond distance of NiAl-(PPh<sub>3</sub>)<sub>2</sub> and NiAl<sub>2</sub> was found to be 2.3222(16)-2.3683(7) Å. For the Ni-P1 and Ni-(P2/P3) bond distances are between 2.169(2)-2.186(2) Å which are also

smaller than the expected of previously reported complexes which are around 2.28 Å.<sup>18</sup> The Bis(diphenyl phosphino) methane ligand brings together/assembles the overall complex variant to be closer than the triphenylphosphine variant, and the regioselectivity and electron density forces to be in close proximity.

### 2.2.3 NiAl-(PMe<sub>3</sub>)<sub>2</sub> Complex

Trimethyl Phosphine is a smaller and strongly donating ligand compared to both dppm and triphenylphosphine.<sup>53,55</sup> This is in part due to the electron-donating methyl groups rather than the phenyl groups. To monitor the effect of the hydride and the Ni-Al interaction, trimethylphosphine was utilized in the synthesis of heterometallic species. Interestingly, the synthesis of NiAl-(PMe<sub>3</sub>)<sub>2</sub> takes longer to proceed in comparison to both PPh<sub>3</sub> and dppm variants discussed above. At first, the synthesis of this complex was performed following the same methodology as NiAl-(PPh<sub>3</sub>)<sub>2</sub>, but since trimethyl phosphine takes longer to react and gives less yield, then the methodology was modified. This reaction is shown in Figure 34. Once the complex was isolated, intriguing data was acquired. The hydride shift in the <sup>1</sup>H NMR spectra is observed at a very upfield chemical shift, which may indicate more Ni-H character. The <sup>31</sup>P {<sup>1</sup>H} NMR spectra is observed as a triplet and doublet, corresponding to the metalloligand, and the trimethyl phosphine moieties, respectively. The single-crystal XRD studies showed further shortening of the Ni-Al interaction which was expected. Overall, these three complexes demonstrate an intriguing trend in the changes of the electronic distribution of the subunits. Further perturbation with even stronger sigma donors was then sought. Below, the experimental for the synthesis and characterization of this compound is described. Including multinuclear NMR spectroscopy and single-crystal X-ray structure depictions.

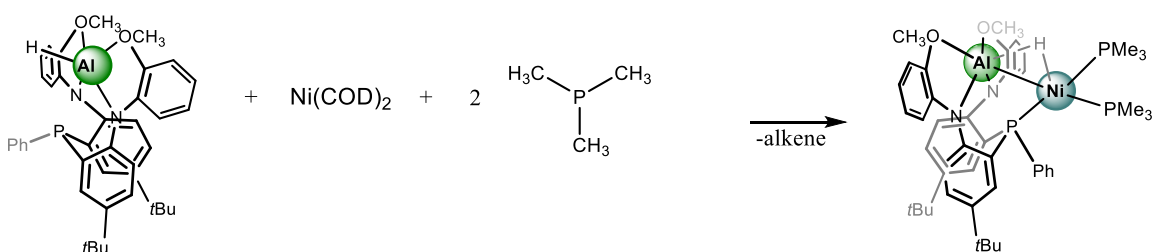


Figure 31: Reaction of LAIH + TMP.

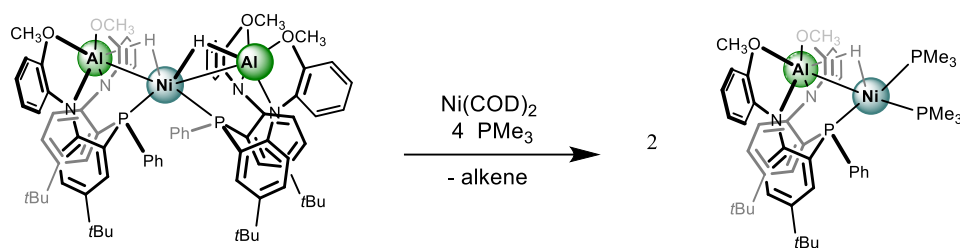


Figure 32: Reaction of NiAl<sub>2</sub> + TMP.

Small scale synthesis: In a glovebox, three different 20 mL scintillation vials were placed with LAIH (20 mg, 0.0311 mmol), Ni(COD)<sub>2</sub> (8.55 mg, 0.0311 mmol), and Trimethyl phosphine (16 mg, 0.0622 mmol). Using a whole pipette of C<sub>6</sub>D<sub>6</sub>, then it is added to the vial with LAIH. Once this is well dissolved, it is transferred to the vial with Trimethyl phosphine. Again, when this is well dissolved and integrated then it is transferred to the vial with the Ni(COD)<sub>2</sub>. The bright yellow solution displayed was then transformed into a burned orange solution. Once that it is all incorporated, the small scale is transferred to a J-young tube with a Teflon-key cap. This J-young tube is taken out from the glovebox and placed in an oil dish with a hot oil bath stirred for 45 min at 60 °C. After that, the J-young tube is allowed to cool down and then it is analyzed using

an NMR. When the NMR is clean, then the j-young tube is taken inside the glovebox and all volatiles were then removed in vacuo and the crude material was triturated with n-pentane 3 x 1.5 mL. The crude solid was then extracted with diethyl ether and dried to afford 39.2 mg of NiAl-(PMe<sub>3</sub>)<sub>2</sub> in ~88% purity (42.81% in benzene, 38.55% in ether, 18.64% in pentane). <sup>1</sup>H NMR (400 MHz, C<sub>6</sub>D<sub>6</sub>, 298K) δ 7.91 (apparent t, <sup>3</sup>J<sub>HH</sub> = 8.9 Hz, 4H, PhH), 7.31 (d, <sup>3</sup>J<sub>HH</sub> = 8.2 Hz, 2H, PhH), 7.25 (apparent t, <sup>3</sup>J<sub>HH</sub> = 8.8 Hz, 2H, PhH), 7.08-7.02 (overlapping multiplets, 5H, PhH), 6.76 (apparent t, <sup>3</sup>J<sub>HH</sub> = 7.4 Hz, 2H, PhH), 6.68 (apparent t, <sup>3</sup>J<sub>HH</sub> = 7.4 Hz, 2H, PhH), 6.35 (d, <sup>3</sup>J<sub>HH</sub> = 7.9 Hz, 2H, PhH), 3.06 (s, 6H, OCH<sub>3</sub>), 1.22 (s, 18H, C(CH<sub>3</sub>)<sub>3</sub>), 0.95 (s, 18H, P(CH<sub>3</sub>)<sub>3</sub>), -3.28 (apparent d, J<sub>HP</sub> = 54.5 Hz, W<sub>1/2</sub> = 96.9 Hz, 1H, Al-H-Ni). <sup>13</sup>C {<sup>1</sup>H} NMR (101 MHz, C<sub>6</sub>D<sub>6</sub>, 298 K) δ 152.40 (d, <sup>2</sup>J<sub>CP</sub> = 14.5 Hz, aryl-C), 151.99 (s, aryl), 139.78 (dt, <sup>1</sup>J<sub>CP</sub> = 36.3 Hz, <sup>2</sup>J<sub>CP</sub> = 5.6 Hz, aryl-C), 138.33 (broad s, aryl-C), 137.39 (d, <sup>2</sup>J<sub>CP</sub> = 5.3 Hz, aryl-C), 132.44 (d, <sup>2</sup>J<sub>CP</sub> = 11.6 Hz, aryl-C), 129.06 (s, aryl-C), 126.91 (d, <sup>2</sup>J<sub>CP</sub> = 8.5 Hz, aryl-C), 126.42 (s, aryl-C), 125.41 (s, aryl-C), 123.01 (broad s, aryl-C), 122.54 (broad s, aryl-C), 121.88 (dt, <sup>1</sup>J<sub>CP</sub> = 44.1 Hz, <sup>2</sup>J<sub>CP</sub> = 9.1 Hz, aryl-C), 119.72 (broad s, aryl-C), 115.67 (d, <sup>2</sup>J<sub>CP</sub> = 6.0 Hz, aryl-C), 110.13 (s, aryl-C), 65.55 (broad s, aryl-C), 55.21 (s, OCH<sub>3</sub>), 51.52 (broad s, aryl-C), 33.84 (s, C(CH<sub>3</sub>)<sub>3</sub>), 31.36 (s, C(CH<sub>3</sub>)<sub>3</sub>), 21.91 (dt, <sup>1</sup>J<sub>CP</sub> = 11.1 Hz, <sup>2</sup>J<sub>CP</sub> = 4.5 Hz, P(CH<sub>3</sub>)<sub>3</sub>). <sup>31</sup>P {<sup>1</sup>H} NMR (161.97 MHz, C<sub>6</sub>D<sub>6</sub>, 298 K) δ -9.2 (t, <sup>2</sup>J<sub>PP</sub> = 9.1 Hz 1P, PPhAr), -21.11 (d, <sup>2</sup>J<sub>PP</sub> = 9.1 Hz 2P, PMe<sub>3</sub>) C<sub>46</sub>H<sub>62</sub>AlN<sub>2</sub>NiO<sub>2</sub>P<sub>3</sub> Theoretical: C % 64.73, H % 7.32, N % 3.28. Determined C % 62.59, H % 7.38, N % 3.03.

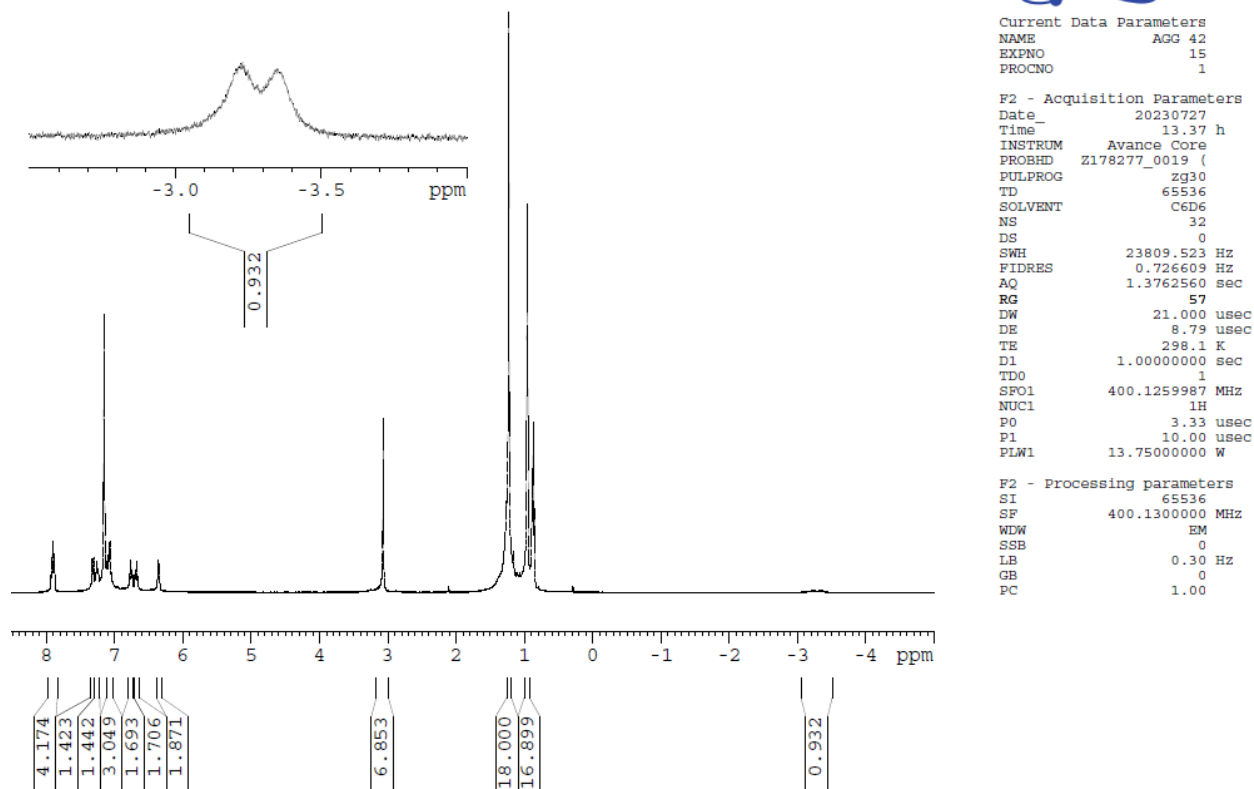


Figure 33:  $^1\text{H}$  NMR spectrum of  $\text{NiAl}(\text{PMe}_3)_2$  in  $\text{C}_6\text{D}_6$ .

The NMR data shows that the main groups in the complex which are the tert-butyls, methoxys, and phenyl groups, and lastly the Ni-H-Al showing at -3.28 ppm as a broad d. This peak is slightly more upfield than the reported  $\text{NiAl}_2$ ,  $\text{NiAl}(\text{PPh}_3)_2$ , and  $\text{NiAl}(\text{dppm})_2$  complexes, compared to -1.50 ppm, -1.78 ppm, and -2.14 ppm.<sup>16</sup> In addition, the trimethylphosphine is easier to identify by  $^{31}\text{P}\{^1\text{H}\}$  NMR, showing the peaks of a t around -9.2 ppm for  $\text{PPhAr}$  and a d around -21.11 ppm for  $\text{PMe}_3$ .

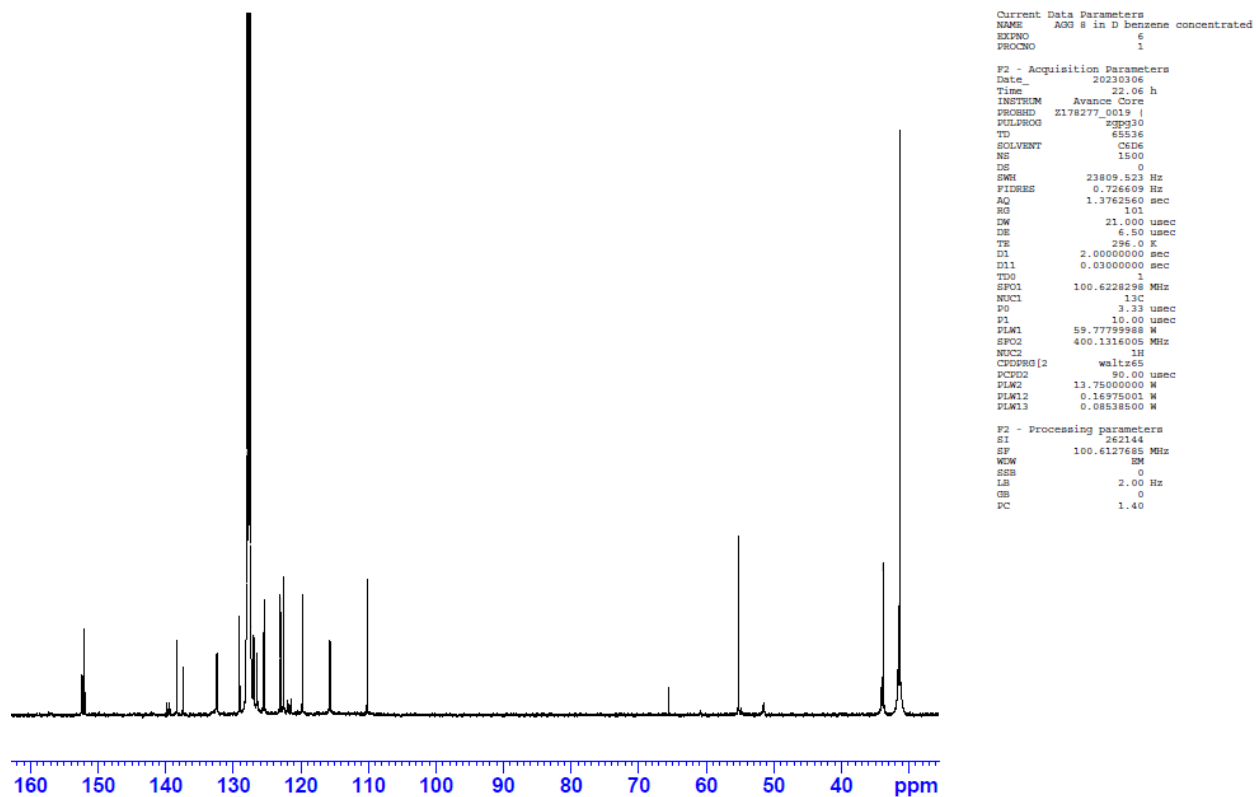


Figure 34:  $^{13}\text{C}\{^1\text{H}\}$  NMR spectrum of  $\text{NiAl}(\text{PMe}_3)_2$  in  $\text{C}_6\text{D}_6$ .



Current Data Parameters  
NAME AGG 8  
EXPNO 16  
PROCNO 1

F2 - Acquisition Parameters  
Date\_ 20230330  
Time 12.44 h  
INSTRUM Avance Core  
PROBHD z178277\_0019 (zpgp30)  
PULPROG zgpg30  
TD 65536  
SOLVENT C6D6  
NS 32  
DS 0  
SWH 65789.477 Hz  
FIDRES 2.007735 Hz  
AQ 0.4980736 sec  
RG 101  
DW 7.600 usec  
DE 6.50 usec  
TE 298.1 K  
D1 2.00000000 sec  
D11 0.03000000 sec  
TD0 1  
SFO1 161.9674942 MHz  
NUC1 31P  
P0 3.33 usec  
P1 10.00 usec  
PLW1 27.58300018 W  
SFO2 400.1316005 MHz  
NUC2 1H  
CPDPRG[2] waltz16  
PCPD2 90.00 usec  
PLW2 13.75000000 W  
PLW12 0.16975001 W  
PLW13 0.08538500 W

F2 - Processing parameters  
SI 262144  
SF 161.9755930 MHz  
WDW EM  
SSB 0  
LB 3.00 Hz  
GB 0  
PC 1.40

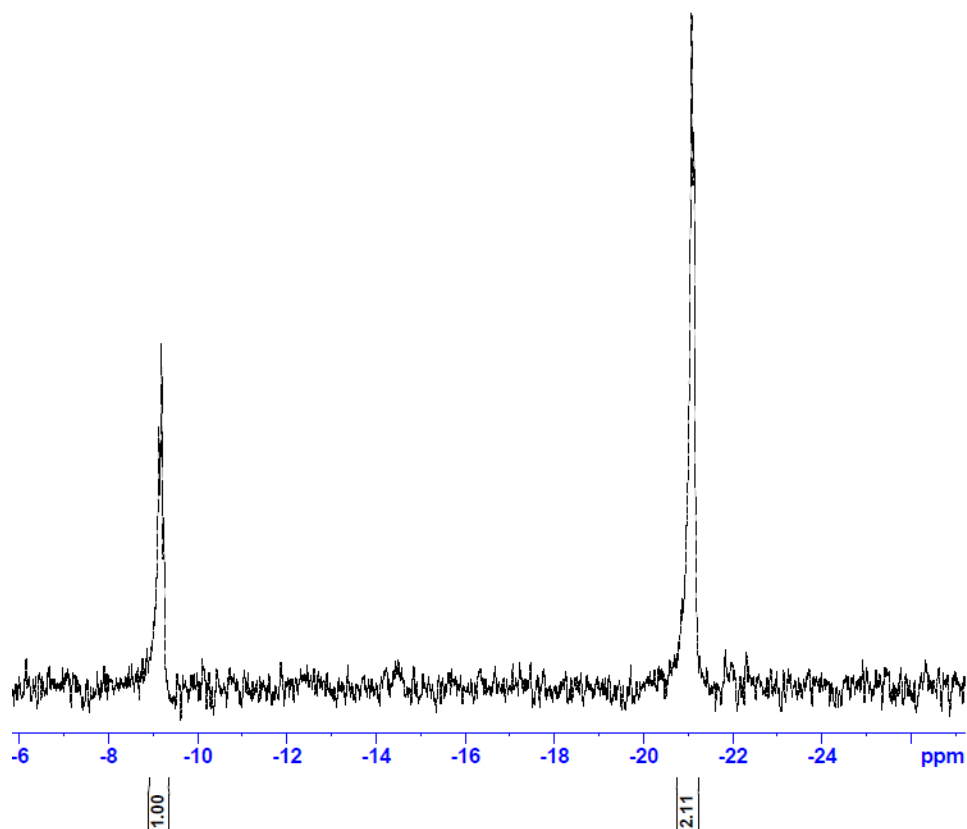


Figure 35:  $^{31}\text{P}\{^1\text{H}\}$  NMR spectrum of  $\text{NiAl}(\text{PMe}_3)_2$  in  $\text{C}_6\text{D}_6$ .

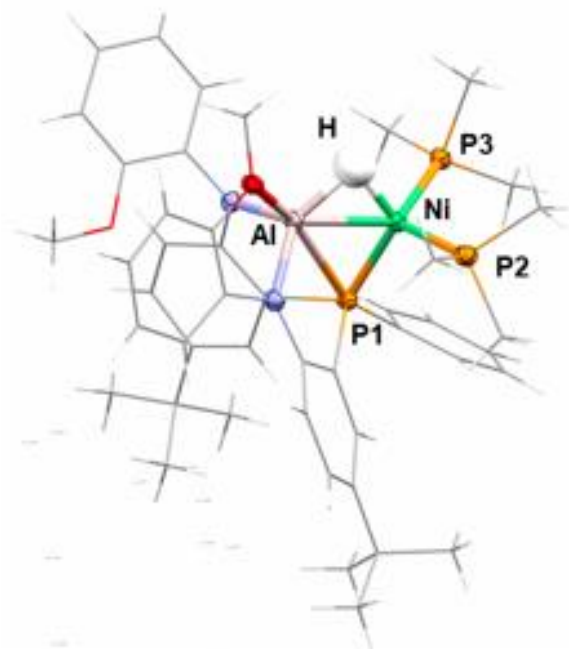


Figure 36: XRD crystal structure of  $\text{NiAl}(\text{PMe}_3)_2$ .

Table 3: Properties of Bond Distance of  $\text{NiAl}(\text{PMe}_3)_2$ .

$\text{NiAl}(\text{PMe}_3)_2$	Bond Distance Å
Ni-H	1.61(4)
	1.67(4)
Al-H	1.68(4)
	1.71(4)
Ni-Al	2.2503(7)
	2.2613(7)
Ni-(P1)	2.1410(6)
	2.1449(6)
Ni-(P2/P3)	2.1570(7)
	2.1612(7)
	2.1674(7)
	2.1706(7)

The crystal structure of NiAl-(PMe<sub>3</sub>)<sub>2</sub>, as shown in Figure 36 and Table 4, is composed of normal van der Waals' shortest bond distance is 1.61-1.67(4) Å which belongs to Ni-H. This is found to be far smaller than the range for NiAl-(dppm)<sub>2</sub> which is 1.43-1.47(13) and bigger for NiAl-(PPh<sub>3</sub>)<sub>2</sub> and NiAl<sub>2</sub> bond distance which is 1.54(4)-1.60(3)Å. This was achievable since the trimethyl phosphine donates its electron density to the Ni center. Then, Al-H is found to be 1.68(4)-1.71(4) Å, which is bigger than NiAl-(dppm)<sub>2</sub> which is 1.55-1.72(12) Å and smaller than the expected Al-H bond distance previously reported of NiAl-(PPh<sub>3</sub>)<sub>2</sub>. The NiAl-(PMe<sub>3</sub>)<sub>2</sub> bond distance between Ni-Al was found to be 2.2503-2.2613(7) Å, which is smaller than the Ni-Al bond distance compared to the NiAl-(dppm)<sub>2</sub>, NiAl-(PPh<sub>3</sub>)<sub>2</sub>, and NiAl<sub>2</sub> was found to be 2.269-2.3683(7) Å. For the Ni-P1 and Ni-(P2/P3) bond distances are between 2.1410(6)-2.1674(7) Å which are also smaller than the expected of previously reported complexes which are around 2.28 Å.<sup>18</sup> The trimethyl phosphine ligand brings together and assembles the overall complex variant to be closer than the triphenylphosphine variant, and the regioselectivity and electron density forces it to be in close proximity.

#### 2.2.4 Anionic Hydride Complex

The only one of the three carbenes that work and proceed to yield a product is Diisopropyl-4,5-dimethyl-Imidazol-2-ylidene (NHC-IPr). NHC-IPr is considered a strong organic base.<sup>15,35,44,63</sup> For this reason, it works, or it mainly employs methyl abstraction. The synthesis of anionic hydride was somewhat surprising but intriguing. It showed that the Al-H-Ni species can be stabilized at a negative charge. The synthesis of the anionic hydride uses NiAl-(PMe<sub>3</sub>)<sub>2</sub> as the precursor as the NiAl<sub>2</sub> species produced different reactivity. Starting with this complex allowed the methyl abstraction to occur from one of the methoxy's from the original structure. Interested

in the impact of aspects such as charge and ancillary ligands of different strength catalysis with the varying complexes using quinoline, H-BPin, and heterometallics, and was explored and is discussed later. The anionic hydride was again characterized by multinuclear NMR and single-crystal XRD. The NMR studies show that the species is desymmetrized and has three phosphine resonances and a hydride appearing upfield of -4.07 ppm. The solid-state structure shows an elongation of the Ni-Al bond which is likely due to the increased negative charge. Below, the experimental for the synthesis and characterization of this compound is described. Including multinuclear NMR spectroscopy and single-crystal X-ray structure depictions

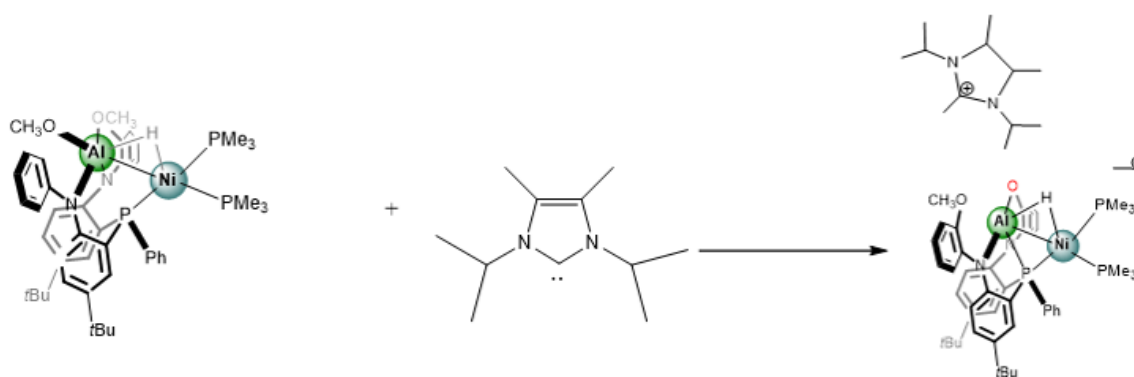


Figure 37: Reaction of NiAl-(PMe<sub>3</sub>)<sub>2</sub> and NHC-IPr.

Small-scale synthesis: In a glovebox, three different 20 mL scintillation vials were placed with NiAl-(PMe<sub>3</sub>)<sub>2</sub> (20 mg, 0.0311 mmol), and Diisopropyl-4,5-dimethyl-Imidazol-2-ylidene (16 mg, 0.0622 mmol). Using a whole pipette of C<sub>6</sub>D<sub>6</sub>, when this is well dissolved and integrated then it was allowed to react for half an hour. The bright yellow solution displayed was then transformed into a bright orange solution. Once that it is all incorporated, the small scale is transferred to a J-young tube with a Teflon-key cap. This J-young tube is taken out from the glovebox and placed in an oil dish with a hot oil bath stirred for 45 min at 60 °C. After that, the J-young tube is

allowed to cool down and then it is analyzed using an NMR. When the NMR is clean, then the j-  
 young tube is taken inside the glovebox and all volatiles are then removed in vacuo and the  
 crude material was triturated with n-pentane 3 x 1.5 mL. The crude solid was then extracted with  
 diethyl ether and dried to afford 34.5 mg of NiAl-(PMe<sub>3</sub>)<sub>2</sub>-NHC-IPr(3) in ~96% purity. <sup>1</sup>H NMR  
 (400 MHz, C<sub>4</sub>D<sub>8</sub>O, 298K): δ 7.72-7.64 (overlapping m, 3H, PhH), 7.54 (dd, <sup>3</sup>J<sub>HH</sub> = 6.1 Hz, <sup>3</sup>J<sub>HH</sub>  
 = 8.2 Hz, 1H, PhH), 7.36 (apparent t, <sup>3</sup>J<sub>HH</sub> = 6.2 Hz, 1H, PhH), 7.22 (apparent t, <sup>3</sup>J<sub>HH</sub> = 7.2 Hz,  
 2H, PhH), 7.17 (apparent t, <sup>3</sup>J<sub>HH</sub> = 7.3 Hz, 1H, PhH), 7.08 (d, <sup>3</sup>J<sub>HH</sub> = 7.1 Hz, 1H, PhH), 6.95  
 (aparent t, <sup>3</sup>J<sub>HH</sub> = 10.7 Hz, 2H, PhH), 6.88 (apparent t, <sup>3</sup>J<sub>HH</sub> = 7.5 Hz, 1H, PhH), 6.76-6.64  
 (overlapping multiplets, 3H, PhH), 6.43 (d, <sup>3</sup>J<sub>HH</sub> = 7.2 Hz, PhH), 6.38 (t, <sup>3</sup>J<sub>HH</sub> = 7.3 Hz, PhH),  
 6.06 (apparent t, <sup>3</sup>J<sub>HH</sub> = 7.2 Hz, 1H, PhH), 5.93 (apparent t, <sup>3</sup>J<sub>HH</sub> = 7.2 Hz, 1H, PhH), 4.31 (sep,  
<sup>3</sup>J<sub>HH</sub> = 7.2 Hz, 2H, CH(CH<sub>3</sub>)<sub>2</sub>), 3.48 (s, 3H, OCH<sub>3</sub>), 2.06 (overlapping s, 9H, imidazolium CH<sub>3</sub>),  
 1.25 (d, <sup>3</sup>J<sub>HH</sub> = 7.2 Hz, 12H, CH(CH<sub>3</sub>)<sub>2</sub>), 1.23 (s, 9H, C(CH<sub>3</sub>)<sub>3</sub>), 1.14 (s, 9H, C(CH<sub>3</sub>)<sub>3</sub>), 0.85 (d,  
<sup>3</sup>J<sub>HH</sub> = 4.2 Hz, 9H), 0.66 (d, <sup>3</sup>J<sub>HH</sub> = 4.2 Hz, 9H), -4.07 (apparent d, J<sub>HP</sub> = 44.8 Hz, W<sub>1/2</sub> = 115.2  
 Hz, 1H, Ni-H-Al). <sup>13</sup>C{<sup>1</sup>H} NMR (101 MHz, C<sub>4</sub>D<sub>8</sub>O, 298 K) δ 158.08 (s, aryl-C), 157.82 (d, J<sub>CP</sub>  
 = 17.5 Hz, aryl-C), 156.07 (s, aryl-C), 150.53 (d, J<sub>CP</sub> = 12.0 Hz, aryl-C), 143.21 (ddd, J<sub>CP</sub> = 26.4  
 Hz, J<sub>CP</sub> = 10.9 Hz, J<sub>CP</sub> = 1.9 Hz, aryl-C), 142.07 (s, aryl-C), 141.76 (s, aryl-C), 139.13 (s, aryl-  
 C), 134.74 (d, J<sub>CP</sub> = 5.5 Hz, aryl-C), 132.80 (d, J<sub>CP</sub> = 12.4 Hz, aryl-C), 132.36 (d, J<sub>CP</sub> = 4.6 Hz,  
 aryl-C), 132.18 (s, aryl-C), 130.33 (s, aryl-C), 127.48 (ddd, J<sub>CP</sub> = 42.9 Hz, J<sub>CP</sub> = 13.3 Hz, J<sub>CP</sub> =  
 8.5 Hz, aryl-C), 125.95 (d, J<sub>CP</sub> = 8.8 Hz, aryl-C), 125.66 (s, aryl-C), 125.05 (s, aryl-C), 124.66 (s,  
 aryl-C), 124.24 (s, aryl-C), 121.99 (s, aryl-C), 120.95 (s, aryl-C), 119.92 (s, aryl-C), 116.45 (dd,  
 J<sub>CP</sub> = 19.0 Hz, J<sub>CP</sub> = 17.5 Hz, aryl-C), 116.16 (d, J<sub>CP</sub> = 6.3 Hz, aryl-C), 116.08 (s, aryl-C), 113.66  
 (s, aryl-C), 113.41 (d, J<sub>CP</sub> = 5.6 Hz, aryl-C), 113.24 (s, aryl-C), 112.41 (s, aryl-C), 111.17 (s, aryl-  
 C), 54.44 (s, CH(CH<sub>3</sub>)<sub>2</sub>), 50.38 (s, OCH<sub>3</sub>), 33.69 (s, C(CH<sub>3</sub>)<sub>3</sub>), 33.35 (s, C(CH<sub>3</sub>)<sub>3</sub>), 31.37 (s,

$C(CH_3)_3$ , 31.11 (s,  $C(CH_3)_3$ ), 22.50 (ddd,  $J_{CP} = 12.6$  Hz,  $J_{CP} = 7.4$  Hz,  $J_{CP} = 5.2$  Hz,  $P(CH_3)_3$ ),  
 21.69 (ddd,  $J_{CP} = 13.2$  Hz,  $J_{CP} = 7.8$  Hz,  $J_{CP} = 5.5$  Hz,  $P(CH_3)_3$ ), 20.27 (s,  $CH(CH_3)_2$ ), 10.24 (s,  
 $^iPrNCCH_3N^iPr$ ), 8.84 (s,  $NCCH_3CCH_3N$ ).  $^{31}P \{^1H\}$  NMR (161.97 MHz,  $C_4D_8O$ , 298 K)  $\delta$  -0.65  
 (d,  $^2J_{PP} = 32.5$  Hz,  $^2J_{PP} = 6.4$  Hz, 1P, PPhAr), -16.65 (dd,  $^2J_{PP} = 30.5$  Hz,  $^2J_{PP} = 6.4$  Hz, 1P,  
 $P(CH_3)_3$ ), -21.91 (s, impurity), -25.45 (dd,  $^2J_{PP} = 30.5$  Hz,  $^2J_{PP} = 32.5$  Hz, 1P,  $P(CH_3)_3$ ).  
 $C_{57}H_{82}AlN_4NiO_2P_3$  Theoretical: C % 66.22, H % 7.99, N % 5.42. Determined C % 65.02, H %  
 8.02, N % 5.07.

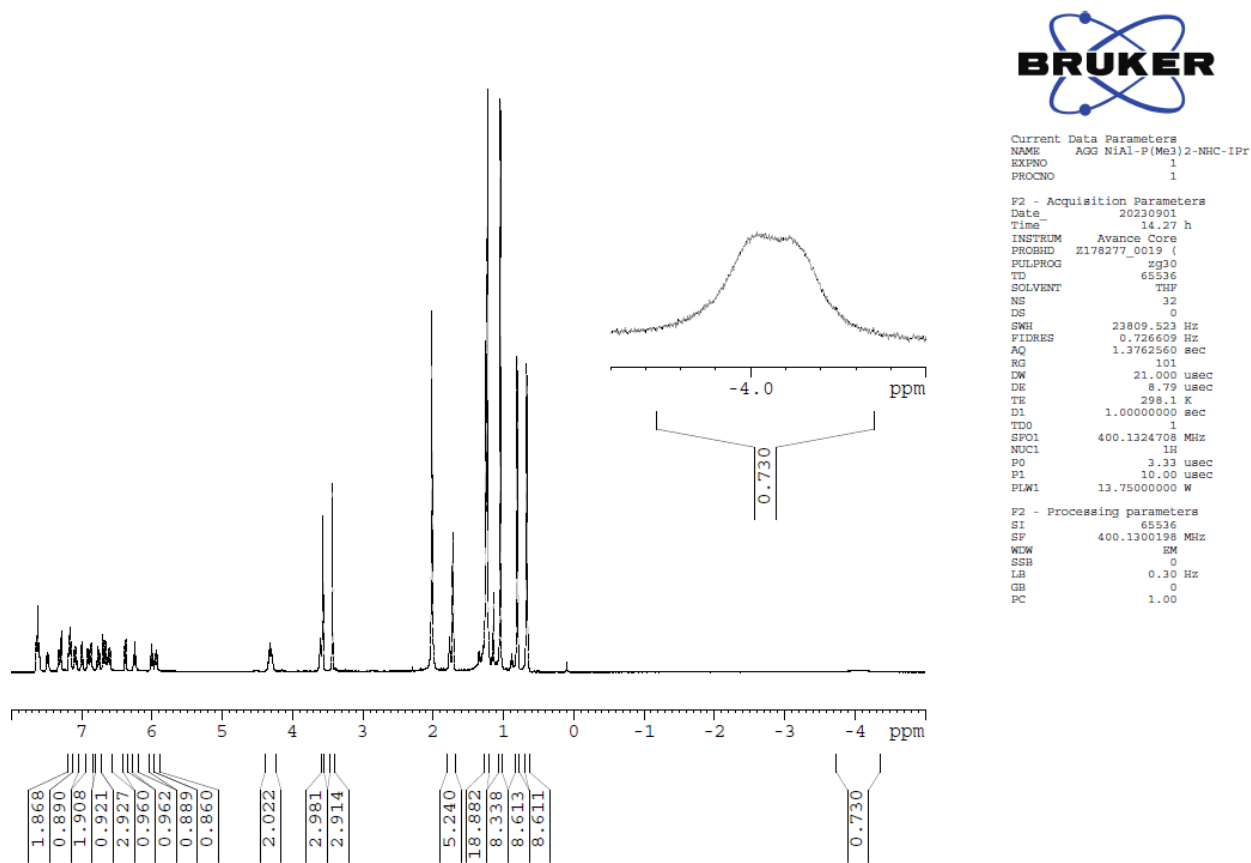


Figure 38:  $^1H$  NMR spectrum of  $NiAl-(PMe_3)_2-NHC-IPr$  in  $C_6D_6$ .

The NMR data shows that the main groups in the complex which are the tert-butyls, methoxys, and phenyl groups, and lastly the Ni-H-Al showing at -4.07 ppm as a broad d. This peak is slightly more upfield than the reported NiAl<sub>2</sub>, NiAl-(PPh<sub>3</sub>)<sub>2</sub>, NiAl-(dppm)<sub>2</sub>, NiAl-(PMe<sub>3</sub>)<sub>2</sub> complexes, compared to -1.50 ppm, -1.78 ppm, -2.14 ppm and -3.28.<sup>16</sup> In addition, the anionic hydride variant is complex to identify by <sup>31</sup>P{<sup>1</sup>H} NMR, showing the peaks of a d around -0.65 ppm for PPhAr, a d around -16.65 ppm for P(Me<sub>3</sub>)<sub>3</sub>, and a t around -25.45 ppm for P(Me<sub>3</sub>)<sub>3</sub>. There is an extra peak of a broad s around -21.91 ppm that is an impurity.

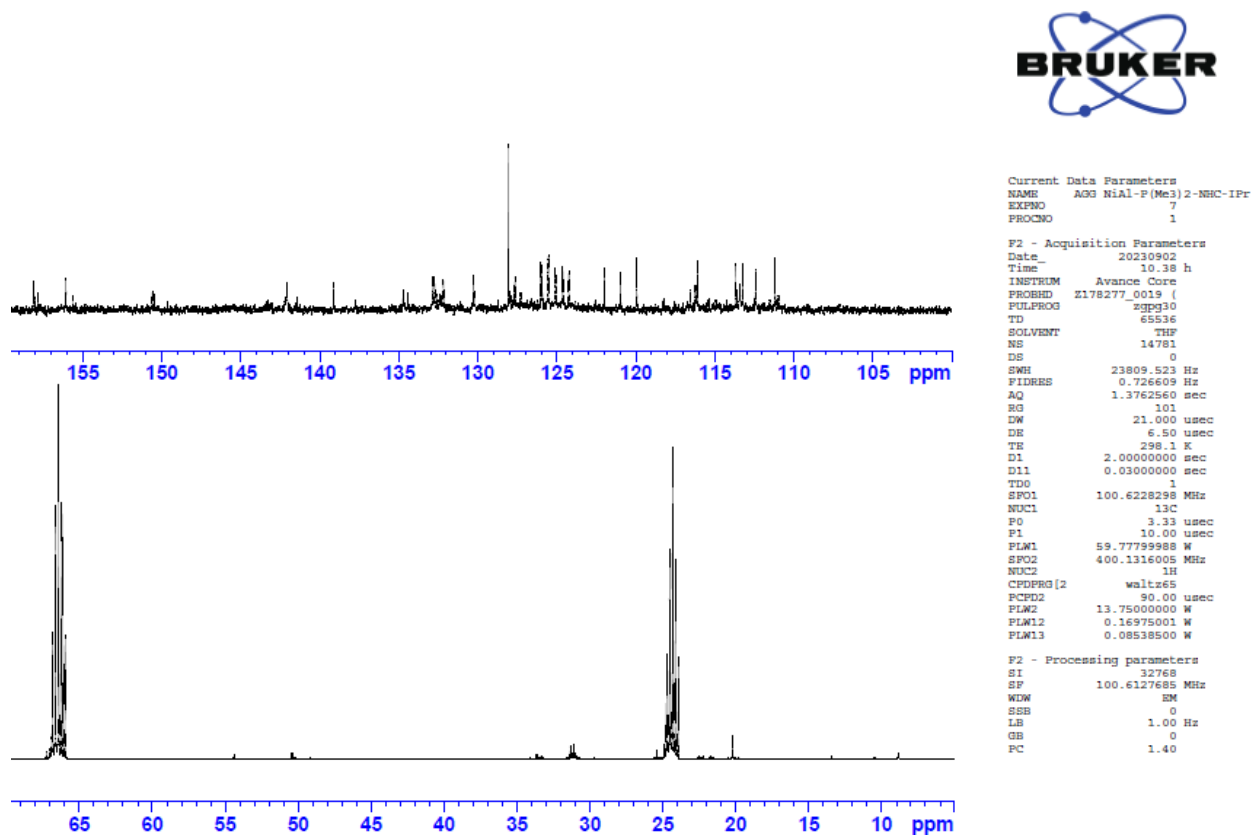


Figure 39: <sup>13</sup>C{<sup>1</sup>H} NMR spectrum of NiAl-(PMe<sub>3</sub>)<sub>2</sub>-NHC-IPr in C<sub>6</sub>D<sub>6</sub>.



Current Data Parameters  
NAME AG3 NiAl-P(Me3)2-NHC-IPr  
EXPNO 2  
PROCNO 1

F2 - Acquisition Parameters  
Date\_ 20230901  
Time 14.33 h  
INSTRUM Avance Core  
PROBHD Z178277\_0019 (zpg30)  
PULPROG zgpg30  
TD 65536  
SOLVENT THF  
NS 64  
DS 0  
SWH 65789.477 Hz  
FIDRES 2.007735 Hz  
AQ 0.4980736 sec  
RG 101  
DM 7.600 usec  
DE 6.50 usec  
TE 298.2 K  
D1 2.00000000 sec  
D11 0.03000000 sec  
TDO 1  
SFO1 161.9674942 MHz  
NUC1 31P  
P0 3.33 usec  
P1 10.00 usec  
PLW1 27.58300018 W  
SFO2 400.1316005 MHz  
NUC2 1H  
CPCPRG2 waltz16  
PCPD2 90.00 usec  
PLW2 13.75000000 W  
PLW12 0.16975001 W  
PLW13 0.08538500 W

F2 - Processing parameters  
SI 262144  
SF 161.9755930 MHz  
WDW EM  
SSB 0  
LB 1.00 Hz  
GB 0  
PC 1.40

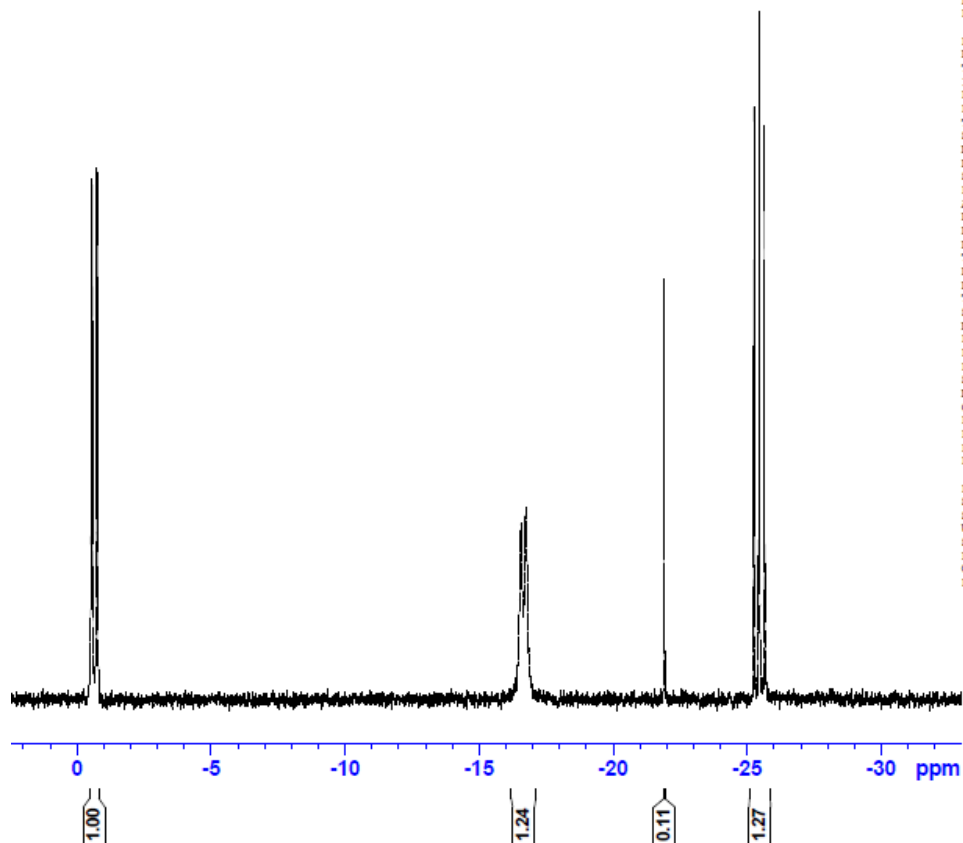


Figure 40:  $^{31}\text{P}\{^1\text{H}\}$  NMR spectrum of  $\text{NiAl}(\text{PMe}_3)_2\text{-NHC-IPr}$  in  $\text{C}_6\text{D}_6$ .

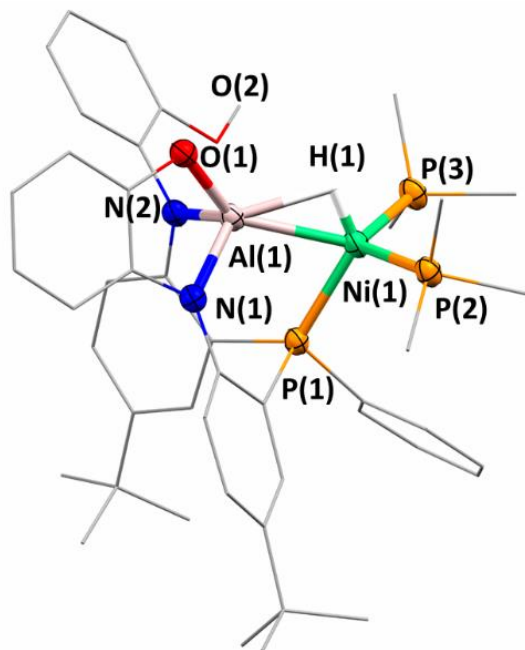


Figure 41: XRD crystal structure of **NiAl-(PMe<sub>3</sub>)<sub>2</sub>-NHC-IPr**.

Table 4: Properties of Bond Distances of NiAl-(PMe<sub>3</sub>)<sub>2</sub>-NHC-IPr(3).

NiAl-(PMe <sub>3</sub> ) <sub>2</sub> -NHC-IPr	Bond distances
Ni-H	1.19(3)
	1.31(3)
Al-H	1.88(3)
	1.75(3)
Ni-Al	2.3336(11)
	2.3358(11)
Ni-(P1)	2.1311(10)
	2.1329(10)
Ni-(P2/P3)	2.1661(11)
	2.1614(11)
	2.1559(11)
	2.1677(10)

The crystal structure of NiAl-(PMe<sub>3</sub>)<sub>2</sub>-NHC-IPr, as shown in Figure 41 and Table 5, is composed of normal van der Waals' shortest bond distance is 1.19-1.31(3) Å which belongs to Ni-H. This is found to be far smaller than the range for NiAl<sub>2</sub>, NiAl-(PPh<sub>3</sub>)<sub>2</sub>, NiAl-(dppm)<sub>2</sub>, and NiAl-(PMe<sub>3</sub>)<sub>2</sub> which is the bond distance which is 1.43(4)-1.67(4)Å. This was achievable since the trimethyl phosphine donates its electron density to the Ni center. Then, Al-H is found to be 1.75-1.88(3) is bigger than NiAl-(PMe<sub>3</sub>)<sub>2</sub> and NiAl-(dppm)<sub>2</sub> bond distance which is 1.55(4)- 1.72(4) Å, and smaller than the expected Al-H bond distance previously reported of NiAl-(PPh<sub>3</sub>)<sub>2</sub>. The NiAl-(PMe<sub>3</sub>)<sub>2</sub>-NHC-IPr bond distance between Ni-Al was found to be 2.3336-2.3358(11), which is bigger than the bond distance of NiAl-(PMe<sub>3</sub>)<sub>2</sub> found to be 2.2503-2.2613(7) Å and similar range to the bond distance compared to the NiAl-(dppm)<sub>2</sub>, NiAl-(PPh<sub>3</sub>)<sub>2</sub>, and NiAl<sub>2</sub> was found to be 2.269-2.3683(7) Å. For the Ni-P1 and Ni-(P2/P3) bond distances are between 2.1559(11)-2.1677(10) Å which are also smaller than the expected of previously reported complexes which are around 2.28 Å.<sup>18</sup> The trimethyl phosphine ligand brings together/assembles the overall complex variant to be closer than the triphenylphosphine variant, and the regioselectivity and electron density forces it to be in close proximity.

### 2.2.5 Analysis of Overall Structural Parameters

Given that all four complexes were isolated by single crystal XRD, it offered the chance to gain insight by comparing bond metrics. Intriguing parameters to monitor are the Ni-Al distances which show a contraction and then an elongation. Furthermore, the bond angles about the coordination sphere at Ni show tetrahedral geometry throughout. The quality of the data sets is good and relevant XRD parameters are shown in the table below.

Table 5: Overall comparison between all complexes. This data was collected from a collaboration between RICE and UTSA.

Compound	NiAl-(PPh <sub>3</sub> ) <sub>2</sub>	NiAl-(dppm) <sub>2</sub>	NiAl-(PMe <sub>3</sub> ) <sub>2</sub>	3
Chemical Formula	C <sub>76</sub> H <sub>74</sub> AlN <sub>2</sub> NiO <sub>2</sub> P <sub>3</sub>	C <sub>204</sub> H <sub>199</sub> Al <sub>2</sub> N <sub>4</sub> Ni <sub>2</sub> O <sub>4</sub> P <sub>10</sub>	C <sub>96</sub> H <sub>126</sub> Al <sub>2</sub> N <sub>4</sub> Ni <sub>2</sub> O <sub>5</sub> P <sub>6</sub>	C <sub>65</sub> H <sub>97</sub> AlN <sub>4</sub> NiO <sub>4</sub> P <sub>3</sub>
Temp	100 K	100 K	100 K	100 K
Crystal system	Monoclinic	Monoclinic	Triclinic	Monoclinic
Space group	P2 <sub>1</sub> /c	P2 <sub>1</sub>	P-1	P2 <sub>1</sub> /n
a/ Å	21.9928(5)	17.4356(2)	13.3950(1)	19.6897(2)
b/ Å	17.5090(4)	48.5980(6)	15.9482(2)	18.2605(2)
c/ Å	17.8697(4)	20.8299(2)	23.2712(3)	40.6637(4)
α/ °	90	90	103.697(1)	90
β/ °	96.555(2)	90.369 (1)	97.850(1)	100.044(1)
γ/ °	90	90	90.485(1)	90
V/ Å <sup>3</sup>	6836.1(3)	17649.5(3)	4780.4(1)	14396.3(3)
Z	4	4	2	8
D <sub>calc</sub> /g cm <sup>-3</sup>	1.191	1.224	1.235	1.086
μ(Mo-Kα) / mm <sup>-1</sup>	1.548	1.658	2.015	1.469
F(000)	2548	6860	1892	5064
Reflection collected	12180	93407	68604	170067
Independent reflections	9918	54808	39743	47860
R(int)	11.41%	3.90%	3.23%	5.64%
R1 (I > 2σ(I)) <sup>a</sup>	6.72%	6.23%	3.78%	7.49%
wR2(all)	18.14%	14.96%	10.03%	16.07%
GOF	1.029	1.071	1.044	1.095

### 2.3 Ancillary Ligands Employed Leading to Auxiliary/Negligible Reactivity

Among the variety of different ligands used for the amplification of reactivity of the parent complex or LAIH, the list of ligands consisted of highly reactive electron-rich and electron-poor groups. Surrounded by different ligands utilized for the entirety of the trials it was used phosphines, N-heterocyclic carbenes, a silane, pyridines, nitriles, acetylenes, and phosphino ethane.

In order of priority, utilizing NHCs offers better and stronger donors than phosphines or any other ligand.<sup>5</sup> For this reason, this set of trials was focused on utilizing phosphines overall. Table 1 summarizes the list of conditions used.

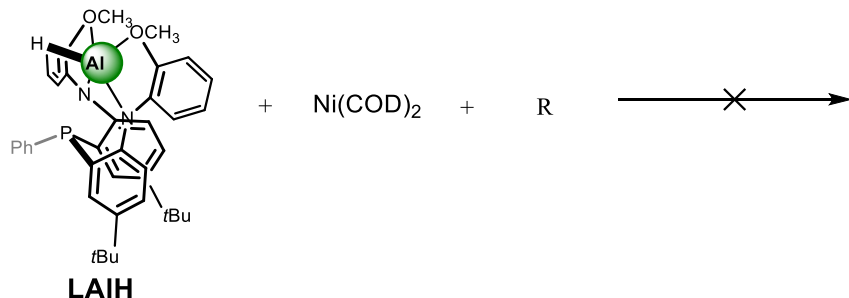


Figure 42: General methodology behind the small-scale reaction with unsuccessful ligands. In this case, R is every ligand listed in Table 1.

Table 6. List of ligands used, # of equivalence, temperature, and attempts.

Ligand	Equivalences	Temperature	Attempts
a. Trimethyl Phosphite	2	RT	2
b. Tri-tert-butyl phosphine	3	RT	2
c. Triphenyl phosphine	2	RT	2
d. 1,3-Bis(2,6-diisopropylphenyl) Imidazol-2-ylidene	2	RT	2
e. Vinyl-Trimethyl Silane	2	RT	1
f. 1,3,4,5-tetramethyl Imidazole (NHC-Me)	4 2	RT	2 2
g. Tricyclo Phosphine (PCy <sub>3</sub> )	2	RT	2
h. Tris(dimethylamino) Phosphine (P(NMe <sub>3</sub> ) <sub>2</sub> )	2	RT	2
i. 2,2'-Dipyridyl	2	RT	2
j. 4-dimethylaminopyridine (DMAP)	2	RT	3
k. Diphenylacetylene	1 2 10	RT	1 1 3
l. 1,2-Bis(Diphenyl Phosphino) Ethane	1	RT	1
m. Benzonitrile	1 2 10	RT	1 2 2

## 2.4 Catalytic Trials with Heterometallics

One of the main motivations for the synthesis sections above is to perform catalytic trials using the new heterometallic complexes and monitor the performance. As discussed in the introduction, catalysis is the ability of a species to lower the activation energy of a reaction without the species being consumed.<sup>7</sup> Catalytic transformations are essential in inorganic chemistry since one of the motivations to synthesize multimetallic complexes for the benefit lowering the barriers to accomplishing catalysis. The main motive of catalytic transformations of our heterotrimetallic and heterobimetallics is to break down N-heterocyclic atoms. We have showed previously that the heterometallic NiAl<sub>2</sub> complex is a highly active catalyst for the hydrofunctionalization of N-heterocycles. Monitoring the impact of the additional ancillary ligands is crucial in better understanding the reasoning behind the amplification of reactivity from the NiAl<sub>2</sub> species to the LAIH species.

In this section, catalytic reactions with H-BPin, quinoline, and 5% of the heterometallic catalysts are conducted. Within the section, two catalytic trials were performed using NiAl<sub>2</sub> and NiAl(PPh<sub>3</sub>)<sub>2</sub>.<sup>16</sup>

### 2.4.1 NiAl<sub>2</sub> Complex Catalysis

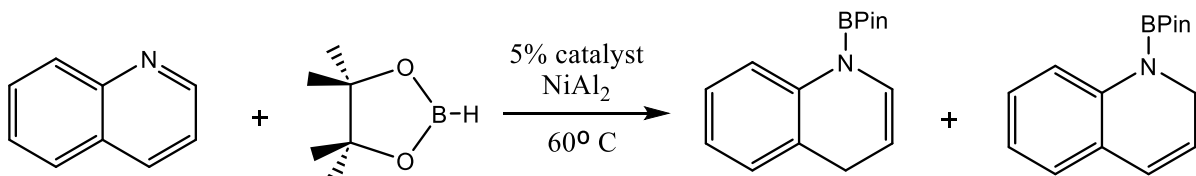


Figure 43: Reaction of Quinoline and H-BPin with 5% NiAl<sub>2</sub> catalyst.<sup>16</sup>

As reported before, figure 44 shows the reaction of Quinoline and H-BPin using 5% NiAl<sub>2</sub>. The catalytic capabilities of NiAl<sub>2</sub> demonstrate the dearomatization of N-heterocycles. To demonstrate comparative reactivity, the catalytic trials needed to be repeated to observe the direct impact of the heterometallic complex. The reaction shows that after an hour of being heated at 60 °C, the NMR spectra shows that catalyst NiAl<sub>2</sub> is not consumed and shows resonances consistent with two new dearomatized N-heterocycles. In this hydroboration of quinoline, it shows the appearance of 1,4 and 1,2 isomers of the dearomatized heterocycle in a 2:1 ratio.<sup>16</sup> This data was presented in the paper by our group. As shown in Figures 44 and 45, the <sup>1</sup>H and <sup>31</sup>P{<sup>1</sup>H} NMR shows the appearance of 1,4 and 1,2 isomers of quinoline in accordingly peaks such as 6.90-6.70 and 6.26 for olefinic-H.<sup>62</sup>

For 1,4-isomer: <sup>1</sup>H NMR (400 MHz, C<sub>6</sub>D<sub>6</sub>, 298K): δ 8.11 (d, <sup>3</sup>J<sub>HH</sub> = 8.2 Hz, 1H, PhH), 7.07 (t, <sup>3</sup>J<sub>HH</sub> = 7.53 Hz, 1H, PhH), 6.90-6.77 (overlapping m, 3H, PPh + olefinic H), 4.81 (dt, <sup>3</sup>J<sub>HH</sub> = 9.56 Hz, <sup>3</sup>J<sub>HH</sub> = 4.25 Hz, 1H, olefinic-H), 3.31 (d, <sup>3</sup>J<sub>HH</sub> = 4.2 Hz, 2H, alkyl-H), 1.02 (s, 12H, BPin), <sup>31</sup>P {<sup>1</sup>H} NMR (161.97 MHz, C<sub>6</sub>D<sub>6</sub>, 298 K) δ 0.08 (broad s, W<sub>1/2</sub> = 188.50 Hz, Ni-H-Al), -28. (s, PPhAr).

For 1,2-isomer:  $^1\text{H}$  NMR (400 MHz,  $\text{C}_6\text{D}_6$ , 298K):  $\delta$  7.91 (d,  $^3J_{\text{HH}} = 7.5$  Hz, 1H, PhH), 7.09 (t,  $^3J_{\text{HH}} = 7.6$  Hz, 1H, PhH), 6.90-6.77 (overlapping m, 2H, PPh), 6.26 (d,  $^3J_{\text{HH}} = 9.2$  Hz, 1H, olefinic-H) 5.57 (dt  $^3J_{\text{HH}} = 9.7$  Hz,  $^3J_{\text{HH}} = 4.1$  Hz 1H, olefinic-H), 4.14 (d,  $^3J_{\text{HH}} = 4.4$  Hz, 2H, alkyl-H), 1.04 (s, 12H, BPin),  $^{31}\text{P}$   $\{^1\text{H}\}$  NMR (161.97 MHz,  $\text{C}_6\text{D}_6$ , 298 K)  $\delta$  0.08 (broad s,  $W_{1/2} = 188.50$  Hz, Ni-H-Al), -28.0 (s, PPhAr),

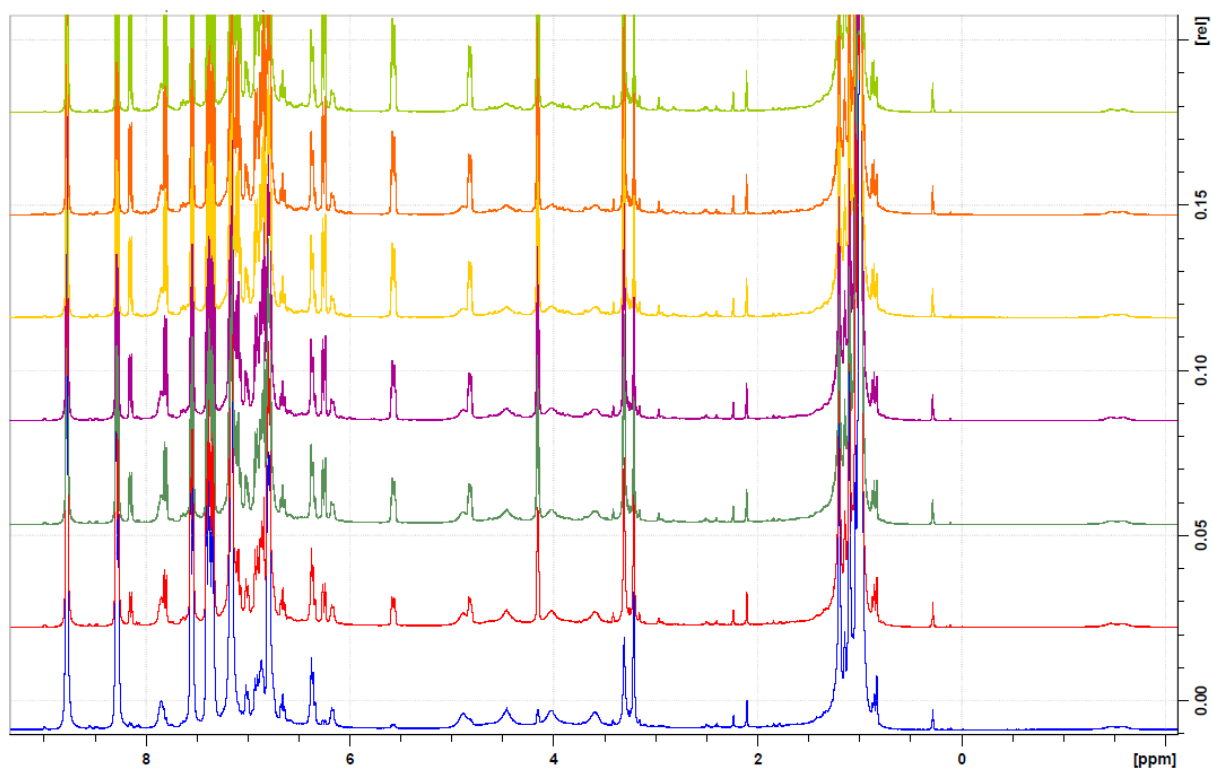


Figure 44:  $^1\text{H}$  NMR spectrum of catalytic reaction using 5 %  $\text{NiAl}_2$  in  $\text{C}_6\text{D}_6$ .

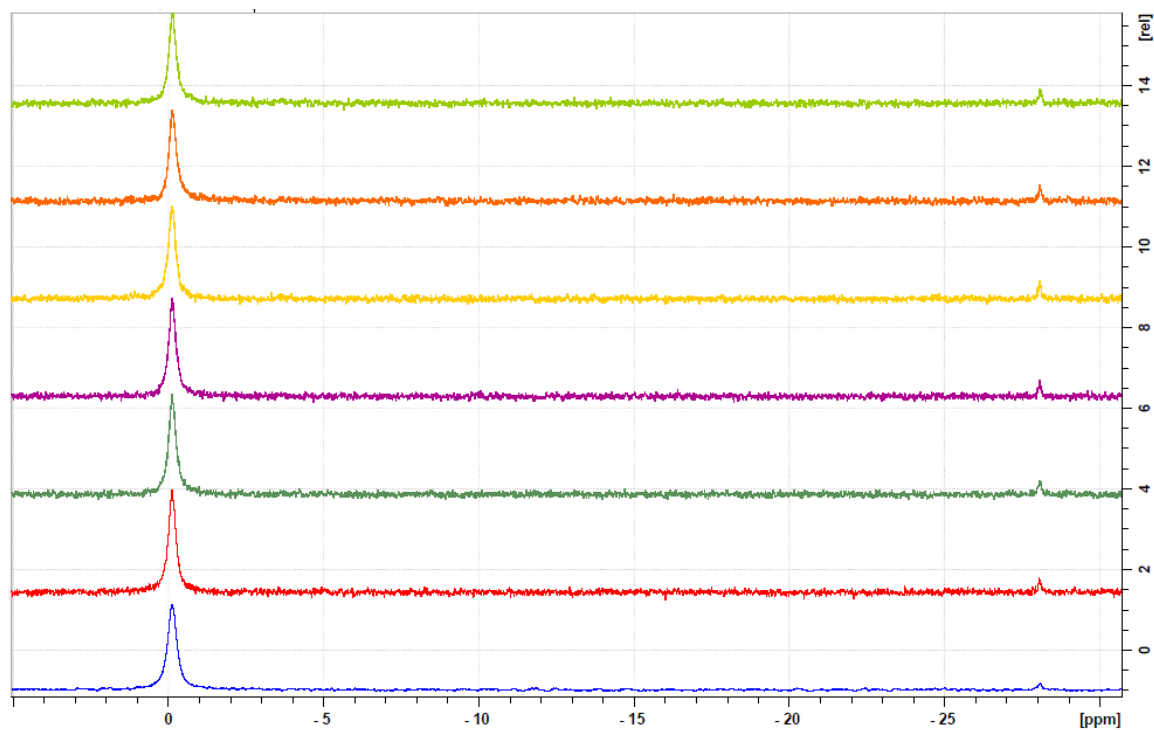


Figure 45:  $^{31}\text{P}\{^1\text{H}\}$  NMR spectrum of catalytic reaction using 5 %  $\text{NiAl}_2$  in  $\text{C}_6\text{D}_6$ .

## 2.4.2 $\text{NiAl}-(\text{PPh}_3)_2$ Complex

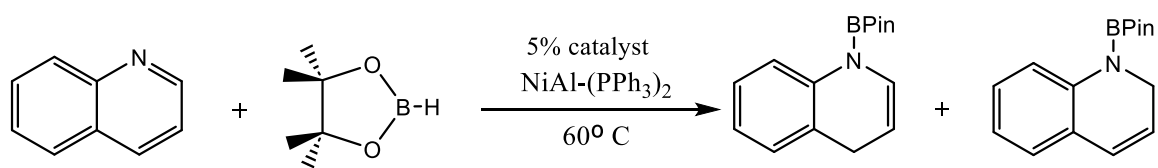


Figure 46: Reaction of Quinoline and H-BPin with 5%  $\text{NiAl}-(\text{PPh}_3)_2$  catalyst

Similarly to  $\text{NiAl}_2$ , as shown in Figure 46 the catalytic reaction was performed with the same parameters but using the heterobimetallic  $\text{PPh}_3$ -coordinated complex. The results showed that dearomatization was still observed in N-heterocycles. In this hydroboration of quinoline, it

shows the appearance of 1,4 and 1,2 isomers of the dearomatized heterocycle in a 2:1 ratio. As shown in Figures 46 and 47, the  $^1\text{H}$  and  $^{31}\text{P}\{^1\text{H}\}$  NMR shows the appearance of 1,4 and 1,2 isomers of quinoline in accordingly peaks such as 6.90-6.70 and 6.26 for olefinic-H.<sup>62</sup> Ongoing studies to monitor the impact of the ancillary ligands in selectivity and activation in catalysis are underway.

For 1,4-isomer:  $^1\text{H}$  NMR (400 MHz,  $\text{C}_6\text{D}_6$ , 298K):  $\delta$  8.12 (d,  $^3J_{\text{HH}} = 8.3$  Hz, 1H, PhH), 7.08 (t,  $^3J_{\text{HH}} = 7.6$  Hz, 1H, PhH), 6.91-6.70 (overlapping m, 3H, PPh + olefinic H), 4.80 (dt,  $^3J_{\text{HH}} = 9.6$  Hz,  $^3J_{\text{HH}} = 4.3$  Hz, 1H, olefinic-H), 3.32 (d,  $^3J_{\text{HH}} = 4.3$  Hz, 2H, alkyl-H), 1.03 (s, 12H, BPin)

For 1,2-isomer:  $^1\text{H}$  NMR (400 MHz,  $\text{C}_6\text{D}_6$ , 298K):  $\delta$  7.91 (d,  $^3J_{\text{HH}} = 7.5$  Hz, 1H, PhH), 7.09 (t,  $^3J_{\text{HH}} = 7.6$  Hz, 1H, PhH), 6.90-6.77 (overlapping m, 2H, PPh), 6.26 (d,  $^3J_{\text{HH}} = 9.2$  Hz, 1H, olefinic-H) 5.57 (dt  $^3J_{\text{HH}} = 9.7$  Hz,  $^3J_{\text{HH}} = 4.1$  Hz 1H, olefinic-H), 4.14 (d,  $^3J_{\text{HH}} = 4.4$  Hz, 2H, alkyl-H), 1.04 (s, 12H, BPin)

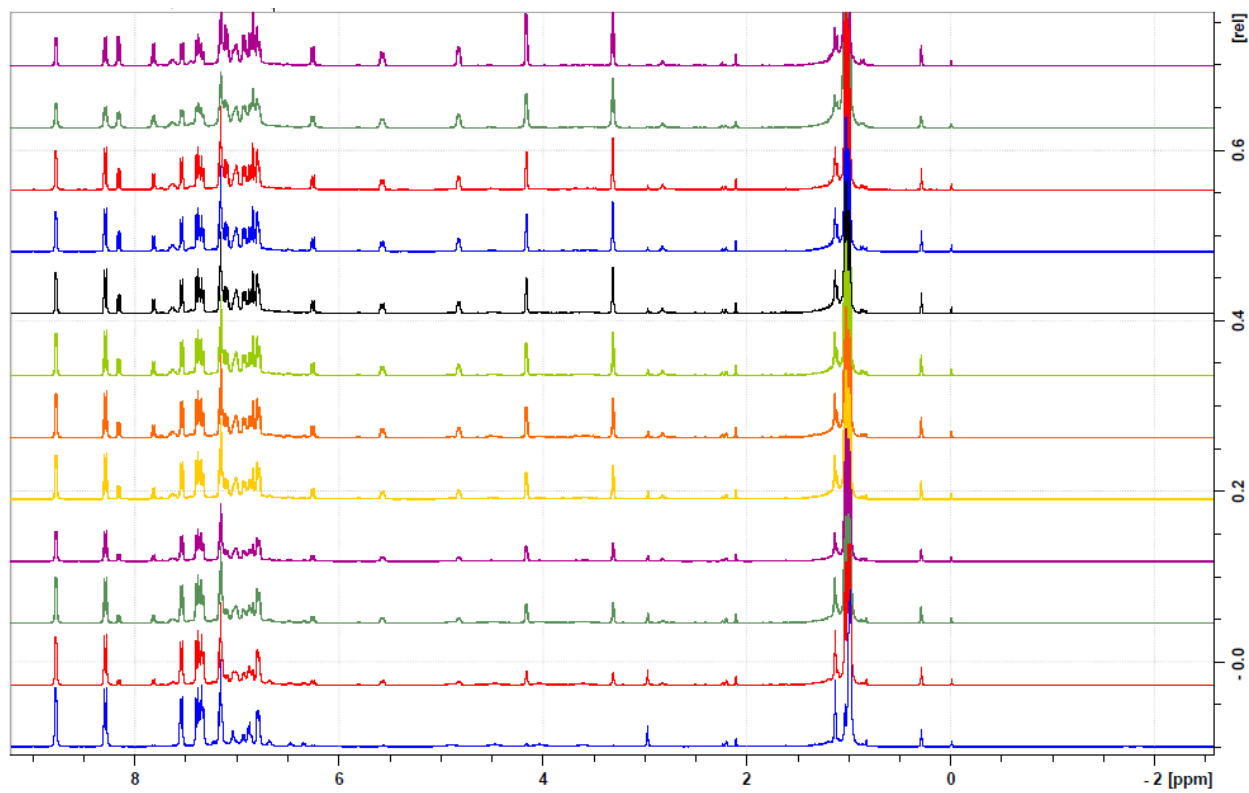


Figure 47:  $^1\text{H}$  NMR spectrum of catalytic reaction using 5 %  $\text{NiAl}(\text{PPh}_3)_2$  in  $\text{C}_6\text{D}_6$ .

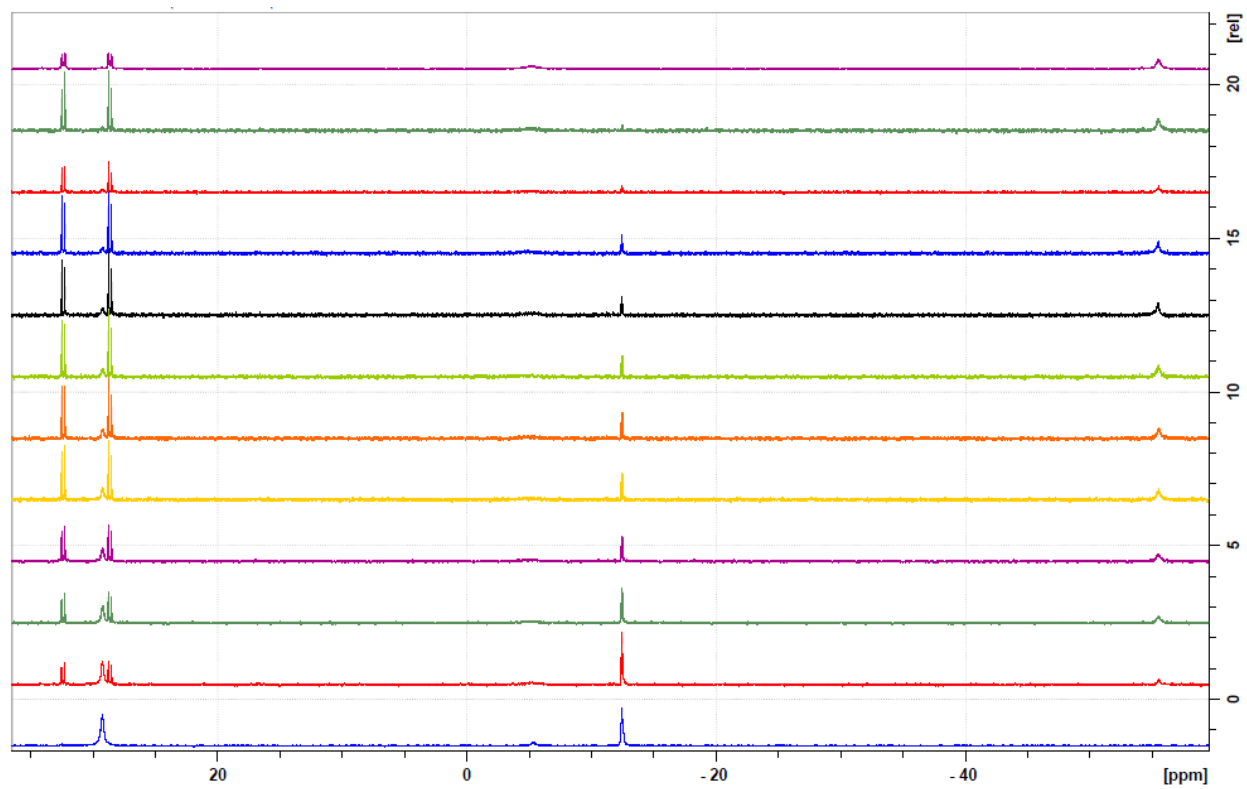


Figure 48:  $^{31}\text{P}\{^1\text{H}\}$  NMR spectrum of catalytic reaction using 5 %  $\text{NiAl}(\text{PPh}_3)_2$  in  $\text{C}_6\text{D}_6$ .

CHAPTER III  
ELECTRONIC STRUCTURE STUDIES OF HETEROMETALLIC HYDRIDES

**3.1 Wiberg Bond Index and QTAIM Analyses of Heterometallic Molecules,  
Heterotrimetallic molecule, and Alane**

Natural Bond Orbital (NBO) analysis and Quantum Theory of Atoms in Molecules (QTAIM) analysis are computational methods that can provide insights into molecular electronic structure and bonding.<sup>2,3,4</sup> Both NBO and QTAIM need to be performed on optimized structures. One of the main results obtained from NBO analysis is the Wiberg Bond Index (WBI)<sup>27</sup>, which is a chemically interpretable bond order value calculated from the population of natural orbitals.<sup>47,57</sup> In this study, we performed the NBO analysis to better understand the electronic structure of these heterocomplexes and to build a connection between experimental and computational observations.

In QTAIM analysis, the real space electron density data is analyzed topologically to obtain chemical information such as bonding. Most information from QTAIM is provided via critical points, where the Laplacian of electron density is zero. A critical point denoted as (3, x) means that at this point, the electron density function is maxima along  $(3-x)/2$  dimensions and is minima along  $(3+x)/2$  dimensions. The main critical points are the following: atom critical point (3, -3), bond critical point (BCP) (3, -1), ring critical point (3, 1), and cage critical point (3, 3).<sup>38</sup> These critical points provide the main components to identifying/providing the principal atoms involved such as the electron density (Rho value,  $\rho$ ), the Laplacian of the electron density ( $\nabla^2(\rho)$ ), the ellipticity (Ellipticity), the electron kinetic energy density ( $k$ ), and the difference

between the bond path length for every geometric bond length (BPL-GB\_1).<sup>39</sup> In this work, we focused on calculating the electron density  $\rho$  value at BCPs to better understand the bonding in the complexes.

In this study, the structure of our four main heterometallic complexes was first optimized using density functional theory (DFT) calculations. The BP86 functional along with def2-SVP (for H, C, N, O, and P) and def2-TZVP (for Al and Ni) basis sets were used.<sup>4,21,22</sup> Vibrational frequency analysis was then performed to verify that all optimized structures have no imaginary frequencies. NBO and QTAIM analysis was then carried out using the optimized structures, using Multiwfn and AIMAll programs.<sup>31,56</sup>

### 3.1.1. Triphenyl Phosphine Ligand

The data reported are the WBIs, the electron density  $\rho$  values at BCPs, and the bond distances of the key bonds: Ni-H, Al-H, and Ni-Al. The higher the value of WBI, the stronger the covalency between the two atoms under investigation. Similarly, the higher the electron density or  $\rho$  value the stronger the bonding between those two. As shown in Table 7, Ni-H has higher WBI, larger  $\rho$ , and shorter distances than Al-H, indicating that the Ni-H bond is stronger than Al-H bond. For Ni-Al, the value for WBI was even lower which is 0.3349, the  $\rho$  value was not found, and the bond distance was longer. The reasoning behind this is due to the ancillary ligand bonded to the complex, in this case, triphenylphosphine.<sup>20</sup> Since triphenylphosphine is an electron-donating ligand, then it is donating its electron density to the main metal in this case Ni.

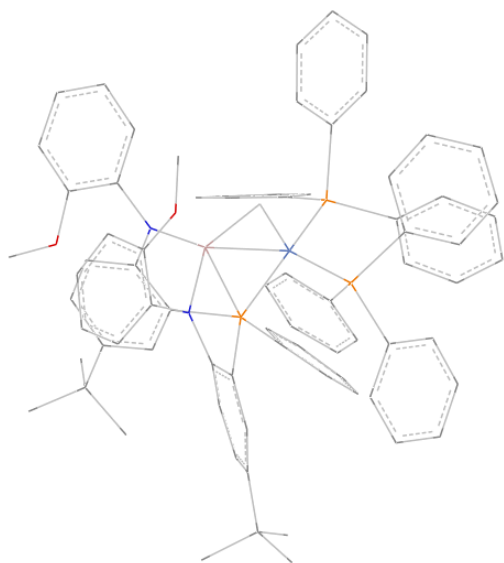


Figure 49: Optimized structure of NiAl-(PPh<sub>3</sub>)<sub>2</sub>.

Table 7. WBIs, Rho values, and Bond distances of NiAl-(PPh<sub>3</sub>)<sub>2</sub>.

NiAl-(PPh <sub>3</sub> ) <sub>2</sub>	WBI	Rho ( $\rho$ )	Bond distance (Å)
Ni-H	0.4746	0.0905	1.6359
Al-H	0.3734	0.0638	1.7126
Ni-Al	0.3475	C.P. not found	2.2640

### 3.1.2. Bis-(Diphenyl Phosphino) Methane Ligand

Bis-(Diphenyl Phosphino) Methane is a bulky electron-donating ligand known as dppm which is expected to have similar bonding pattern as triphenylphosphine. Same as in the triphenylphosphine ligand, here the Ni-H bond also appears stronger than Al-H. As shown in

Table 8, Ni-H has higher WBI, larger rho, and shorter distances than Al-H, indicating that the Ni-H bond is stronger than the Al-H bond. The experimental bond distance for Ni-H was found to be 1.43(13)-1.47(13) Å compared to the theoretical which is 1.6357 Å. For Al-H, the experimental bond distance was found to be 1.55(12)-1.72(12) Å compared to the theoretical which is 1.7300 Å. Experimental bond lengths involving H are not accurate due to the limitation of X-Ray crystallography. The theoretical bond distances correlate with the For Ni-Al, the value for WBI was even lower which is 0.3554, the Rho value was not found, and the bond distance was longer which is 2.2778 Å. The experimental bond distances of Ni-Al are found to be lower than the theoretical, these were found to be 2.269(4)-2.276(4) Å. The reasoning behind this is due to the ancillary ligand bonded to the complex, in this case, bis(diphenyl phosphino) methane.<sup>25</sup> Since bis(diphenyl phosphino) methane is an electron-donating ligand, then it donates its electron density to the main metal in this case Ni.

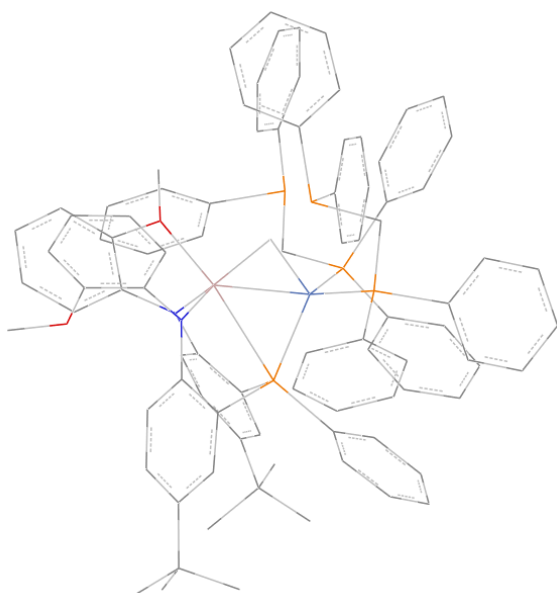


Figure 50: Optimized structure of NiAl-(dppm)<sub>2</sub>.

Table 8. WBIs, Rho values, and Bond distances of NiAl-(dppm)<sub>2</sub>.

NiAl-(dppm) <sub>2</sub>	WBI	Rho ( $\rho$ )	Bond distance (Å)
Ni-H	0.4883	0.09095	1.6357
Al-H	0.3735	0.06525	1.7300
Ni-Al	0.3554	C.P. not found	2.2778

### 3.1.3. Trimethyl Phosphine Ligand

Similarly to the NiAl-(PPh<sub>3</sub>)<sub>2</sub>, the trimethyl phosphine donates its electron density to the nickel center, which indicates that the WBIs are higher and the bond distance between Ni-H is closer or lower than Al-H. As shown in Table 9, Ni-H has higher WBI, larger rho, and shorter distances than Al-H, indicating that the Ni-H bond is stronger than the Al-H bond. The experimental bond distance for Ni-H was found to be 1.61(4)-1.67(4) Å compared to the theoretical which is 1.6578 Å. For Al-H, the experimental bond distance was found to be 1.68(4)-1.71(4) Å compared to the theoretical that is 1.7268 Å. The theoretical bond distances correlate with the For Ni-Al, the value for WBI was even lower which is 0.3848, the Rho value was not found, and the bond distance was longer which is 2.2542 Å. The experimental bond distances of Ni-Al were found to be lower than the theoretical, these were found to be 2.2503(7)-2.2613(7) Å. The reasoning behind this is due to the ancillary ligand bonded to the complex, in this case, trimethyl phosphine.<sup>55</sup> Since trimethyl phosphine is an electron-donating ligand, then it donates its electron density to the main metal in this case Ni.

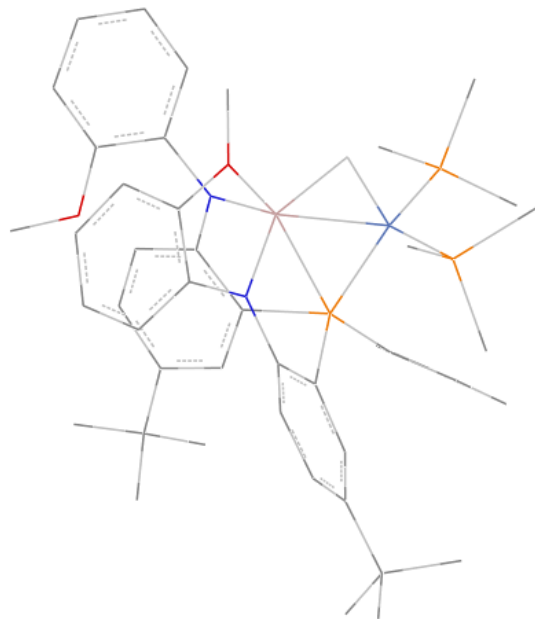


Figure 51: Optimized structure of NiAl-(PMe<sub>3</sub>)<sub>2</sub>.

Table 9. WBIs, Rho values, and Bond distances of NiAl-(PMe<sub>3</sub>)<sub>2</sub>.

NiAl-(PMe <sub>3</sub> ) <sub>2</sub>	WBI	Rho (ρ)	Bond distance (Å)
Ni-H	0.4868	0.0876	1.6578
Al-H	0.3946	0.0655	1.7265
Ni-Al	0.3848	C.P. not found	2.2542

### 3.1.4. Diisopropyl-4,5-dimethyl-Imidazol-2-ylidene Ligand

We also modeled the experimentally synthesized anionic hydride derived from NiAl-(PMe<sub>3</sub>)<sub>2</sub>, since this was synthesized differently and is considered an ion the approach to work on the trimethyl phosphine donates its electron density to the nickel center, which indicates that the

WBIs are higher and the bond distance between Ni-H is closer or lower than Al-H. As shown in Table 10, Ni-H has higher WBI, larger rho, and shorter distances than Al-H, indicating that the Ni-H bond is stronger than the Al-H bond. The experimental bond distance for Ni-H was found to be 1.19(3)-1.31(3) Å compared to the theoretical which is 1.6204 Å. For Al-H, the experimental bond distance was found to be 1.88(3)-1.75(3) Å compared to the theoretical that is 1.7340 Å. The theoretical bond distances correlate with the For Ni-Al, the value for WBI was even lower which is 0.3348, the Rho value was not found, and the bond distance was longer which is 2.3430 Å. The experimental bond distances of Ni-Al are found to be lower than the theoretical, these were found to be 2.3336(11)-2.3358(11) Å. The reasoning behind this is due to the ancillary ligand bonded to the complex, in this case, trimethyl phosphine and Diisopropyl-4,5-dimethyl-Imidazol-2-ylidene.<sup>63</sup> Since trimethyl phosphine and Diisopropyl-4,5-dimethyl-Imidazol-2-ylidene are electron-donating ligands, then it donates its electron density to the main metal in this case Ni.

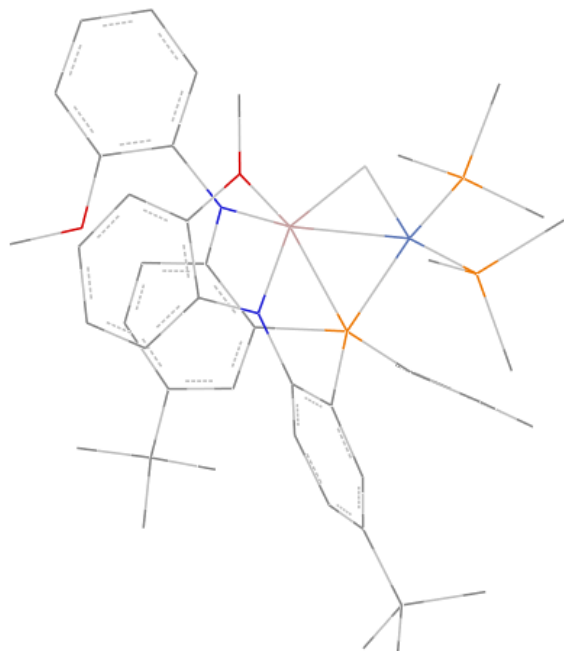


Figure 52. Optimized structure of NiAl-P(Me<sub>3</sub>)<sub>2</sub> + NHC-IPr.

Table 10. WBIs, Rho values and Bond distances of NiAl-P(Me<sub>3</sub>)<sub>2</sub> + NHC-IPr.

(NiAl-P(Me <sub>3</sub> ) <sub>2</sub> + NHC-IPr)	WBI	Rho (ρ)	Bond distance (Å)
Ni-H	0.5220	0.0936	1.6204
Al-H	0.3670	0.0631	1.7340
Ni-Al	0.3348	C.P. not found	2.3430

### 3.1.5. Overall

Along with the optimized structure of all complexes, Table 11 shows the comparison between WBIs and Rho values between complexes. As observed, the biggest WBI is 0.522 along with the Rho value is 0.0936 for the Ni-H bond for the NiAl-(PMe<sub>3</sub>)<sub>2</sub>-NHC-IPr or Anionic hydride. The reason behind this is due to having a charge in this complex which makes the atoms to be closer to each other. The smallest WBI is 0.4846 of NiAl-(PPh<sub>3</sub>)<sub>2</sub> and the smallest Rho value is 0.0876 of NiAl-(PMe<sub>3</sub>)<sub>2</sub> for the Ni-H bond. For the Al-H bond, the biggest WBI is 0.3946 and the Rho value is 0.0655 belonging to NiAl-(PMe<sub>3</sub>)<sub>2</sub>, and the smallest WBI is 0.3670 and the Rho value is 0.0631 and belongs to the anionic hydride. For the Ni-Al bond, the biggest WBI is 0.3348 for NiAl-(PMe<sub>3</sub>)<sub>2</sub>, and the smallest is 0.3348 for the anionic hydride. The strongest Ni-H character belongs to the Anionic hydride and the least is between NiAl-(PMe<sub>3</sub>)<sub>2</sub> since exhibits a higher Al-H character; however, NiAl-(PPh<sub>3</sub>)<sub>2</sub> is similar since the WBI is smaller for Ni-H.

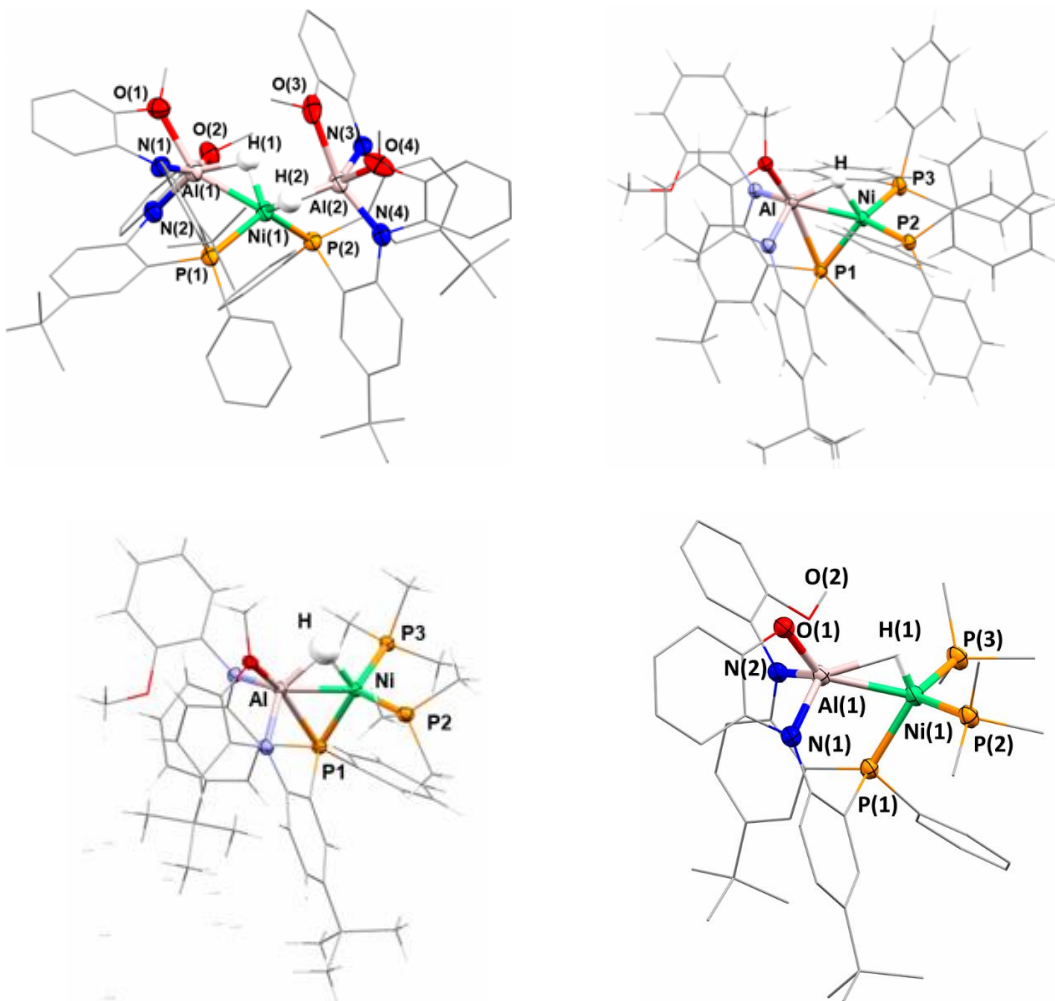


Figure 53: Experimental molecular structure of all complexes.

Table 11. Overall comparison table of WBIs and Rho values between all complexes.

Bond	NiAl <sub>2</sub> (1)	LAIH	2-(dppm) <sub>2</sub>	2-(PPh <sub>3</sub> ) <sub>2</sub>	2-(PMe <sub>3</sub> ) <sub>2</sub>	3
Ni-H	WBI: 0.4668-0.4803 Rho: 0.08673 0.09320	n/a	WBI: 0.4883 Rho: 0.0909	WBI: 0.4746 Rho: 0.0905	WBI: 0.4868 Rho:0.0876	WBI: 0.5220 Rho: 0.0936
Al-H	WBI: 0.3643-0.3943 Rho: 0.06667 0.06731	WBI: 0.7610 Rho: 0.08037	WBI: 0.3735 Rho: 0.0652	WBI: 0.3734 Rho: 0.0638	WBI: 0.3946 Rho:0.0655	WBI: 0.3670 Rho: 0.0631
Ni-Al	WBI: 0.2982-0.3054 Rho: C.P. not found	n/a	WBI: 0.3554 Rho: C.P. not found	WBI: 0.3475 Rho: C.P. not found	WBI: 0.3848 Rho: C.P. not found	WBI: 0.3348 Rho: C.P. not found

### 3.2 T1 Time Analysis of Heterometallic Molecules, Heterotrimetallic molecule, and Alane

The spin-lattice relaxation time, or longitudinal relaxation time is defined as a measurement of how the nucleus needs to reach equilibrium with its surroundings or its ground state in the direction of B<sub>0</sub>.<sup>19</sup> Also known as T1 Time analysis, it is one of the methods to understand the net magnetization vector of a substance under analysis.<sup>19</sup> T1 time measurements have found usage in organometallic chemistry through differentiation through seminal studies by Crabtree which

differentiate metal-hydrides from dihydrogen coordination.<sup>14</sup> Transition-metal dihydrogen complexes are common for 2<sup>nd</sup> and 3<sup>rd</sup> row-late transition metals and are generally indistinguishable from metal-hydrides through single-crystal X-ray diffraction.<sup>11</sup> Chemical shift, while providing some details through chemical shift, also does not distinguish between the two. T1 time analysis has proven useful here. Given the short H-H distances in metal dihydrogen complexes and the spin-active nature of H atoms, T1 time analysis of dihydrogen ligands are often two orders of magnitude less than metal hydrides (1-5 ms vs 100-500 ms).<sup>14</sup> T1 times of metal hydrides also serve as a way to characterize the hydride and the electronic impact by neighboring ligands within a transition metal complex. Determining the T1 time at room temperature offers some insight and can be used to some degree to differentiate protons, their surrounding atoms, bonding, and general dynamics between these atoms.<sup>12</sup> The T1 times for the series of complexes have been determined at room temperature. While T1(min) studies are reported elsewhere and are useful in gaining insight into the nature of the hydride, the T1 values observed here are consistent with known metal hydride complexes in multimetallic systems and provide further support for the bridged nature of the metal hydride. To fully characterize these complexes, we have reported a T1 times analysis of the series of complexes discussed above. some of the majority of the relaxation time constant of the complexes.

In Figures 54 to 56, it shows the data for NiAl-(PPh<sub>3</sub>)<sub>2</sub> complex structure along with T1 Plots for C<sub>6</sub>D<sub>6</sub> and THF, the T1 times were found to be 235.2 ms and 464.79 ms. In Figures 57 to 59, it shows the data for NiAl-(PMe<sub>3</sub>)<sub>2</sub> complex along with T1 Plots C<sub>6</sub>D<sub>6</sub> and THF were found to be 452.5 ms and 483.3 ms. Since the anionic hydride is only soluble in THF, there is only data with this solvent. In Figures 60 to 61, it shows the data for the Anionic hydride complex along with the T1 Plot was found to be 243.7 ms. In Figures 62 to 63, it shows the data for the LAIH complex

along with the T1 plot, the T1 time was found to be 293.6 ms in C<sub>6</sub>D<sub>6</sub>. In Figures 64 to 66, it shows the data for the NiAl<sub>2</sub> complex, the T1 plots were found to be 227.1 ms in C<sub>6</sub>D<sub>6</sub> and 363.2 ms in THF. As shown in Table 12, the overall T1 time values for all the complexes, here are reported that the biggest T1 time for C<sub>6</sub>D<sub>6</sub> is LAIH, and the smallest is NiAl<sub>2</sub>, and for THF is NiAl-(PMe<sub>3</sub>)<sub>2</sub> and NiAl<sub>2</sub>.

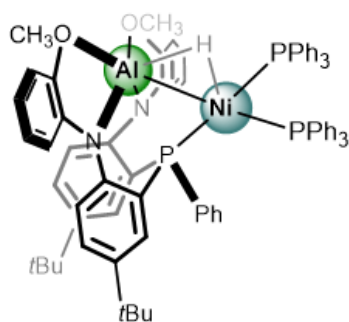


Figure 54: Structure of NiAl-(PPh<sub>3</sub>)<sub>2</sub>.

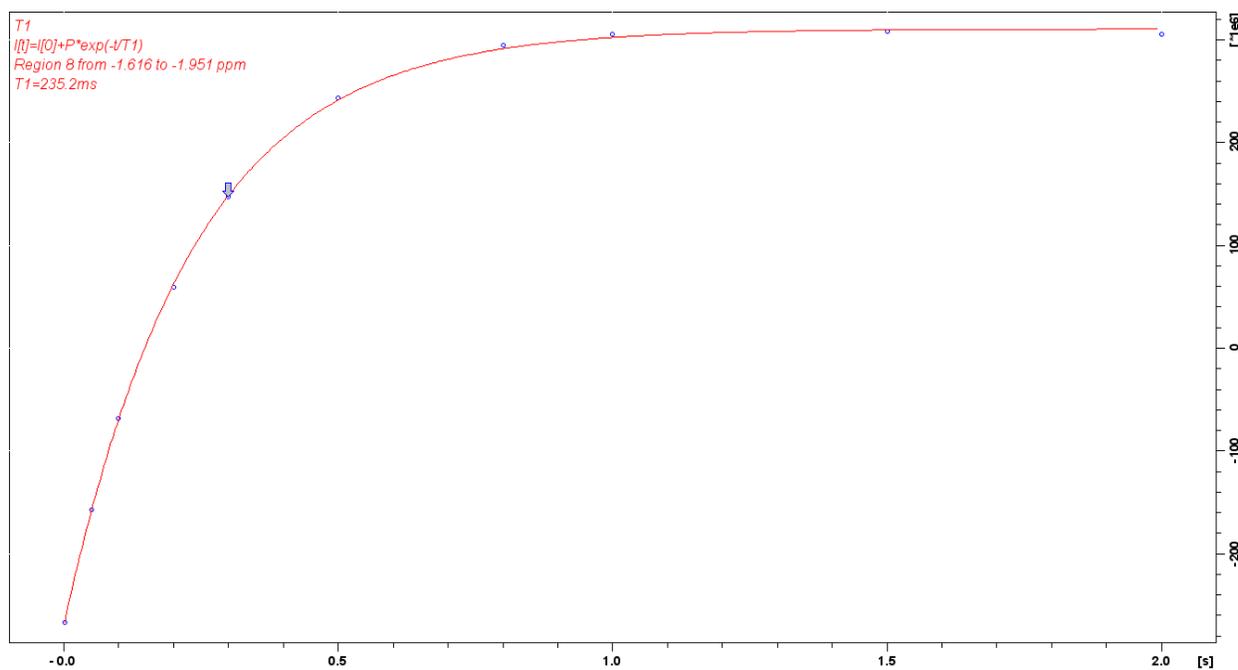


Figure 55: T1 Time Plot NiAl-(PPh<sub>3</sub>)<sub>2</sub> in C<sub>6</sub>D<sub>6</sub>.

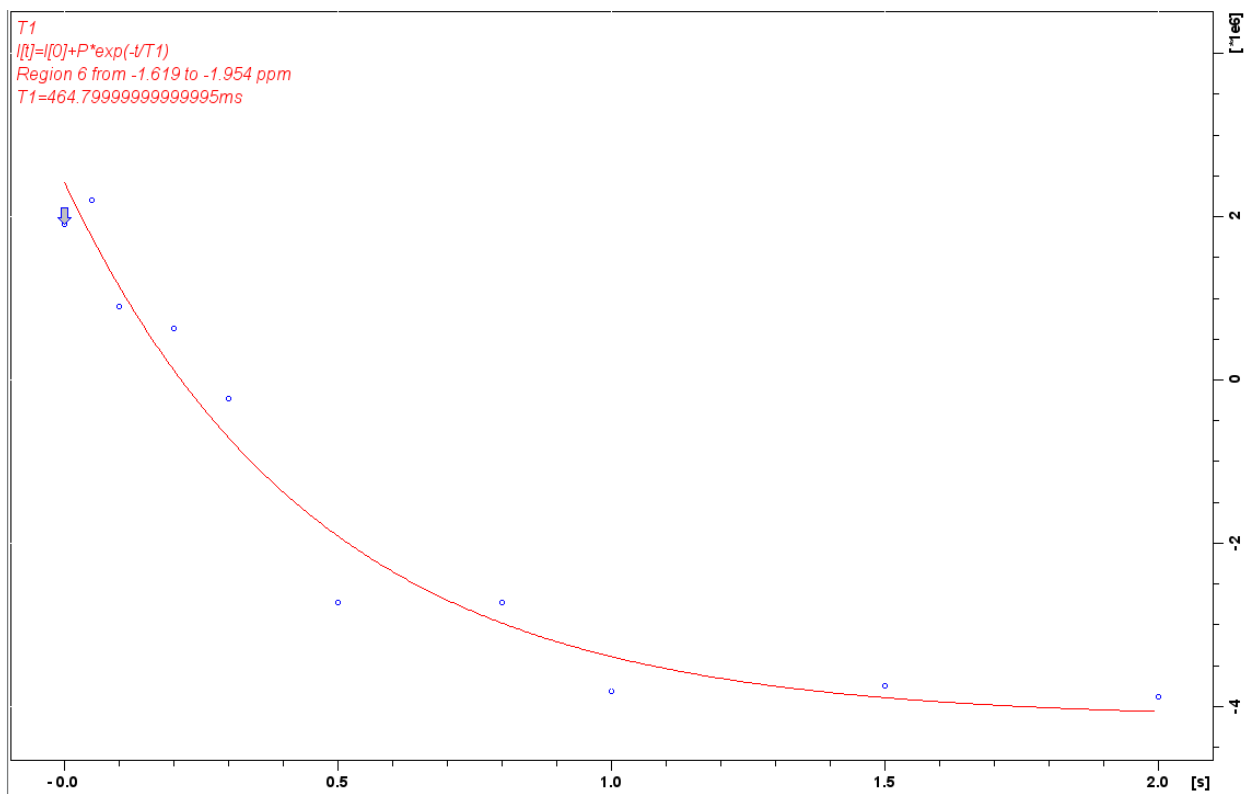


Figure 56: T1 Time Plot NiAl-(PPh<sub>3</sub>)<sub>2</sub> in THF.

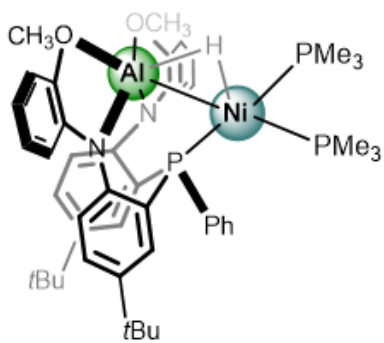


Figure 57: Structure of NiAl-(PMe<sub>3</sub>)<sub>2</sub>.

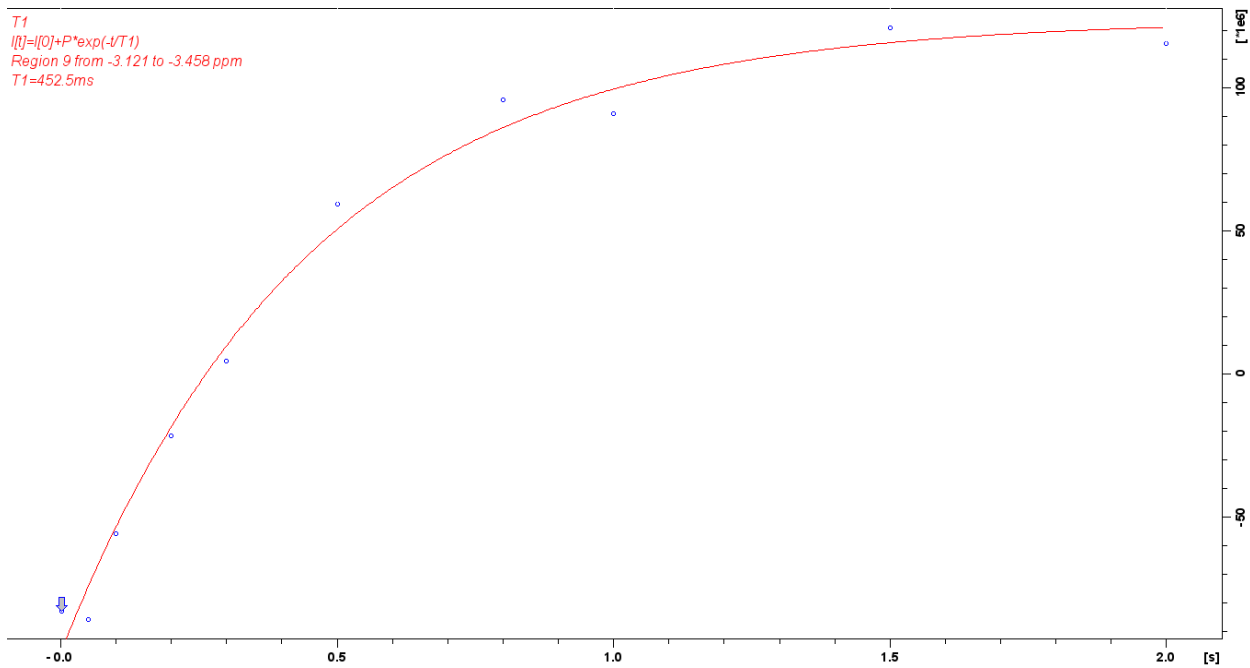


Figure 58: T1 Time Plot NiAl-(PMe<sub>3</sub>)<sub>2</sub> in C<sub>6</sub>D<sub>6</sub>.

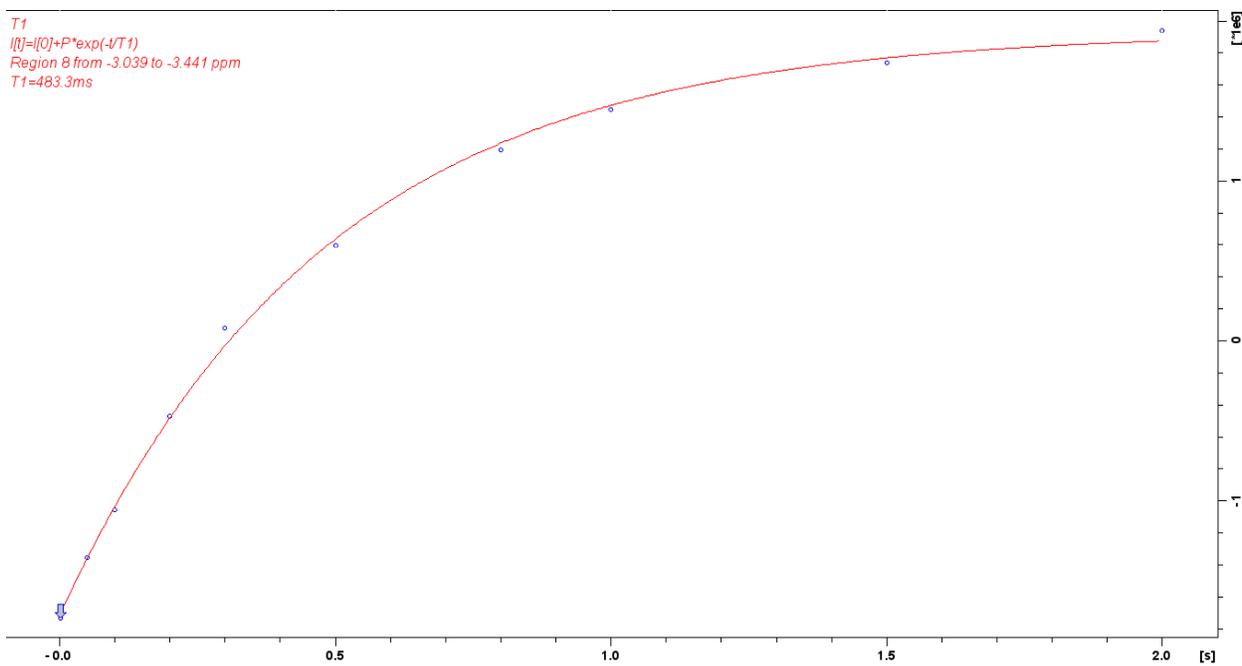


Figure 59: T1 Time Plot NiAl-(PMe<sub>3</sub>)<sub>2</sub> in THF.

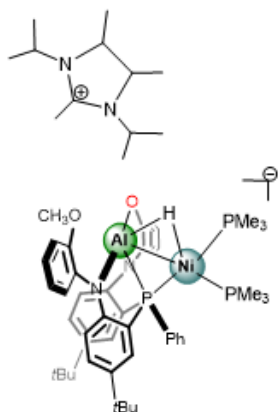


Figure 60: Structure of NiAl-(PMe<sub>3</sub>)<sub>2</sub>-NHC-IPr.

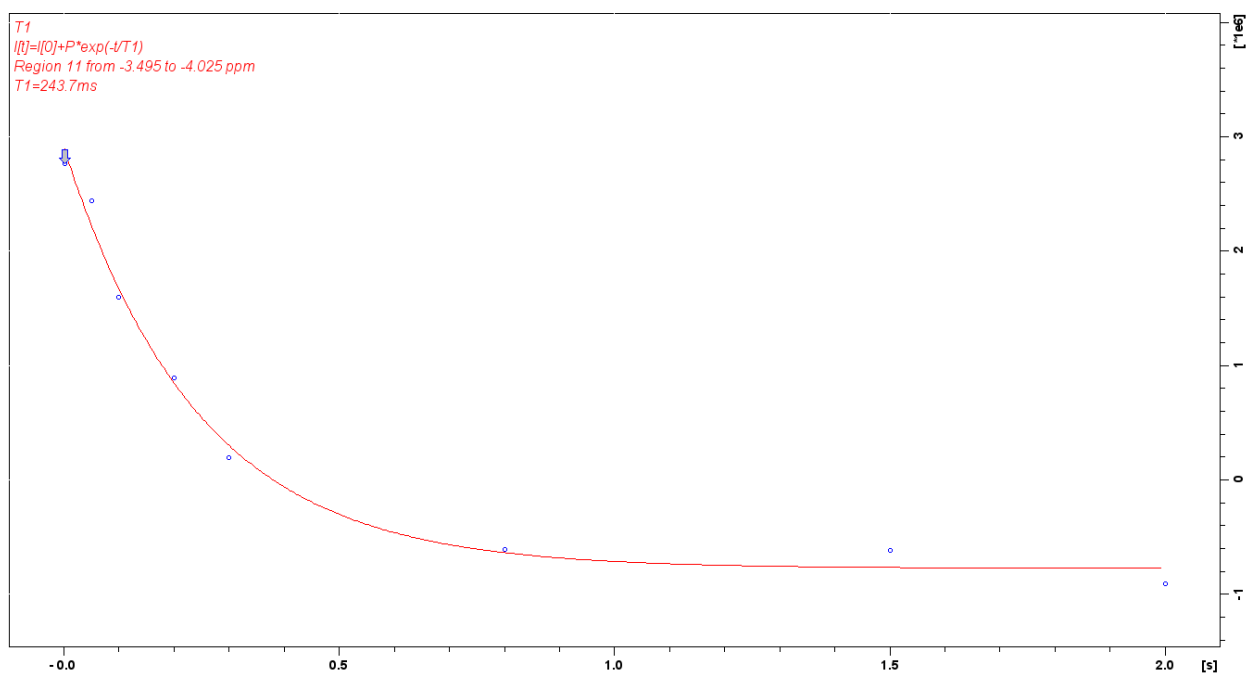


Figure 61: T1 Time Plot NiAl-(PMe<sub>3</sub>)<sub>2</sub>-NHC-IPr in THF.

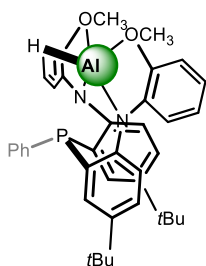


Figure 62: Structure of LAIH.

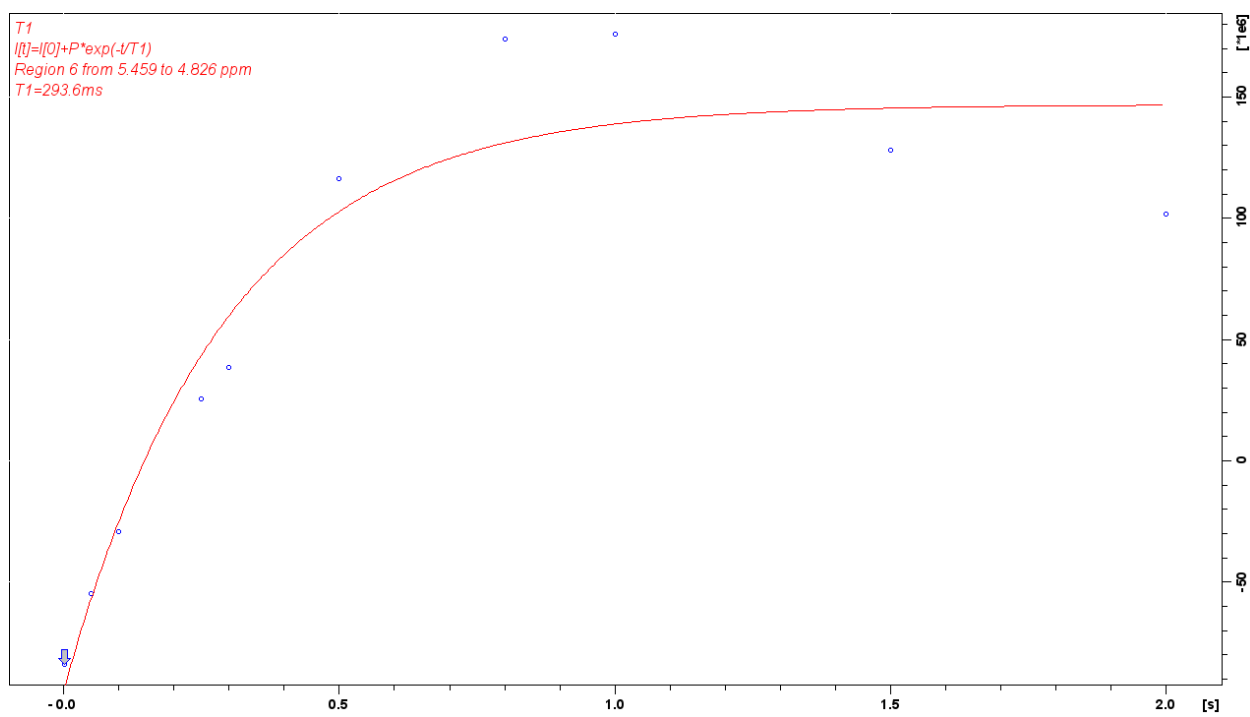


Figure 63: T1 Time Plot LAIH in C<sub>6</sub>D<sub>6</sub>.

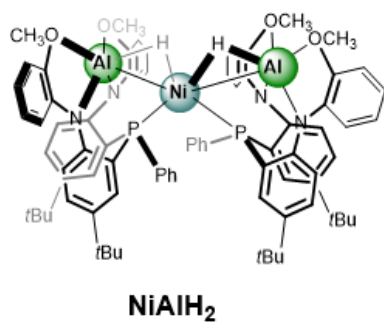


Figure 64: Structure of NiAl<sub>2</sub>.

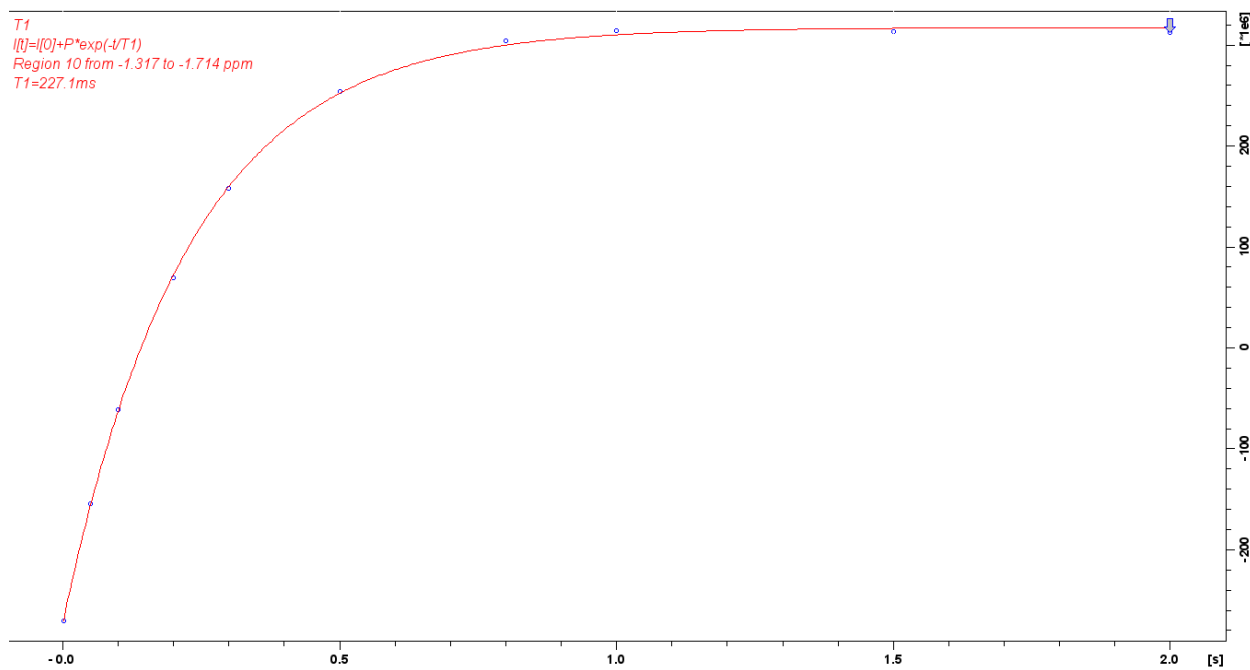


Figure 65: T1 Time of NiAl<sub>2</sub> in C<sub>6</sub>D<sub>6</sub>.

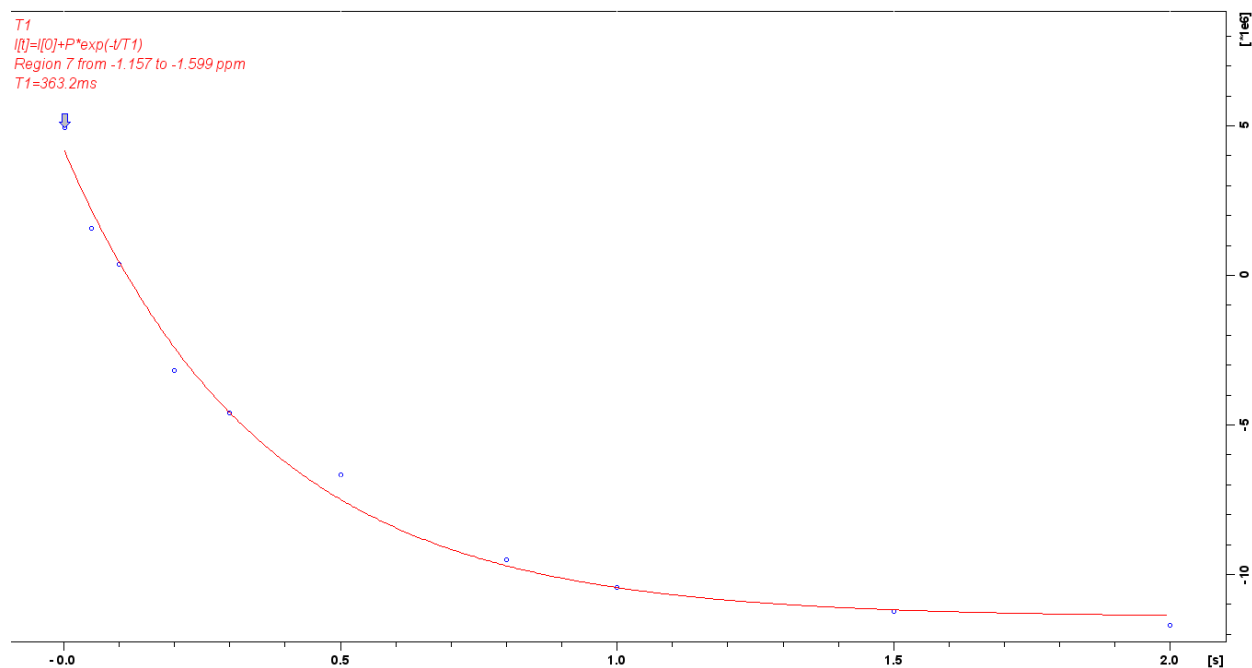


Figure 66: T1 Time of NiAl<sub>2</sub> in THF.

Table 12. Overall comparison table of T1 times between all complexes.

Analysis	NiAl <sub>2</sub>	LAIH	2-(PPh <sub>3</sub> ) <sub>2</sub>	2-(PMe <sub>3</sub> ) <sub>2</sub>	2-(PMe <sub>3</sub> ) <sub>2</sub> -NHC-IPr
T1	C <sub>6</sub> D <sub>6</sub> :	C <sub>6</sub> D <sub>6</sub> :	C <sub>6</sub> D <sub>6</sub> :	C <sub>6</sub> D <sub>6</sub> :	C <sub>6</sub> D <sub>6</sub> : 243.7 ms
	227.1 ms	293.6 ms	235.2 ms	452.5 ms	
	THF:		THF:	THF:	
	363.2 ms		464.8 ms	483.3 ms	

## CHAPTER IV

### CONCLUSION

In summary, this work builds on the rare reports of three-center-two-electron bonding within a Ni-H-Al subunit. The subunit features a Ni center and sterically accessible Lewis-acidic Al centers with a degree of covalency within the shared hydride moiety. To understand the impact of the Al-H-Ni subunit in electronic structure, the synthesis of similar heterometallic complexes was mainly performed utilizing ancillary ligands. Here is reported a series of small-scale studies of LAIH or NiAl<sub>2</sub> complex using ancillary ligands, in which the purpose is to reach enhance modulation of covalency in heterobimetallic complexes in heterobimetallic complexes. Having explored a variety of potential ancillary ligands, it was found that the main four successful ligands were triphenylphosphine, trimethyl phosphine, bis(diphenyl phosphino) methane and Diisopropyl-4,5-dimethyl-imidazol-2-ylidene (NHC-IPr). The synthesis of the well-defined heterometallic complexes with varying electronic parameters, reported in the previous chapters, demonstrates that covalency between with Ni-H-Al subunit can be modulated.

After an extensive investigation of attempts to incorporate 17 different potential ancillary ligands, it was found that sigma donors were the best suitors in the high-yielding synthesis of heterometallic complexes. All attempts were analyzed and characterized by multinuclear NMR spectroscopy. For the isolated species, the NMR resonance of their hydride ligand showed a upfield chemical shift. In order the NiAl-(PPh<sub>3</sub>)<sub>2</sub>, NiAl-(dppm)<sub>2</sub>, NiAl-(PMe<sub>3</sub>)<sub>2</sub>, and anionic hydride were found to be at -1.78 ppm, -2.14 ppm, -3.28 ppm, and -4.07 ppm. In addition, some catalysis trials were conducted using H-BPin and quinoline with 5% of catalyst in this case NiAl<sub>2</sub>

and NiAl-(PPh<sub>3</sub>)<sub>2</sub>. As shown in the NMR spectra for both complexes, the formation of 1,4 and 1,2 isomers of dearomatized quinoline is noted. As shown in Figures 44-45 and 46-47, the <sup>1</sup>H and <sup>31</sup>P{<sup>1</sup>H} NMR shows the appearance of 1,4 and 1,2 isomers of dearomatized quinoline in accordingly peaks such as 6.90-6.70 and 6.26 for olefinic-protons.<sup>62</sup> For these and many other reasons, our strategy demonstrated that it is simple to obtain different types of the same electronic structure complex along with similar features of types of structures. The effectiveness of the heterometallic complexes in catalytic trials for hydrofunctionalization are under continued investigation.

Computational studies complement the information provided by the XRD results from our crystal structures. Computational studies were performed using the BP86 functional along with def2-SVP (for H, C, N, O, and P), and def2-TZVP (for Al and Ni).<sup>4,21,22</sup> By performing geometry optimization (Opt), vibrational frequency (Freq) calculation, and wavefunction analysis including Natural Bond Order (NBO) and Quantum Theory of Atoms in Molecules (QTAIM), we gain insight into the electronic structure to complement the findings produced through experimental chemistry using software called Multiwfn and AIMAll.<sup>2,3,31,56</sup> These data show that based on the highest WBI and Rho value for Ni-H is the anionic hydride variant, which means this complex exhibits the strongest covalency within the other complexes. In addition, the T1 time was performed in a variety of temperatures. The T1 time analysis proves that all our complexes are metal hydrides since the T1 times are two orders of magnitude higher than the dihydrogen ligand. The shortest room temperature T1 time experiment is 227.1 ms for NiAl<sub>2</sub> and the longest T1 time experiment at room temperature is 452.5 ms for NiAl-(PMe<sub>3</sub>)<sub>2</sub> with C<sub>6</sub>D<sub>6</sub> and for THF the smallest one is 363.2 ms again or NiAl<sub>2</sub> and the highest one is 483.3 ms for NiAl-(PMe<sub>3</sub>)<sub>2</sub>. Further studies are needed to elaborate on these studies. Combined synthetic and

theoretical studies complement our findings that the addition of ancillary ligands can modulate the covalency in heterobimetallic subunits.

The fundamental part of my work was developing an understanding of heterometallic sigma complexes and their electronic structure. Due to our findings, a potential advancement may lead to how ligand design plays an important role in heterometallic catalysis. Incorporation of different donors allows us to vary the degree of electrophilicity at the Lewis-acidic metal center which can play a crucial part in the hydrofunctionalization catalysis. A continued challenge is to balance the steric accessibility of the Lewis-acidic metal since the unbalance may lead to decomposition of the generated species by lack of donors surrounding the Lewis-acidic metal. There are several important aspects to take away from this project, an important part was that adding the different ancillary ligands changes the degree of Ni-H vs Al-H character which was able to probe both computationally and experimentally. This project continues to develop a vast encyclopedia of heterometallic complexes to expand our understanding of the Ni-H-Al subunit, and with this to explore the interaction between some other metals. Meanwhile, our well-defined systems are still under investigation, we desire to identify new routes to access precise regio divergence in a single complex while exploring modulating the covalency in the specific subunit.

#### **4.1 Future Work**

Expanding on these results including the further exploration of ancillary ligands to perturb the electron density distribution will better aid our understanding of the electronic structure within these rare Ni-H-Al subunits. If our catalytic activity studies demonstrate our complexes are successful in hydrofunctionalization, our well-defined heterometallic complexes may facilitate the hydrofunctionalization of more challenging substrates. To further our knowledge in the

modulation of covalency and mechanistic studies, it is important to explore the mechanistic studies of hydrofunctionalization since insertion studies are important to improve methodology. Having a better understanding of these potential computational studies will lead to improving our synthetic methods for our heterometallic complexes and then they will be fully understood. Then, we will be able to expand to obtain plenty of other complexes using some other different ancillary ligands.

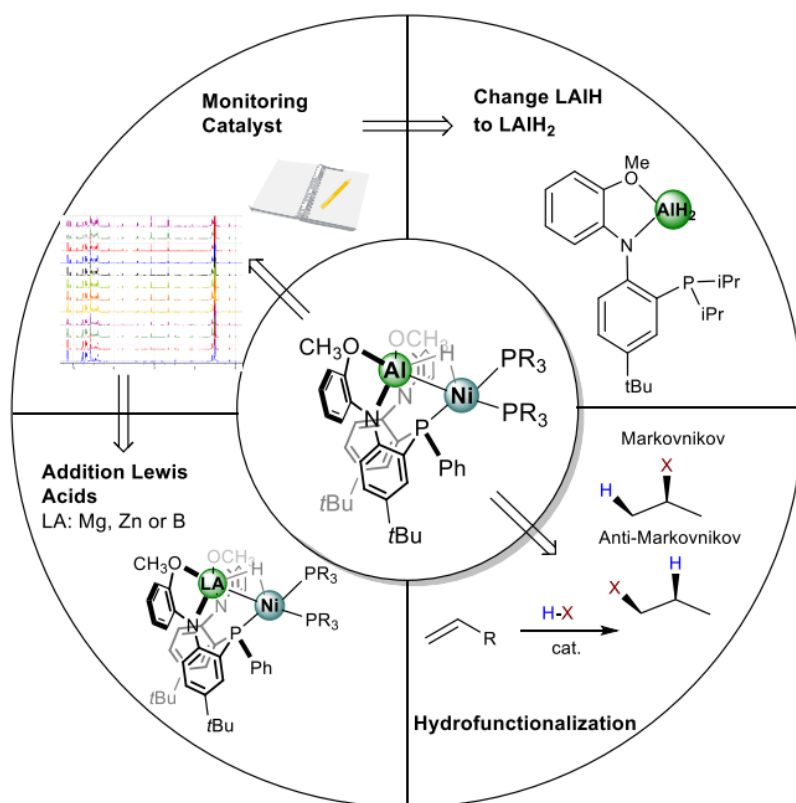


Figure 67: Future work.

## REFERENCES

- (1) Acharya, A. K.; Chang, Y. A.; Jones, G. O.; Rice, J. E.; Hedrick, J. L.; Horn, H. W.; Waymouth, R. M. Experimental and Computational Studies on the Mechanism of Zwitterionic Ring-Opening Polymerization of  $\delta$ -Valerolactone with N-Heterocyclic Carbenes. *The Journal of Physical Chemistry B* **2014**, *118* (24), 6553–6560.
- (2) Bader, R. F. Atoms in Molecules. *Accounts of Chemical Research* **1985**, *18* (1), 9–15.
- (3) Bader, R. F. A Quantum Theory of Molecular Structure and Its Applications. *Chemical Reviews* **1991**, *91* (5), 893–928.
- (4) Becke, A. D. Density-functional exchange-energy approximation with correct asymptotic behavior. *Physical Review A*, **1988**. *38*(6), 3098–3100.
- (5) Bonanno, J. B.; Henry, T. P.; Wolczanski, P. T.; Pierpont, A. W. Evidence for strong tantalum-to-boron dative interactions in  $(\text{SiOx})_3\text{Ta}(\text{BH}_3)$  and  $(\text{SiOx})_3\text{Ta}(\text{H}_2\text{-B, Cl-BCl}_2\text{Ph})$  (SiOx =  $\text{tBu}_3\text{SiO}$ ). *Inorg. Chem.* **2006**, *46* (4), 1222–1232.
- (6) Buchwalter, P.; Rosé, J.; Braunstein, P. Multimetallic Catalysis Based on Heterometallic Complexes and Clusters. *Chemical Reviews* **2014**, *115* (1), 28–126.
- (7) Cai, Y.; Jiang, S.; Rajeshkumar, T.; Maron, L.; Xu, X. A Planar Nickelaspiropentane Complex with Magnesium-Based Metalloligands: Synthesis, Structure, and Synergistic Dihydrogen Activation. *Journal of the American Chemical Society* **2022**, *144* (36), 16647–16655.
- (8) Cammarota, R. C., & Lu, C. C. Tuning nickel with Lewis acidic group 13 metalloligands for catalytic olefin Hydrogenation. *Journal of the American Chemical Society*, **2015**, *137*(39), 12486–12489.
- (9) Chen, Q.; Qin, D.; Ouyang, L.; Yang, X.; Zhang, Y. Understanding Solid Phase Diffusion-Bonding Process of Ni (000)/ $\alpha$ - $\text{Al}_2\text{O}_3$  (0001) Interface. *Energy Storage and Saving* **2023**, *2* (3), 495–502.
- (10) Clifford, A. F.; Mukherjee, A. K. Iron Carbonyl Complexes of Triphenylphosphine, Triphenylarsine, and Triphenylstibine. *Inorganic Chemistry* **1963**, *2* (1), 151–153.

- (11) Cotton, F. A.; Luck, R. L. Variable temperature T<sub>1</sub> studies on rhenium hydrido phosphine complexes, REH<sub>5</sub>(PPh<sub>3</sub>)<sub>3</sub>, PR<sub>3</sub> = PMePh<sub>2</sub> and PPh<sub>3</sub>, ReH<sub>7</sub>(PPh<sub>3</sub>)<sub>2</sub>, and Re<sub>2</sub>H<sub>8</sub>(PPh<sub>3</sub>)<sub>4</sub>. classical or nonclassical hydrides? *Inorganic Chemistry* **1989**, 28 (1), 6–8.
- (12) Cotton, F. A.; Luck, R. L.; Root, D. R.; Walton, R. A. Variable-Temperature <sup>1</sup>H NMR spectra and T<sub>1</sub> measurements on the Dinuclear Octahydride Complexes Re<sub>2</sub>H<sub>8</sub>(PR<sub>3</sub>)<sub>4</sub> (PR<sub>3</sub> = PPh<sub>3</sub>, PEt<sub>2</sub>Ph, PMe<sub>2</sub>Ph, PMe<sub>3</sub>) and the Monohydride Complexes Cp<sub>2</sub>ReH and Re<sub>2</sub>HCl<sub>3</sub>(CO)<sub>2</sub>(dppm)<sub>2</sub> (dppm = Ph<sub>2</sub>CH<sub>2</sub>PPh<sub>2</sub>). *Inorganic Chemistry* **1990**, 29 (1), 43–47.
- (13) Cotton, F. A.; Takats, J. Structure of Triphenylphosphine-(Pentahaptocyclopentadienyl) Copper (I). *Journal of the American Chemical Society* **1970**, 92 (8), 2353–2358.
- (14) Crabtree, R. H. *The Organometallic Chemistry of the Transition Metals*; John Wiley & Sons, Inc, 2019.
- (15) Cui, H.; Cui, C. Silylation of N-Heterocyclic Carbene with Aminochlorosilane and - Disilane: Dehydrohalogenation vs. Si–Si Bond Cleavage. *Dalton Transactions* **2011**, 40 (44), 11937.
- (16) De Leon, E.; Gonzalez, F.; Bauskar, P.; Gonzalez-Eymard, S.; De Los Santos, D.; Shoshani, M. M. Amplifying Reactivity of Metal Hydrides: A Heterotrimetallic NiAl<sub>2</sub>(μ<sub>2</sub>-H)<sub>2</sub> Catalyst for the Dearomatization of N-Heterocycles. *Organometallics* **2023**, 42 (6), 435-440
- (17) DePriest, J.; Zheng, G. Y.; Goswami, N.; Eichhorn, D. M.; Woods, C.; Rillema, D. P. Structure, Physical, and Photophysical Properties of Platinum(II) Complexes Containing Bidentate Aromatic and Bis(Diphenylphosphino)Methane as Ligands. *Inorganic Chemistry* **2000**, 39 (9), 1955–1963.
- (18) Dera, P.; Lazarz, J. D.; Lavina, B. Pressure-Induced Development of Bonding in NiAs Type Compounds and Polymorphism of NiP. *Journal of Solid State Chemistry* **2011**, 184 (8), 1997–2003.
- (19) Dietrich, O.; Gaass, T.; Reiser, M. F. T<sub>1</sub> relaxation time constants, influence of oxygen, and the oxygen transfer function of the human lung at 1.5 T—a meta-analysis. *European Journal of Radiology* **2017**, 86, 252–260.
- (20) Dunne, B. J.; Orpen, A. G. Triphenylphosphine: A Redetermination. *Acta Crystallographica Section C Crystal Structure Communications* **1991**, 47 (2), 345–347.
- (21) F. Weigend, “Accurate Coulomb-fitting basis sets for H to Rn,” *Phys. Chem. Chem. Phys.* **2006**, 8 1057-65.
- (22) F. Weigend and R. Ahlrichs, “Balanced basis sets of split valence, triple zeta valence and quadruple zeta valence quality for H to Rn: Design and assessment of accuracy,” *Phys. Chem. Chem. Phys.* **2005**, 7 3297-305.

- (23) Govindarajan, M.; Karabacak, M. Spectroscopic properties, NLO, HOMO–LUMO and NBO analysis of 2,5-Lutidine. *Spectrochimica Acta Part A: Molecular and Biomolecular Spectroscopy* **2012**, *96*, 421–435.
- (24) Graziano, B. J., Vollmer, M. V., & Lu, C. C. Cooperative bond activation and facile intramolecular aryl transfer of nickel–aluminum pincer-type complexes. *Angewandte Chemie*, **2021**, *133*(27), 15214–15221.
- (25) Grim, S. O.; Walton, E. D. Unsymmetrical Bis-Phosphorus Ligands. 12. Synthesis and Nuclear Magnetic Resonance Studies of Some Derivatives of Bis(Diphenylphosphino)Methane. *Inorganic Chemistry* **1980**, *19* (7), 1982–1987.
- (26) Harman, W. H.; Peters, J. C. Reversible H<sub>2</sub> Addition across a Nickel–Borane Unit as a Promising Strategy for Catalysis. *Journal of the American Chemical Society* **2012**, *134* (11), 5080–5082.
- (27) Harper, L. K., Shoaf, A. L., & Bayse, C. A. Predicting trigger bonds in explosive materials through Wiberg Bond index analysis. *Chem Phys Chem*, **2015**, *16*(18), 3886–3892.
- (28) Hill, A. F. An unambiguous electron-counting notation for metallaboratranes. *Organometallics* **2006**, *25* (20), 4741–4743.
- (29) Jafarpour, L., Stevens, E. D., & Nolan, S. P. A sterically demanding nucleophilic carbene: 1,3-bis(2,6-diisopropylphenyl)imidazol-2-ylidene). thermochemistry and catalytic application in olefin metathesis. *Journal of Organometallic Chemistry*, **2000**, *606*(1), 49–54.
- (30) Keim, W. Nickel: An element with wide application in industrial homogeneous catalysis. *Angewandte Chemie International Edition in English*, **1990**, *29*(3), 235–244.
- (31) Keith, Todd A. TK Gristmill Software, Overland Park KS, USA, 2019 (aim.tkgristmill.com)
- (32) Kuhn, N., & Kratz, T. Synthesis of Imidazol-2-ylidenes by Reduction of Imidazole-2(3H)-thiones. *Synthesis*, **1993**, *1993*(06), 561–562.
- (33) Kurt, M.; Babu, P. C.; Sundaraganesan, N.; Cinar, M.; Karabacak, M. Molecular structure, vibrational, UV and NBO analysis of 4-chloro-7-nitrobenzofurazan by DFT calculations. *Spectrochimica Acta Part A: Molecular and Biomolecular Spectroscopy* **2011**, *79* (5), 1162–1170.
- (34) Lai, Q., Cosio, M. N., & Ozerov, O. V. Ni complexes of an Alane/tris(phosphine) ligand built around a strongly Lewis acidic tris(*n*-pyrrolyl)aluminum. *Chemical Communications*, **2020**, *56*(94), 14845–14848.

- (35) Li, Y.; Ma, B.; Cui, C. Reactivity of an NHC-Stabilized Silylene towards Ketones. Formation of Silicon Bis-Enolates vs. Bis-Silylation of the C=O Bond. *Dalton Transactions* **2015**, 44 (31), 14085–14091.
- (36) Maiola, M. L.; Buss, J. A. Accessing Ta/Cu architectures via metal-metal Salt Metatheses: Heterobimetallic C–H bond activation affords  $\mu$ -hydrides. *Angewandte Chemie International Edition* **2023**, 62 (48).
- (37) Matsuzaka, H.; Kodama, T.; Uchida, Y.; Hidai, M. Metallo-selective substitution reactions by amines or phosphines in HRUCO<sub>3</sub>(CO)<sub>12</sub>. infrared and Proton and Cobalt-59 NMR studies of HRuCO<sub>3</sub>(CO)<sub>12-x</sub>L<sub>x</sub> (L = amines or phosphines; x = 0-2) and crystal structure of HRuCO<sub>3</sub>(CO)<sub>11</sub>(PPh<sub>3</sub>). *Organometallics* **1988**, 7 (7), 1608–1613.
- (38) Matta, C. F. Special issue: Philosophical aspects and implications of the quantum theory of atoms in molecules (QTAIM). *Foundations of Chemistry* **2013**, 15 (3), 245–251.
- (39) Mojica-Sánchez, J. P. Applications of the Quantum Theory of Atoms in Molecules in Chemical Reactivity. *Chemical Reactivity* **2023**, 1–14.
- (40) Murphy, L. J.; Hollenhorst, H.; McDonald, R.; Ferguson, M.; Lumsden, M. D.; Turculet, L. Selective Ni-catalyzed hydroboration of CO<sub>2</sub> to the formaldehyde level enabled by new PSIP ligation. *Organometallics* **2017**, 36 (19), 3709–3720.
- (41) Murugesan, K., Wei, Z., Chandrashekhar, V. G., Jiao, H., Beller, M., & Jagadeesh, R. V. General and selective synthesis of primary amines using Ni-based homogeneous catalysts. *Chemical Science*, **2020**, 11(17), 4332–4339.
- (42) Ocampo, M. V. L.; Murray, L. J. Metal-Tuned Ligand Reactivity Enables CX(2) (X = O, S) Homocoupling with Spectator Cu Centers. *J Am Chem Soc* **2024**, 146 (1), 1019-1025.
- (43) Odachowski, M.; Marschner, C.; Blom, B. A Review on 1,1-Bis(Diphenylphosphino) Methane Bridged Homo- and Heterobimetallic Complexes for Anticancer Applications: Synthesis, Structure, and Cytotoxicity. *European Journal of Medicinal Chemistry* **2020**, 204, 112613.
- (44) Page, M. J.; Mahon, M. F.; Whittlesey, M. K. Formation and Reactivity of the Cyclometallated N-Heterocyclic Carbene Complexes [Ru(Nhc')(Dppe)(Co)h]. *Dalton Transactions* **2011**, 40 (31), 7858.
- (45) Parkin, G. A simple description of the bonding in transition-metal borane complexes. *Organometallics* **2006**, 25 (20), 4744–4747.
- (46) Puddephatt, R. J. Chemistry of Bis(Diphenylphosphino)Methane. *Chemical Society Reviews* **1983**, 12 (2), 99.

- (47) Reed, A. E., Weinstock, R. B., & Weinhold, F. Natural population analysis. *The Journal of Chemical Physics*, **1985**, 83(2), 735–746.
- (48) Semba, K.; Nagase, K.; Asano, H.; Hara, N.; Nakao, Y. Synthesis and reactivity of Al–Ni bimetallic complexes. *Polyhedron* **2024**, 251.
- (49) Seo, Y.-S., Jung, Y.-S., Yoon, W.-L., Jang, I.-G., & Lee, T.-W. The effect of Ni content on a highly active Ni–Al<sub>2</sub>O<sub>3</sub> catalyst prepared by the homogeneous precipitation method. *International Journal of Hydrogen Energy*, **2011**, 36(1), 94–102.
- (50) Shoshani, M. M. Cooperative heterometallic platforms enabling selective C–H bond activation and functionalization of pyridines. *Cell Reports Physical Science*, **2023**, 4(4), 101213.
- (51) Shubina, E. S.; Belkova, N. V.; Krylov, A. N.; Vorontsov, E. V.; Epstein, L. M.; Gusev, D. G.; Niedermann, M.; Berke, H. Spectroscopic evidence for *intermolecular* m–h···h–or hydrogen bonding: interaction of WH(CO)<sub>2</sub>(NO)<sub>2</sub> hydrides with Acidic Alcohols. *Journal of the American Chemical Society* **1996**, 118 (5), 1105–1112.
- (52) Sobaczynski, A. P.; Bauer, T.; Kempe, R. Heterometallic Hydride Complexes of Rare-Earth Metals and Ruthenium through C–H Bond Activation. *Organometallics* **2012**, 32 (5), 1363–1369.
- (53) Takaya, J.; Iwasawa, N. Synthesis, structure, and catalysis of palladium complexes bearing a group 13 Metalloligand: Remarkable effect of an aluminum-metalloligand in hydrosilylation of CO<sub>2</sub>. *Journal of the American Chemical Society* **2017**, 139 (17), 6074–6077.
- (54) Tasker, S. Z., Standley, E. A., & Jamison, T. F. Recent advances in homogeneous nickel catalysis. *Nature*, **2014**, 509(7500), 299–309.
- (55) Thomas, R.; Eriks, K.; Holmes, R. R.; Carter, R. P.; Lanpher, E. Trimethylphosphine. *Inorganic Syntheses* **1967**, 59–63.
- (56) Tian Lu, Feiwu Chen, Multiwfn: A Multifunctional Wavefunction Analyzer, *J. Comput. Chem.* **2012**, 33, 580-592.
- (57) Weinhold, F.; Landis, C. R.; Glendening, E. D. What is NBO analysis and how is it useful? *International Reviews in Physical Chemistry* **2016**, 35 (3), 399–440.
- (58) Xiao, S.; Trogler, W. C.; Ellis, D. E.; Berkovitch-Yellin, Z. Nature of the Frontier Orbitals in Phosphine, Trimethylphosphine, and Trifluorophosphine. *Journal of the American Chemical Society* **1983**, 105 (24), 7033–7037.
- (59) Yang, C.; Zhang, F.; Deng, G. J.; Gong, H. Amination of Aromatic Halides and Exploration of the Reactivity Sequence of Aromatic Halides. *J Org Chem* **2019**, 84 (1), 181-190.

- (60) Yang, H.; Whitten, J. L. Chemisorption of Hydrogen on the Nickel (111) Surface. *The Journal of Chemical Physics* **1988**, *89* (8), 5329–5334.
- (61) Yartys, V. A.; Denys, R. V.; Maehlen, J. P.; Frommen, C.; Fichtner, M.; Bulychev, B. M.; Emerich, H. Double-Bridge Bonding of Aluminium and Hydrogen in the Crystal Structure of  $\gamma$ -AlH<sub>3</sub>. *Inorganic Chemistry* **2006**, *46* (4), 1051–1055.
- (62) Zhang, F.; Song, H.; Zhuang, X.; Tung, C.-H.; Wang, W. Iron-Catalyzed 1,2-Selective Hydroboration of *n*-Heteroarenes. *Journal of the American Chemical Society* **2017**, *139* (49), 17775–17778. DOI:10.1021/jacs.7b11416.
- (63) Zhukhovitskiy, A. V.; Kobylanskiy, I. J.; Wu, C.-Y.; Toste, F. D. Migratory insertion of carbenes into Au(III)–C bonds. *Journal of the American Chemical Society* **2017**, *140* (1), 466–474.

## VITA

Aleida G. Gonzalez (aleida.gonzalez01@utrgv.edu) is a first-generation college student who completed her Bachelor of Science in Chemistry in the Spring of 2019. During her undergraduate studies, Aleida was awarded the Research Initiative for Scientific Enhancement (RISE) scholarship and started working on the identification of biochemical properties of medicinal plants such as *Moringa Oleifera* under the advice of Dr. Arnulfo O. Mar. During the Summer of 2017, Aleida was part of the NSF-International Research Experience for Students (IRES): Research in Catalysis and Photocatalysis in Lyon, France. There she worked on the project “Fluorous Solvent Droplet Catalysis in Fluorous Tag Oligosaccharide Synthesis” under the advice of Dr. Peter Goekjian. In summer 2018, she participated in the Chemistry NSF-Research Experience for Undergraduates (REU) at Clemson University. I worked on the project “Synthesis and Characterization of Plasmonic Nanoparticles Assemblies” by Dr. George Chumanov. Later in 2022, Dr. Tatiana A. Estrada-Medoza published an article entitled, “Silicate as a Versatile Matrix for the Aqueous Synthesis of Metal Sulfide Nanoparticles” which Ms. Gonzalez co-authored. In Fall 2022, she started her graduate studies under the advice of Dr. Manar M. Shoshani and Dr. Haoyuan Chen. During her MSc in biochemistry and molecular biology, Aleida was awarded the COS Dean’s Graduate Assistantship while finishing her Master’s degree. Her project is based on “A Novel Strategy to Influence Reactivity of Ni-H-Al Subunit in Heterometallic Complexes by Addition of Varying Ancillary Ligands” then graduating with a Master of Science in Biochemistry and Molecular Biology July 2024.